Impact of Wettability on Rock Mechanics and Oil Recovery

A Comparative Study on Different Outcrop Chalks

by

Jaspreet Singh Sachdeva

Thesis submitted in fulfilment of
the requirements for the degree of
PHILOSOPHIAE DOCTOR
(PhD)

University
of Stavanger

Faculty of Science and Technology
Department of Energy Resources
2020

University of Stavanger
NO-4036 Stavanger
NORWAY
www.uis.no

ISBN: 978-82-7644-905-1
ISSN: 1890-1387
PhD: Thesis UiS No. 502

This dissertation is dedicated to my parents
who instilled in me the virtues of perseverance
and commitment and relentlessly encouraged
me to strive for excellence.

Acknowledgements

I would like to express my sincere gratitude to everyone who helped and encouraged me in various ways in carrying out my PhD work. Their contributions are sincerely appreciated and gratefully acknowledged.

First and foremost, I would like to thank Dr. Anders Nermoen, Prof. Merete Vadla Madland and Dr. Reidar Inge Korsnes for their guidance, advices and suggestions throughout the term of my PhD. Without their valuable assistance, always generously and unstintingly given, the completion of this work would have been immeasurably more difficult. Dr. Korsnes' cheerful mood and love for the same taste in music as me made my time spent in the laboratories completely worthwhile.

I am also indebted to The National IOR Centre of Norway for introducing me to so many industry stalwarts in Improved Oil Recovery and Rock Mechanics field of studies and helping me learn so much more than what I had wished for at the start of my PhD. I would also like to thank everyone at the Department of Energy Resources and Department of Energy and Petroleum Engineering, University of Stavanger, for their support and cooperation.

I would also like to give my special thanks to Dr. Kim Andre Vorland and Dr. Ola Kjetil Siqveland for their invaluable help in carrying out the experimental work. During this work, the constant association with all my PhD colleagues, especially Tijana Voake, Dhruvit Satishchandra Berawala and Shreyansh Divyankar, and their valuable suggestions are highly appreciated. I would also like to thank *Folken* in Stavanger for providing me with a second home in Norway.

I really appreciate the time spent with the Hibernia EOR group at the Memorial University of Newfoundland, Canada, as an exchange researcher and would like to extend my heartiest gratitude to Prof. Lesley Anne James and Mr. Edison Sripal for teaching me so much through experimental studies and long discussions. The time spent in St. John’s also provided me with an opportunity to meet many new people, including Rishikesh Nair, which I will cherish forever.

My special thanks go to my parents Mr. Amarjeet Singh Sachdeva and Mrs. Kulvinder Kaur Sachdeva for their continuous encouragement, love and support during my thesis work. Their morale boosting support during these years cannot be described in words. I also express my gratitude to my brother Mr. Darshanjeet Singh Sachdeva, my sister-in-law Ms. Harkirtan Kaur Sachdeva and my beautiful niece Suhaavi Kaur Sachdeva for continuously inspiring me to achieve new heights.

I am also very grateful to all my extended family members and friends across the globe for believing in me and for providing their support at all times.

I, once again, thank everyone for their never-ending support and encouragement that they have provided me at various stages of my PhD period.

Jaspreet Singh Sachdeva

Summary

Chalk reservoirs are highly fractured and are known for their remarkable storage capacity as a reservoir rock for the petroleum industry. Chalk is a sedimentary carbonate rock primarily made up of calcium carbonate (calcite, $CaCO_3$) and is a very important reservoir rock in the Norwegian and Danish Continental Shelfs. Water flooding has been used as a secondary production method in chalk reservoirs as it provides pressure maintenance to the reservoir and is a proven improved oil recovery (IOR) method to produce more oil from the production facilities. Ekofisk field in the Norwegian Continental Shelf is a successful example of production by water flooding method, where seawater is used as the injection fluid. The initial estimated oil recovery was 18% as mentioned in the initial development plan of the field and today's estimates lie well above 50%.

However, seawater has also shown to enhance reservoir compaction due to water weakening of the chalk formation. It can, for example, lead to buckling and loss of well pipes, arching of overburden rocks leading to stress redistributions, and the porosity/permeability decline of the producible formation, all physical effects that alter the ultimate recovery and recovery rates of oil-bearing chalk reservoirs.

The detection of subsidence of the Ekofisk field in the Norwegian North Sea around 35 years ago has been linked to the compaction of chalk formations due to porosity reduction associated with field production. It attracted the attention of oil and gas researchers across the globe and since that time, considerable research has been carried out concerning chalk behavior, especially on how the pore fluid composition alters the mechanical properties of chalk.

Research on chalk, so far, has primarily been carried out on water-wet systems. The studies have shown that when reactive brines are injected through chalk at elevated temperatures, chemical reactions occur

between the rock and the injected brine, which affects chalk mechanical stability. It has been found that the divalent ions, such as magnesium (Mg^{2+}), calcium (Ca^{2+}) and sulfate (SO_4^{2-}) play an important role in defining chalk mechanics. Mg^{2+} ions in the injected brines lead to dissolution of calcite, which in turn leads to precipitation of new mineral phases such as magnesite, huntite, talc, anhydrite etc. Both Mg^{2+} and SO_4^{2-} ions also adsorb on the chalk surface leading to a reduction in the strength of the rock.

This project deals with the mechanical effects and oil production upon brine injection through wettability-altered samples from two chalk types. **Paper I** and **Paper III** give the results from the mechanical tests performed on Kansas chalk and Mons chalk, respectively. Both chalk types were saturated by a mixture of oil (60% - 40% by volume of Heidrun oil and heptane) and 1.1 M sodium chloride (NaCl) brine and aged for three weeks at 90°C. The wettability index of the altered samples was estimated using chromatographic separation tests by co-injecting sulfate ions, that adsorb on the water-wet mineral surfaces, and non-affine tracer. A good repeatability was observed for both chalk types.

In the triaxial test program, unaged water-wet and aged wettability-altered samples were hydrostatically loaded to 1.5 times yield stress so stiffness and strength could be determined. The samples were kept at the same stress level over time to monitor the volumetric creep. After a stagnant creep period of 15 days, magnesium chloride ($MgCl_2$) brine was flushed through both chalk types. A different set of Kansas samples from the same chalk block were also flooded by seawater. The effluents were taken at frequent intervals of time and tested using Ion Chromatography for effluent concentration. The oil production from the wettability-altered samples was also continuously monitored.

The combined observations of the bulk volume, oil volume and estimated solid volume (from effluent analyses) were used to calculate pore volume and thereby oil saturation with time.

Paper I showed that the wettability-altered Kansas chalk samples were stiffer and stronger than the water-wet samples, and when the stress was kept at 1.5 times yield the creep curves overlapped. During the flow-through period, the changes in ion composition were insensitive to the presence of oil, and ongoing water weakening for wettability-altered samples was the same as in the water-wet samples. Further, it was found that oil was only produced during the first 2–3 pore volumes (PVs) of injected brine. Afterwards, no oil was produced even though the chemical reactions took place and pore volume reduced.

Paper III showed that both water wet and wettability-altered Mons chalk samples gave comparable trends during the stagnant phase and the following $MgCl_2$ injection phase when the stress was kept at 1.5 times yield. They also showed that the non-equilibrium chemical reactions were insensitive to the initial wettability. The oil production observations, however, showed that 43% of the total oil was recovered during early-stage compaction from Mons chalk with no flow, whereas Kansas chalk did not produce any oil. No tail-end oil production was observed due to compaction or non-equilibrium brine flow in any of the two chalk types.

Paper II dealt with evaluating the extent to which chemical interactions induced by the $MgCl_2$ brine injection modify the water wetness of wettability-altered chalk samples. These tests were performed at low effective stresses. In situ wettability measurements were carried out using chromatographic separation and were performed every 10 days to estimate the evolution in mineral surface area in contact with water. The results showed an increased delay time for the sulfate ion, linked to an increase of the mineral surface area, which was observed in both water-wet and wettability-altered cores but was found to be more dominating in the wettability-altered samples. This implied that oil, which was adsorbed on the mineral surfaces, got mobilized in addition to an increased overall specific surface area as new magnesium-bearing minerals precipitated and grew during the $MgCl_2$ brine flow. This was supported by continuous effluent analysis displaying a reduced magnesium and increased calcium concentration. As in **Paper I** and **Paper III**, the nonequilibrium chemical reactions did not lead to additional oil recovery.

The main objective of **Paper IV** was to evaluate the degree to which the wettability in chalk core samples can be controlled in the laboratory. Kansas chalk samples saturated with the same 1.1M NaCl brine and oil mixture (60% - 40% by volume of Heidrun oil and heptane), as in Paper I, II and III, were aged at a constant temperature of 90°C with aging time as the laboratory control variable. A multimodal method incorporating contact angle measurements, wettability index via USBM test, and SEM-MLA analysis was applied in evaluating wettability. It was observed that an aging period of 21 days was enough to obtain a stable wettability at the specified aging conditions.

Paper V dealt with exploring elastic and plastic parameters during deviatoric loading and time-dependent deformation. A series of experiments were performed at 130°C to study the effect of four different fluids, viz., distilled water (DW), NaCl-brine, $MgCl_2$-brine and seawater (SSW), on Mons outcrop chalk. The cores were deviatorically loaded and left to creep at a constant value of 69-73% of the axial yield stress obtained from reference tests with the same brine. The results showed that SSW had the lowest yield stress followed by NaCl and $MgCl_2$, and highest for DW. The final creep strain was highest for SSW and was 1.3-1.5 times higher than for other brines. The core initially saturated by SSW showed the highest plastic component of the total strain inferring that the ions in SSW does play an important role in inducing permanent damage.

The main aim of **Paper VI** was to check how the mechanical strength of chalk depends on the chemistry of pore fluids. Experiments were performed at uni-axial strain conditions maintaining constant overburden stress during pore pressure depletion and subsequent compaction phase. Significant differences were observed during the depletion and time-dependent compaction phase. The oil-saturated core was stronger than core saturated by brine-oil mixture, while the brine-saturated core accumulated most strain. During compaction, seawater was injected that led to additional strain; most so in the oil-saturated core, intermediate additional strain in the brine-oil mixed core, and least additional strain was observed in the brine-saturated core. This is in line with earlier results on how the ion composition of seawater significantly impacted chalk mechanics. It was also observed that the seawater induced weakening is abrupt, and it is more prominent when there is less water in the core originally.

Abbreviations and Symbols

W_i	Wettability index
A_1	Area under the secondary drainage capillary pressure curve
A_2	Area under the primary imbibition capillary pressure curve
S_w	Water saturation
A_{mw}	Area between thiocyanate and sulfate concentration curves for wettability-altered sample
A_{ww}	Area between thiocyanate and sulfate concentration curves for water-wet sample
σ	Stress / Stress tensor
σ_{ij}	Normal components of stress
τ_{ij}	Shear components of stress
r	Radial direction
θ	Tangential direction
z	Axial direction
ε	Strain / Strain tensor
t	Time
L_o	Original length of sample
$L(t)$	Length of sample at time t

ΔL	Change in length of sample
ε_{ij}	Normal components of strain
Γ_{ij}	Shear components of strain
σ'	Effective stress
α	Biot coefficient
P_f	Pore pressure
E	Young's / Elastic modulus
ν	Poisson's ratio
ε_{vol}	Volumetric strain
V_o	Original volume of sample
ΔV	Change in volume of sample
ε_r	Radial strain
ε_θ	Tangential strain
ε_z	Axial strain
r_o	Original radius of sample
Δr	Change in radius of sample
X	Conversion factor to convert axial strain to volumetric strain
σ'_{hyd}	Effective hydrostatic stress
K	Bulk modulus of material

P_{conf} / σ_{rad}	Confining pressure
f_{area}	Area factor that relates the area of the core plug to the area of the chamber in the triaxial cell
P_{pist}	Hydraulic pressure in the piston chamber of the triaxial cell
P_{fric}	Friction of the piston / friction pressure in the triaxial cell
$\sigma_{elastic}$	Linear elastic stress
V_b	Bulk volume of sample
ε_p	Strain component due to change in pore volume of sample
ε_s	Strain component due to change in solid volume of sample
ΔV_s	Change in the solid volume of sample
$M_{s,o}$	Original solid mass of core plug
$M_s(t)$	Mass evolution of core plug with time
$\rho_{s,o}$	Original solid density of core plug
$\rho_s(t)$	Density evolution of core plug with time
$m_{Ca}(t)$	Amount of calcium produced from the core plug at time t
$m_{Ca,total}$	Total amount of calcium produced from the core plug
$\rho_{s,f}$	Final solid density of core plug
η	Fitting parameter that makes the observed replacement of calcium by magnesium from ion chromatography data match the observed loss in dry mass before and after test

q_{in} / Q	Injection flow rate
n_{Mg}	Molar weight of magnesium = 24 g/mol
n_{Ca}	Molar weight of calcium = 40 g/mol
$c_{in,Mg}$	Inlet molar concentration of magnesium
$c_{out,Mg}$	Outlet molar concentration of magnesium
$c_{in,Ca}$	Inlet molar concentration of calcium
$c_{out,Ca}$	Outlet molar concentration of calcium
V_s	Solid volume of sample
V_p	Pore volume of sample
ΔV_p	Change in the pore volume of sample
ΔV_b	Change in the bulk volume of sample
$V_{b,o}$	Original bulk volume of sample
$V_{p,o}$	Original pore volume of sample
φ	Porosity of the core plug
S_{wi}	Irreducible / Initial water saturation
P_c	Capillary pressure
ω	Angular rotation speed of centrifuge
$\widehat{C_k}$	Reduced concentrations of sulfate and thiocyanate ions
Mg^{2+}	Magnesium ion
Ca^{2+}	Calcium ion

SO_4^{2-}	Sulfate ion
Na^+	Sodium ion
Cl^-	Chloride ion
SCN^-	Thiocyanate ion
BET	Brunauer–Emmett–Teller
BSE	BackScattered Electron
$CaCO_3$	Calcium Carbonate / Calcite
DW	Distilled Water
EDX	Energy Dispersive X-ray
EOR	Enhanced Oil Recovery
FEG	Field Emission Gun
FEG-SEM	Field Emission Gun Scanning Electron Microscopy
HFW	High Full Well
IC	Ion Chromatography
IOR	Improved Oil Recovery
LVDT	Linear Voltage Differential Transducer
$MgCO_3$	Magnesium Carbonate / Magnesite
$MgCl_2$	Magnesium Chloride
NaCl	Sodium Chloride
PV	Pore Volume

PV_i	Initial Pore Volume
SCAL	Special Core Analysis
SEM-MLA	Scanning Electron Microscope - Mineral Liberation Analysis
SSA	Specific Surface Area
SSW	Synthetic Seawater
USBM	United States Bureau of Mines

List of publications

Paper I:

Sachdeva, J.S., Nermoen, A., Korsnes, R.I., and Madland, M.V. (2019). Impact of Initial Wettability and Injection Brine Chemistry on Mechanical Behaviour of Kansas Chalk. *Transport in Porous Media*, **128**(2), 755-795. https://doi.org/10.1007/s11242-019-01269-z.

Paper II:

Sachdeva, J.S., Muriel, H., Nermoen, A., Korsnes, R.I., and Madland, M.V. (2019). Chalk Surface Area Evolution during Flow of Reactive Brines: Does Oil Play a Role? *Energy & Fuels*, **33**(6), 4890-4908. https://doi.org/10.1021/acs.energyfuels.9b00515.

Paper III:

Sachdeva, J.S., Nermoen, A., Korsnes, R.I., and Madland, M.V. (2019). Effect of Initial Wettability on Rock Mechanics and Oil Recovery: Comparative Study on Outcrop Chalks. Submitted to *Transport in Porous Media*, publication under review.

Paper IV:

Sachdeva, J.S., Sripal, E.A., Nermoen, A., Korsnes, R.I., Madland, M.V., and James, L.A. (2018). A Laboratory Scale Approach to Wettability Restoration in Chalk Core Samples. Paper SCA2018-117 presented at the International Symposium of the Society of Core Analysts, Trondheim, Norway, 27-30 August.

Paper V:

Sachdeva, J.S., Nermoen, A., Korsnes, R.I., and Madland, M.V. (2017). Elastic and Plastic Behavior of Chalks at Deviatoric Stress Condition: Experiments Performed with Four Different Brines. Paper Tu P030 presented at the IOR Norway 2017 – 19th European Symposium on Improved Oil Recovery, Stavanger, Norway, 24-27 April.

Paper VI:

Sachdeva, J.S., Nermoen, A., Madland, M.V., and Korsnes, R.I. (2016). How Wetting Conditions Dictate Chalk Mechanics at Uni-axial Strain Conditions – Insights from Experiments Performed at In-situ Stress, Temperature and Pore Pressure. Paper SCA2016-068. *International Symposium of the Society of Core Analysts 2016*, Snowmass, Colorado, USA.

Additional contributions

Sachdeva, J.S., Nermoen, A., Korsnes, R.I., and Madland, M.V. (2019). Impact of Initial Wettability and Injection Brine Chemistry on Chalk Mechanics of Kansas and Mons Outcrops. *IOR Norway 2019,* Stavanger, Norway.

Sachdeva, J.S., Nermoen, A., Korsnes, R.I., and Madland, M.V. (2019). Impact of Wettability on Geomechanics and Oil Recovery / Observations on Outcrop Chalk. *Workshop on Wettability Characterization and Alteration of Heterogeneous Carbonate Reservoir Rocks*, NORCE, Stavanger, Norway, March 18.

Sachdeva, J.S., Nermoen, A., Korsnes, R.I., and Madland, M.V. (2018). How the Presence of Oil and Water Affects Chalk Mechanics at Isotropic Stresses. Extended Abstract. *80th EAGE Conference and Exhibition 2018*, Copenhagen, Denmark.

Sachdeva, J.S., Nermoen, A., Korsnes, R.I., and Madland, M.V. (2018). Effect of presence of oil and water on chalk mechanics. *IOR Norway 2018*, Stavanger, Norway.

Minde, M.W., Sachdeva, J.S., Zimmermann, U., Madland, M.V., Korsnes, R.I., and Nermoen, A. (2018). Mineral alterations in water wet and mixed wet chalk due to flooding of seawater-like brines. *IOR Norway 2018*, Stavanger, Norway.

Sachdeva, J.S., Nermoen, A., Madland, M.V., and Korsnes, R.I. (2016). How Wetting Conditions Dictate Chalk Mechanics at Uni-axial Strain Conditions – Insights from Experiments Performed at In-situ Stress, Temperature and Pore Pressure. Lunch and Learn. *University of Stavanger 2016*.

Sachdeva, J.S., Nermoen, A., Madland, M.V., Korsnes, R.I., and Siqveland, O.K. (2016). Which processes are at play during wettability alteration and water induced compaction of chalks? *IOR Norway 2016*, Stavanger, Norway.

Table of Contents

List of Figures

List of Tables

1 Introduction

Approximately 50-60% of the known oil and gas reserves worldwide are found in rocks made up of calcium carbonate ($CaCO_3$) originating from the deposition of the shells or skeletal material in shallow, warm ocean waters (Roehl and Choquette 1985; Lucia 1992; Flügel 2004; Burchette 2012). Due to a decrease in the amount of recoverable reserves using current technologies / strategies, it is of paramount importance to develop and implement measures that could increase the recovery of oil from such reservoirs. This, in turn, would also guide the ways to effectively produce from the reservoirs which are still undiscovered or undeveloped. This will help to increase the recovery rates and reduce the environmental footprint.

Several major oil and gas fields on the Norwegian Continental Shelf (NCS) are producing from chalk reservoirs. Chalks are often found in deep basins as well as on drowned shelves developed from lithification of fine-grained skeletons of planktonic microorganisms, that contain the calcite, during diagenetic processes (Lucia 1992). Chalk rocks of today can be characterised as soft, white, porous sedimentary carbonate rocks formed in marine environments by the sedimentation of calcite shells. They are very fascinating granular materials because their mechanical properties depend on the physico-chemical interplay with the pore fluids. In addition to being a rock-type that contain great hydrocarbon potential, chalks can also be used to study the organisms living in the ocean and the paleoclimate at which the sediments were deposited. They are often highly porous and low permeable because of the sub-micrometer sizes of the pores and skeletal remains.

Seawater is often injected into chalk reservoirs as means of pressure support and secondary means of improved oil recovery. However, seawater injection into chalk leads to enhanced compaction of the reservoir rock. This compaction is a result of both pore pressure depletion early in the field life, and water weakening induced by seawater injection at later stages (Gauer et al. 2002). The compaction by pore volume reduction has been suggested to be an important driving mechanism for mobilizing resident fluids towards production facilities and, hence compaction is of great potential for improving oil recovery, especially if oils are mobile (Sulak and Danielsen 1989; Sulak 1991; Hermansen et al. 2000). Now the mobility of the different fluids is a function of the surface affinity of oil and water, so it is not self-evident that pore volume reduction leads to improved oil recovery rates. This is one of the hypotheses that is put to test in this study.

Reservoir compaction, however, has also shown to induce seafloor subsidence affecting the equipment resting on the sea floor (Sulak and Danielsen 1989; Maury et al. 1996; Nagel 1998; Sylte et al. 1999; Gauer et al. 2002). Seafloor subsidence was detected at the Ekofisk field in the Norwegian North Sea in 1984 (Wiborg and Jewhurst 1986; Sulak and Danielsen 1989). Serious concerns were raised relating to buckling and loss of well pipes, arching of overburden rocks leading to stress redistributions, and the porosity/permeability decline of the producible formation, all physical effects that alter the ultimate recovery and recovery rates of oil bearing chalk reservoirs (Thomas et al. 1987; Teufel et al. 1991; Maury et al. 1996; Hermansen et al. 1997; Nagel 1998; Kristiansen et al. 2005; Doornhof et al. 2006). This subsidence had a consequence on the safety of the equipment, as well as safety of the personnel on the platforms. The height of the platform deck above sea was not enough to avoid the highest waves, hence the platforms were jacked-up by six meters (Overview Greater Ekofisk Area 2019). Since then, considerable research has been carried out concerning chalk behavior in general, and mechanical properties in particular. Johnson and Rhett (1986) and Schroeder and Shao (1996) concluded that the pore collapse deformation of high porosity chalk accounted for most of the reservoir compaction and subsidence. Piau and Maury (1994) mentioned the action of local shear forces exerted by oil/water menisci on grains

(Andersen et al. 1992) and suggested the existence of very localized and quasi-instantaneous chemical actions of brines on grain-to-grain contacts as possible weakening mechanisms. Lord et al. (1998), Heugas and Charlez (1990), and Piau and Maury (1994) pointed out that mineral dissolution at grain-to-grain contacts was needed to be considered in order to explain the water weakening effect.

Later, research focused on understanding how the mechanical behavior of chalk is dictated by the pore fluid chemistry (Risnes 2001; Hellmann et al. 2002a, 2002b; Risnes et al. 2003; Madland et al. 2008; Korsnes et al. 2008; Neveux et al. 2014a, 2014b). These studies dealt with how aqueous chemistry affected mechanical stiffness and plastic failure strength during hydrostatic stress build-up, and the time-dependent deformation during creep. The analysis of the effluent brines and the chemical and micro-structural changes to the minerals in the rock have shown that the injected brines are not in equilibrium with the rock surface. As such, over time changes of the load bearing framework affect the creep deformation rates at constant stress condition during continuous brine flow (Korsnes et al. 2006a, 2006b, 2008; Madland et al. 2008, 2011; Megawati et al. 2011, 2013).

The chemical composition and microscopic structure of the mineral phases that constitutes the chalk, i.e. the load bearing structure, are subject to change when being exposed to continuous flooding of reactive brines over significant times. A reactive brine is composed of surface-active divalent ions, such as magnesium (Mg^{2+}), calcium (Ca^{2+}) and sulfate (SO_4^{2-}), that interacts with the calcite surface and changes its microscopic structural framework, whereas a weakly reactive brine consists of monovalent ions such as sodium (Na^{+}) and chloride (Cl^{-}) that show a lower affinity for calcite surface compared to the divalent ions.

Heggheim et al. (2005) observed that sulfate ions in the injected synthetic seawater (SSW) brine led to a reduced yield and caused weakening of chalk. The point to be noted here is that these tests were run at ambient conditions and there was no flooding during loading phase. The cores were aged for four weeks at 130°C. Korsnes et al. (2008) also observed the same effect by demonstrating that flooding SSW containing sulfate ions through chalk yielded at a significantly lower stress compared to the samples flooded by SSW without sulfate ions. This reduction in yield, at that time, was concluded to have been caused due to the precipitation of anhydrite. Megawati et al. (2013) further showed using sodium sulfate as the injection brine that if the brine contains only sulfate as the surface-active ion, the reduction in yield is due to its adsorption on the charged calcite surface. The interaction between neighbouring charged surfaces (electrical double layer) gives rise to repulsive electrostatic forces. This leads to a disjoining pressure between grains that eases grain re-organization and allows for pore collapse at lower stresses because the normal load between grain-grain reduces the frictional forces. This process has been employed to explain (a) yielding at lower effective stresses than when saturated by brines without surface-active ions (Korsnes et al. 2008; Liteanu et al. 2013) and (b) additional rates of compaction (Nermoen et al. 2014) when seawater was injected.

When magnesium chloride ($MgCl_2$) brine is injected through chalk, dissolution of calcite $CaCO_3$ and precipitation of magnesite $MgCO_3$ occur (Madland et al. 2011; Nermoen et al. 2015; Zimmermann et al. 2015; Minde et al. 2017, 2018a, 2018b; Andersen et al. 2018). These dissolution/precipitation processes lead to enhanced bulk volume creep rates in chalk compared to when flooded with weakly reactive sodium chloride (NaCl) brine (Madland et al. 2009, 2011). Megawati et al. (2011) also showed similar results while flooding chalk with $MgCl_2$ brine. Further, Nermoen et al. (2015) showed that the compaction rate was sensitive to the injection rate. At higher flooding rates, the rate of dissolution of calcite and precipitation of Mg-bearing minerals increased. The solid volume changed because the sample lost mass and the mineral density increased (density of magnesite is 3.0 g/cm^3 and calcite is 2.7 g/cm^3). Further, the solid volume changes led to a reduction in bulk volume, and the grains unlocked and reorganized to reduce pore volume. Long-term $MgCl_2$ flooding tests (516 days and 1072 days) on Liège water-wet chalk (Belgium) altered the mineralogy from calcite to Mg-bearing minerals dominated by magnesite (Nermoen et al. 2015; Zimmermann et al. 2015; Minde et al. 2017; Borromeo et al. 2018). These observations are in line with modeling results reported in Hiorth et al. (2013).

In addition, the divalent magnesium ions have also shown to adsorb on available surface sites leading to desorption of calcium ions from the internal calcite surface (Ahsan and Fabricius 2010; Alam et al. 2010; Nermoen et al. 2018a), resulting in stiffening and strengthening of chalk due to a lower internal repulsive electrostatic force.

It has also been suggested that chemical reactions between the injected non-equilibrium brines and chalk surface lead to additional oil recovery (Hiorth et al. 2010) either due to rock dissolution or change in the surface charge during brine injection that affects rock wettability. For chemical reactions to be non-negligible, tens (or hundreds) of pore volumes are required. So, for chemical reactions to play a role in enhancing the oil recovery, it must be to mobilize oil after the initial displacement.

Megawati et al. (2015) and Andersen et al. (2018) studied five different chalk types and found a dependence of the non-carbonate content on how the mechanical creep behavior was affected by $MgCl_2$ brine injection. Injecting this brine into impure chalks (Liège, Aalborg and Kansas) led to an immediate increased creep rate. However, in pure chalks (Mons and Stevns Klint) the creep response was delayed by a time lag of several weeks before a tertiary-like creep developed. These rock samples were never exposed to oil, which enabled the aqueous solution to contact the minerals directly.

Both ongoing adsorption/desorption and dissolution/precipitation processes, that describe the interactions between the pore fluid and the mineralogical surfaces, have shown to change several of the parameters that describe chalk mechanical behavior, such as elastic stiffness, plastic strength and time-dependent deformation rates.

Further on, wettability of chalk has been studied to understand how wettability affects multiphase fluid flow, and how alterating the wetting state impacts oil production (Standnes and Austad 2000a, 2000b; Zhang and Austad 2005; Zhang et al. 2006; Strand et al., 2007; Fathi et al. 2010). Prior to flooding and imbibition experiments, reservoir chalk or outcrop chalk is cleaned with solvents and distilled water rendering it water wet. The water-wet chalk surface prefers water coating the grains, and will spontaneously imbibe water, which on pore level controls the flow of oil. Hence, to obtain realistic oil production curves, the wettability of these chalk samples must be changed to a neutral-wet / oil-wet state. This is a standard routine in these experiments and is done by flooding crude oil and water, and then aging over time at high temperature before the wettability can be determined and any additional experiments can be performed. The aged core samples are, then, imbibed and/or flooded and the oil production is quantified as a function of the injected brine composition.

1.1 Objectives

Most of the geomechanical experiments performed so far have exclusively been performed on samples that have never been exposed to oil such that the mineral phases were considered water wet. This has enabled the aqueous solution to contact the minerals directly, and as such, the applicability of the water weakening mechanism to oil reservoir samples has been debated. The question has been to what degree the load bearing structure, especially the grain contacts, are prone to the documented water weakening because the minerals within an oil reservoir chalk sample can sometimes be partially or completely covered with organic oil components that inhibit the adsorption and dissolution/precipitation processes.

Therefore, this study deals with the combined effect of initial wettability and injection brine chemistry on the mechanical response in chalk. Figure 1 shows how wettability, rock mechanics, multiphase flow in porous media and chemical reactions by rock-fluid interactions define the chalk core dynamics.

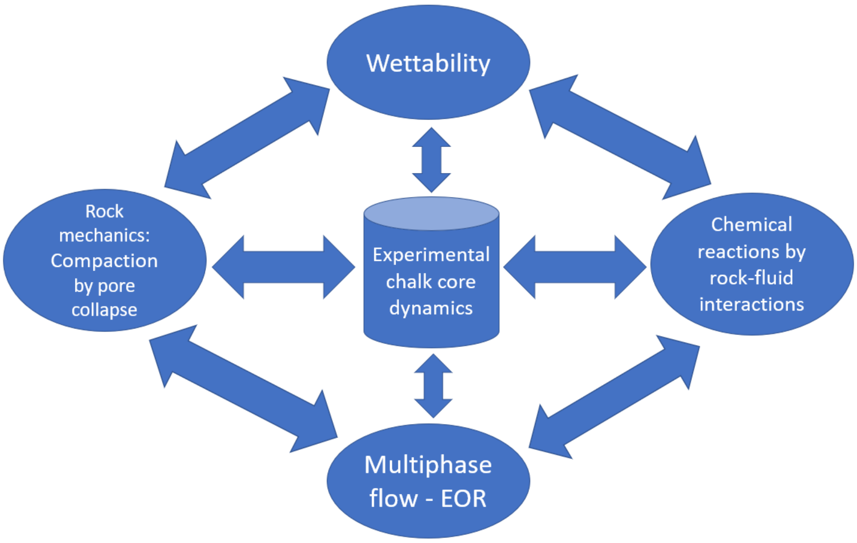

Figure 1. Relationship of chalk core dynamics to various experimentally derived parameters.

Hence, the main research goals of this study are defined in the following points:

1. Defining and evaluating the impact of initial wettability on chalk mechanics.
2. Defining and evaluating the effect of injection brine chemistry on the mechanical response in wettability-altered chalk.
3. Quantifying and understanding the effect of compaction on enhanced oil recovery.
4. Understanding the effect of non-equilibrium rock-fluid interactions on enhanced oil recovery.

1.2 Thesis Outline

This thesis is divided into five main sections. They are:

Section 2 covers the theory related to rock mechanics that has been applied in this work. It includes the basics of stress and strain, their relationship using Hooke's law and the definition of the elastic moduli. It also includes the explanation of drained conditions used in this study. Section 3 covers the materials and methods used in this work, while section 4 presents the main results from the work performed and the discussion of these results. The last section, section 5, provides the concluding remarks and the scope of future work.

Three journal papers (**Paper I**, **Paper II** and **Paper III**) and one conference proceeding (**Paper IV**), that document the main body of this PhD thesis, are attached in the end. Two more conference proceedings (**Paper V** and **Paper VI**) are also attached, however they are not discussed in the main body of this thesis as they do not directly complement the main objective of this work but are performed as extra work during the tenure of the PhD.

2 Theory

In this chapter, the key underlying processes of rock mechanics, used in this study of how chalk mechanics, multiphase flow and mineral wettability are related, are presented.

Rock Mechanics is an applied science of the mechanical behavior of rock masses. It is the study of deformation resulting from the strain of rocks in response to applied stresses. Most materials have an ability to resist and recover from deformations produced by forces. This ability is called elasticity. It is the foundation for all aspects of rock mechanics.

2.1 Stress and strain

Stress is defined as force per unit area. A stress tensor is used to describe the stresses in a porous body. For a cylindrical core plug, a stress tensor σ is defined by,

$$\sigma_{ij} = \begin{bmatrix} \sigma_{rr} & \tau_{r\theta} & \tau_{rz} \\ \tau_{\theta r} & \sigma_{\theta\theta} & \tau_{\theta z} \\ \tau_{zr} & \tau_{z\theta} & \sigma_{zz} \end{bmatrix} \tag{1}$$

where τ_{ij} defines the shear components and σ_{ij} defines the normal components of stress, with $ij = \{r, \theta, z\}$ denoting the radial (r), tangential (θ) and axial (z) directions. When there is no net translational or rotational force acting in the solid body (i.e., $\tau_{r\theta} = \tau_{\theta r}$, $\tau_{rz} = \tau_{zr}$ and $\tau_{\theta z} = \tau_{z\theta}$), a stress tensor can be defined by six independent components only. The off-diagonal elements vanish (τ_{ij}) when the stress tensor is rotated to find the principal directions. For every point inside a body under static equilibrium there are three directions, called the principal directions, where the stress vector is normal to the plane and there is no shear component. These normal stress vectors are called principal stresses. In cylindrical geometries, the principal directions align with the r, θ and z directions.

Now, when a force is applied on a body, there is some change in the dimensions. The most commonly accepted definition of strain defines it as the ratio of elongation in the length of the body ΔL to its original length L_o. Hence, the strain ε at any given time t is given by,

$$\varepsilon(t) = -\frac{L(t) - L_o}{L_o} = -\frac{\Delta L}{L_o} \tag{2}$$

where $L(t)$ is the length of the body at time t. This sign convention is consistent with that of positive compressive stresses, i.e. a positive strain is associated with contraction. This definition of strain is applicable to small finite deformations. In cylindrical coordinates, a strain tensor ε is defined by,

$$\varepsilon_{ij} = \begin{bmatrix} \varepsilon_{rr} & \mathit{\Gamma}_{r\theta} & \mathit{\Gamma}_{rz} \\ \mathit{\Gamma}_{\theta r} & \varepsilon_{\theta\theta} & \mathit{\Gamma}_{\theta z} \\ \mathit{\Gamma}_{zr} & \mathit{\Gamma}_{z\theta} & \varepsilon_{zz} \end{bmatrix} \tag{3}$$

where $\mathit{\Gamma}_{ij}$ defines the shear components and ε_{ij} defines the normal components of strain. As is the case with the stress tensor, the shear strains also balance each other (i.e., $\mathit{\Gamma}_{r\theta} = \mathit{\Gamma}_{\theta r}$, $\mathit{\Gamma}_{rz} = \mathit{\Gamma}_{zr}$ and $\mathit{\Gamma}_{\theta z} = \mathit{\Gamma}_{z\theta}$), thereby reducing the number of parameters required to describe the deformation of a volume to six. The off-diagonal elements vanish ($\mathit{\Gamma}_{ij}$) when the strain tensor is rotated to find the principal directions.

2.2 Effective stresses - Biot coefficient

In porous rocks, the external load is transmitted through the solids at inter-granular contacts. At the same time, some of the externally applied load is carried by the fluid pressure within the pores, thereby reducing the influence of the applied stress. The observed deformation is therefore subjected to the interaction between the fluid pressure and the solid stresses into the effective stress relation. The magnitude of the fluid-to-solid force exchange is given by the fluid-solid contact area. This area is related to the degree of cementation and the spacing between grain contacts. Hence, an equivalent effective stress variable σ' is calculated from the applied stress σ minus a fraction of the pore pressure P_f. This fraction α is given by the cemented cross-area and is termed the Biot coefficient, which always lies between 0 and 1. Hence, the effective stress is defined by,

$$\sigma' = \sigma - \alpha P_f \tag{4}$$

In tensor form, the effective stress is given by,

$$\sigma' = \begin{bmatrix} \sigma_{rr} - \sigma P_f & \tau_{r\theta} & \tau_{rz} \\ \tau_{\theta r} & \sigma_{\theta\theta} - \sigma P_f & \tau_{\theta z} \\ \tau_{zr} & \tau_{z\theta} & \sigma_{zz} - \sigma P_f \end{bmatrix} \tag{5}$$

2.3 Elastic moduli

For small stresses and/or strains (i.e. in the limit of linear elasticity) and assuming homogeneous and isotropic materials, Hooke's law can be used to relate stresses and strains. It assumes that the deformation is immediate, linear and reversible. The elastic parameters that describe the stress-strain relation of a volume element along the principal directions are given via the matrix equation,

$$\begin{bmatrix} \varepsilon_r \\ \varepsilon_\theta \\ \varepsilon_z \end{bmatrix} = \frac{1}{E} \begin{bmatrix} 1 & -\nu & -\nu \\ -\nu & 1 & -\nu \\ -\nu & -\nu & 1 \end{bmatrix} \begin{bmatrix} \sigma'_r \\ \sigma'_\theta \\ \sigma'_z \end{bmatrix} \tag{6}$$

where E defines the Young's/Elastic modulus and ν defines the Poisson's ratio. In cylindrical coordinates, the volumetric strain can be expressed by the radial ε_r, axial ε_z and tangential ε_θ strains.

Young's modulus E is a measure of the stiffness of the sample, i.e. the sample resistance against being compressed by a uniaxial stress. For a spatial direction r, Young's modulus is defined by,

$$\varepsilon_r = \frac{1}{E}\sigma_r \tag{7}$$

This is applicable only when a sample behaves linearly to the applied stress, which is sometimes the case for small stress and strain increments.

Poisson's ratio ν is a measure of lateral expansion in the perpendicular directions relative to longitudinal contraction due to the applied stress in the r direction,

$$\nu = -\frac{\varepsilon_\theta}{\varepsilon_r} = -\frac{\varepsilon_z}{\varepsilon_r} \tag{8}$$

For hydrostatic tests, the stresses in all spatial directions are equal, hence $\sigma_r' = \sigma_\theta' = \sigma_z' = \sigma_{hyd}'$ where σ_{hyd}' is used to define the effective hydrostatic stress. Hence equation (6) becomes,

$$\varepsilon_{vol}E = 3(1-2\nu)\sigma_{hyd}' \tag{9}$$

where ε_{vol} defines the volumetric strain. Equation (9) can be written as,

$$K\varepsilon_{vol} = \sigma_{hyd}' \tag{10}$$

where K defines the bulk modulus of a material in the elastic region in hydrostatic tests. Thus, $E = 3(1-2\nu)K$.

2.4 Time-dependent deformation (creep)

Creep is defined as the time-dependent deformation at constant stress condition. In the plastic phase during pore collapse, the material strength is associated with the rate of creep. The creep rate is simply given by the partial derivative with respect to time of the observed volumetric creep,

$$\dot{\varepsilon}_{vol} = \frac{\partial \varepsilon_{vol}}{\partial t} \tag{11}$$

There are three stages of creep following a change in the stress state (Figure 2). These are:

- Primary creep (steadily declining creep rate),
- Secondary creep (constant creep rate), and
- Tertiary creep (accelerated creep rate).

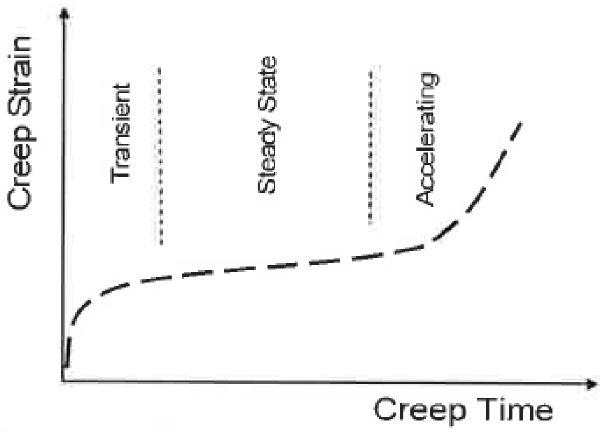

Figure 2. Strain versus time for a creeping material (Fjær et al., 2008).

2.5 Drained test conditions

In testing of low permeability materials, e.g. chalk, drained condition means that the flooding rate of injection fluids must be kept sufficiently low in order to avoid unacceptable pressure build-up when the sample deforms.

In drained tests (Fjær et al. 2008) the pore pressure inside the sample is maintained at a prescribed value by keeping the outlet through the pistons and the cells open, and the fluids can escape (hence constant effective stress). There are two types of tests usually performed:

a) when the outlets are kept open to the atmosphere so that the pore pressure will be zero ($P_f = 0$). In that case from equation (4),

$$\sigma' = \sigma \tag{12}$$

b) when the tests are run at prescribed and constant pore pressure conditions or at actual reservoir conditions. Then the pore pressure must be kept at that prescribed value or at the reservoir pressure level.

The drained tests performed in this study on chalk were run at a prescribed pore pressure value of 0.7 MPa.

2.6 Yield analysis

During stress build-up, the axial and radial strains in the sample are measured. The onset of plastic behavior is identified as the departure from linearity in a plot of effective stress as function of observed strain. For low stress changes, the stress-strain relation is more-or-less linear in accordance with Hooke's law. A linear curve can be fitted to the measurements made in the linear elastic regime, which is then extended into the plastic regime. The onset of yield (i.e. when non-linearity is observed in the stress-strain relation) has been defined to occur when the residual stress R, defined as the difference between the extrapolated linear elastic stress ($\sigma_{elastic} = c_e \varepsilon_z + b_e$) and the imposed effective stress, *i.e.* $R = |\sigma_{elastic} - \sigma_z'|$, exceeds a certain threshold.

2.7 Bulk volume estimates for hydrostatic tests due to non-uniform deformation

After hydrostatic testing, the plug is non-homogenously deformed such that the bulk volume is given by the sum of truncated wedges. The diameter D_i is measured at intervals h_i along the plug and any variations in the diameter is incorporated in the total bulk volume V_b estimated by,

$$V_b = \sum_i \frac{\pi h_i}{12} \left(D_i^2 + D_{i+1}^2 + D_i D_{i+1}\right) \tag{13}$$

2.8 Time-dependent evolution of volumetric strain

The volumetric strain ε_{vol} is defined as the ratio of the volumetric change ΔV divided by the original volume V_o,

$$\varepsilon_{vol} = -\frac{\Delta V}{V_o} \tag{14}$$

In some of the experiments in this study, only the axial strain development was measured. Hence, an assumption was introduced in order to convert the axial strain measurements to estimate the volumetric strain. A conversion factor X was introduced such that,

$$\varepsilon_{vol} = X\varepsilon_{ax} \tag{15}$$

which was assumed to be constant throughout the test. The conversion factor was determined by matching the volumetric strain to the volume of the core after the experiment.

In compressive hydrostatic systems, the porous rocks deform by reducing its bulk volume. The total bulk volume change is caused by changes in both pore and solid volumes. Hence, the volumetric strain can be additively partitioned into a mechanical component and a chemical component given by (Nermoen et al. 2016),

$$\varepsilon_{vol} = \varepsilon_p + \varepsilon_s \tag{16}$$

where ε_p is the strain component due to change in the pore volume and ε_s is the strain component due to change in the solid volume. This is valid in a porous material of solids and voids where the pore volume reduction is associated with re-organization of grains during compaction, and the solid volume reduction is associated with rock-fluid interactions during reactive flow.

2.9 Evolution in solid volume with time

The evolution of the solid mass over time is calculated from the difference in the concentrations of the injected fluid and the produced effluent fluids. Now if the density evolution of the solid mass is known, the change in solid volume ΔV_s can be calculated by,

$$\Delta V_s(t) = \frac{M_s(t)}{\rho_s(t)} - \frac{M_{s,o}}{\rho_{s,o}} \tag{17}$$

In this equation, the mass (M_s) and the density (ρ_s) before ($M_{s,o}$ and $\rho_{s,o}$, respectively) and after the triaxial test are measured quantities. As function of time, however, the values of mass $(M_s(t))$ and density $(\rho_s(t))$ must be calculated.

- To calculate the density at a given time during the experiment $\rho_s(t)$, a function is used that depends on the amount of calcium produced from the plug at that time $m_{Ca}(t)$, and the initial ($\rho_{s,o}$) and final ($\rho_{s,f}$) densities such that,

$$\rho_s(t) = \rho_{s,o} + ((\rho_{s,f} - \rho_{s,o})(m_{Ca}(t)/m_{Ca,total})) \tag{18}$$

- The solid volume evolution with time was estimated from the ion chromatography (IC) using equation (17) in which the solid rock mass and the average density is varied with time. The IC data for magnesium (Mg) and calcium (Ca) is used to interpolate the mass of the core at a given time t according to,

$$\begin{aligned} M_s(t) = M_{s,0} + \eta \int_0^t q_{in}(n_{Mg}(c_{in,Mg} - c_{out,Mg}) \\ - n_{Ca}(c_{in,Ca} - c_{out,Ca})).\, dt \end{aligned} \tag{19}$$

where η is a fitting parameter that makes the observed replacement of Ca by Mg from IC-data match the observed loss in dry mass before and after test, q_{in} is the injected flow rate (liter/day), molar weights $n_{Mg} = 24$ g/mol and $n_{Ca} = 40$ g/mol, and c_{in} and c_{out} are the inlet and outlet molar concentrations in (mol/liter) of Mg and Ca, and t is measured in days.

2.10 Porosity evolution during compaction and flow of non-equilibrium brines

The basic equations used to quantify the porosity evolution through time are given based on the work presented by Nermoen et al. (2015, 2018b). The bulk volume of a porous material V_b is given by,

$$V_b = V_s + V_p \tag{20}$$

where V_s is the solid volume and V_p is the pore volume of the material. Any changes in the solid and pore volumes lead to changes in the bulk volume, hence,

$$\Delta V_b = \Delta V_s + \Delta V_p \tag{21}$$

Porosity (φ) is the percentage of pore space in a rock. It is defined as the ratio of the pore volume to the bulk volume and is given by,

$$\varphi = \frac{V_p}{V_b} = 1 - \frac{V_s}{V_b} \tag{22}$$

Hence, if during an experiment both pore and bulk volumes are changing dynamically, the time evolution of porosity is given by,

$$\varphi(t) = \frac{V_{p,o} + \Delta V_p(t)}{V_{b,o} + \Delta V_b(t)} \tag{23}$$

where the original pore volume $V_{p,o}$ and bulk volume $V_{b,o}$ of the rock/material are known quantities.

Replacing equation (21) in equation (23),

$$\varphi(t) = \frac{V_{p,o} + \Delta V_b(t) - \Delta V_s(t)}{V_{b,o} + \Delta V_b(t)} \tag{24}$$

Now volumetric strain ε_{vol} at any given time t is given by,

$$\varepsilon_{vol}(t) = -\frac{\Delta V_b(t)}{V_{b,o}} \tag{25}$$

The negative sign in the volumetric strain is in line with the geotechnical engineering that inward deformation is positive. The original porosity is given by equation (22),

$$\varphi_o = \frac{V_{p,o}}{V_{b,o}} \tag{26}$$

Hence, equation (24) becomes,

$$\varphi(t) = \frac{\varphi_o - \varepsilon_{vol}(t) - \Delta V_s(t)/V_{b,o}}{1 - \varepsilon_{vol}(t)} \tag{27}$$

This equation is used to analyze how the porosity evolves with time when the overall bulk and solid volumes change through time.

3 Materials and Methods

3.1 Model rock material

In the presented study, chalk is used as a model rock material. This model material is selected because of its economic and technological relevancy as host rock for hydrocarbon resources. The phenomenon that its geomechanical property is affected by the injection of brines is not unique to chalk, this has also been observed for other rocks. However, since the specific surface area of chalk material is high, the surface-processes also affect the bulk behavior.

Other examples that also possess a huge surface area include clays (that have even a higher surface area than chalk material), while other siliciclastic rocks (beach deposits, riverbeds etc.) have larger rounded grains with lower surface area making the rock-fluid interactions less dominating for the overall observed behavior.

A typical picture of the structure of chalk material from Kansas outcrop is presented in Figure 3.

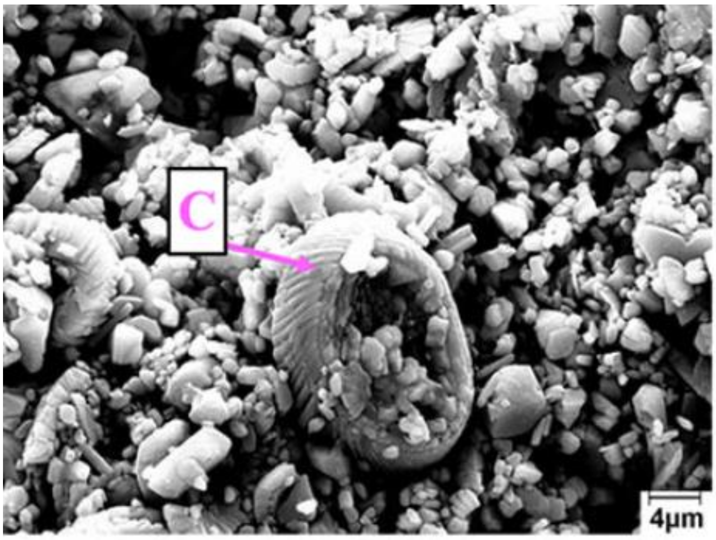

Figure 3. Scanning Electron Microscope (SEM) image of unflooded Kansas outcrop chalk material. ‘C’ denotes the coccolithophore ring observed in the sample surrounded by diagenetic calcite and clay minerals (Andersen et al. 2018).

3.1.1 Outcrop chalks in this study

It is relatively easy to obtain reservoir cores using well established coring methods. However, due to the capital linked to the extraction of the cores and limited availability, experimental studies are mostly performed on outcrop materials used as analogue models for the reservoir rocks. It is believed that the observed behavior of the interplay between geomechanics, multiphase transport (oil/water and EOR), chemical interactions, and wettability changes on outcrops are also applicable to reservoir cases. There are several outcrops across the globe and their applicability to various North Sea chalk reservoirs is always up for discussion. These outcrop chalk samples differ in their chemical composition and mechanical properties (Hjuler and Fabricius 2009).

Two types of outcrop chalks have been used in this study. They are collected from quarries in Kansas, USA (Niobrara Formation) and Mons, Belgium (Trivières Formation). These two outcrop chalks are the endmember cases where the Kansas chalk is stiffer with a low porosity and has gone through more chemical reworking, while the Mons chalk is softer possessing a high porosity and has been exposed to lesser amount of diagenetic overprint.

3.1.1.1 Kansas: Niobrara Formation

Chalk samples were collected from the Fort Hays Member of the Niobrara Formation from west-central Kansas (USA). This chalk is from Late Cretaceous geological age. The Kansas chalk type is reported to have a non-carbonate content of 1-3% (Tang and Firoozabadi 2001; Megawati et al. 2013) and mainly consist of quartz, clay and pyrite (Runnels and Dubins 1949; Hattin and Cobban 1977; Longman et al. 1998). Porosity of chalk from the Niobrara Formation is in the range 35-39% (**Paper I**, **Paper II**, **Paper IV and Paper VI**) and permeability has been reported in the range 1-4 mD (**Paper IV**; Korsnes et al. 2006a; Megawati et al. 2013; Andersen et al. 2018). Tang and Firoozabadi (2001) argue that it is a good analogue to some clean North Sea reservoir chalks in regard to porosity, capillary pressure, and absolute and relative permeability.

3.1.1.2 Mons: Trivières Formation

The chalk from Mons is taken from the Trivières Formation. This chalk belongs to Late Cretaceous geological age and is very pure (> 99 weight percent (wt %) calcite). Porosity is in the range 41-44% (**Paper III** and **Paper V**). The chalk from the Trivières Formation has a high degree of intact coccoliths (Richard et al. 2005). Mons chalk is pure coccolithic mudstone. Large amounts of very small coccoliths and broken calcite crystals of organic origin form the solid framework for this type of chalk (Andersen et al. 2018).

3.2 Core preparation

Cylindrical core samples were drilled in parallel from single Kansas and Mons chalk blocks and were radially adjusted to a diameter of 38.1 mm. The samples were then cut to desired lengths and dried at 110°C overnight after which the initial dry mass was measured. The carbonate mineralogy is not affected by the drying conditions (MacDonald 1956). They were vacuumed before saturation by distilled water (DW) within the vacuum chamber, before saturated mass measurement. The mass difference between the dry and saturated sample was used to estimate the pore volume and saturation porosity.

The samples were divided into two test series:

- Samples for wettability determination by comparing chromatographic separation of reference unaged water-wet samples (Kansas Kww1 to Kww7, refer **Paper I**; Kansas KA1, refer **Paper II**; and Mons Mww1 to Mww3, refer **Paper III**) to wettability-altered samples (Kansas Kmw1 to Kmw4, refer **Paper I**; Kansas KA2 to KA4, refer **Paper II**; and Mons Mmw1 to Mmw3, refer **Paper III**).
- Samples for chemo-mechanical compaction during flow in triaxial cell. These samples were divided into two sub-series: a) 100% water saturated samples ('water-wet samples'): Kansas K1, K2, K5 and K6, refer **Paper I**, and Mons M1 and M2, refer **Paper III**; and b) wettability-altered samples containing a non-zero oil saturation ('wettability-altered samples'): Kansas K3, K4, K7 and K8, refer **Paper I**, and Mons M3 and M4, refer **Paper III**.

The detailed properties of the samples used in this work are mentioned in **Paper I**, **Paper II** and **Paper III**. The properties of the samples mentioned in **Paper IV**, **Paper V** and **Paper VI** provide additional information to supplement this work.

It is assumed that the wettability index results obtained from the wettability-altered samples through the wettability determination program apply to the wettability-altered samples used in the triaxial test program.

3.3 Description of fluids

3.3.1 Brines used

In the wettability determination program, two versions of artificial seawater were used (**Paper I**, **Paper II** and **Paper III**). The SW1T brine contained SO_4^{2-} and SCN^- tracer ions, while SW0T did not (Table 1). Total dissolved solids of SW1T and SW0T equal the SSW case. Four other brines were used during the triaxial test program (Table 1):

- 1.1 M NaCl brine for initial saturation was used to simulate initial resident formation fluids (**Paper I**, **Paper II**, **Paper III**, **Paper IV**, **Paper V** and **Paper VI**). This brine was also used as the injection brine in **Paper VI**.
- 0.657 M NaCl (**Paper II** and **Paper V**) and 0.219 M $MgCl_2$ (**Paper I**, **Paper III** and **Paper V**) brines, with equal ionic strength to seawater (0.657), were used as injection brines. These two brines were used to simulate the fluid injection at Ekofisk. $MgCl_2$ brine injection also focusses on the adsorption / desorption and dissolution / precipitation effects from the Ca-Mg exchange (Madland et al. 2009, 2011).
- SSW (**Paper I**, **Paper V** and **Paper VI**) was also used as an injection brine to model the processes occurring when seawater contacts the Ekofisk hydrocarbon reservoir. SSW interacts with the chalk by both adsorption of surface-active divalent sulfate ions and dissolution / precipitation processes due to presence of magnesium ions (Madland et al. 2011). It is also active in precipitation processes (such as anhydrite precipitation) even in the absence of magnesium ions.

Table 1. Composition of brines used in the tracer tests and during flow-through tests.

	Wettability determination program		**Triaxial test program**			
Ions	**SW0T**	**SW1T**	**1.1 M NaCl**	**0.657 M NaCl**	**0.219 M $MgCl_2$**	**SSW**
	mol/l	**mol/l**	**mol/l**	**mol/l**	**mol/l**	**mol/l**
HCO_3^-	0.002	0.002	0	0	0	0.002
Cl^-	0.583	0.492	1.100	0.657	0.438	0.525
SO_4^{2-}	0	0.024	0	0	0	0.024
SCN^-	0	0.024	0	0	0	0
Mg^{2+}	0.045	0.045	0	0	0.219	0.045
Ca^{2+}	0.013	0.013	0	0	0	0.013
Na^+	0.46	0.393	1.100	0.657	0	0.450
Li^+	0	0.024	0	0	0	0
K^+	0.010	0.034	0	0	0	0.010
Ionic Strength	0.643	0.647	1.100	0.657	0.657	0.657
TDS (g/l)	33.39	33.39	64.28	38.40	44.52	33.39

3.3.2 Oil used

A 60%-40% volume mixture of crude oil from the Heidrun field offshore Norway and heptane was used (**Paper I**, **Paper II**, **Paper III**, **Paper IV** and **Paper VI**) for two main reasons: (a) Lowering the acid number: high acid number leads to more oil-wet cores, and (b) Reducing the oil viscosity: less pressure is required to displace the oil. After the dilution, the oil was centrifuged and filtered through a 5 μm Millipore filter to remove any asphaltene precipitates.

The properties of Heidrun crude oil are reported in Table 2. The acid number of the Heidrun oil was 2.82 mg KOH/g and oil mixture was 2.12 mg KOH/g measured according to the Fan and Buckley (2007) procedure.

Table 2. Properties of Heidrun Crude oil at 25°C

Color	**Density (kg/m^3)**	**Viscosity (cP)**	**TAN (mg KOH/g)**	**Asphaltene content (%)**
Light brown	858	6	2.82	< 1

3.4 Triaxial cells

Cylindrical plugs were mounted into the triaxial cell that allowed for continuous measurements of the axial and radial strains at elevated stresses and temperature (Figure 4). The triaxial cell was equipped with a heating element and a regulating system with precise temperature control. Three pumps were connected to the triaxial cell to control the piston pressure (P_{pist}), confining pressure (P_{conf} / σ_{rad}) and flow rate (Q). The pore pressure on the downstream side (P_p) was controlled by a back-pressure regulator ensuring constant pore pressure (0.7 MPa). An external Linear Voltage Differential Transducer (LVDT) monitored the change in length of the core plug (L) and an internal extensometer monitored the change in diameter of the core plug. The way in which the experimental setup was designed, the axial stress was given by P_{conf} plus P_{pist} minus the friction of the piston (P_{fric}) times an area-factor (f_{area}) that relates the area of the plug to the area of the piston in upper chamber,

$$\sigma_z = P_{conf} + f_{area}(P_{pist} - P_{fric}) \tag{28}$$

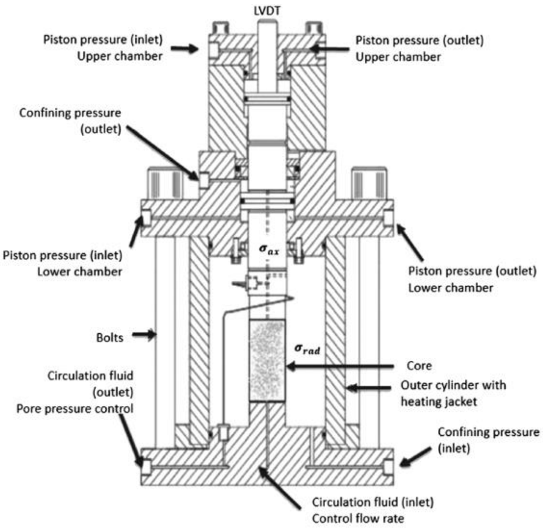

Figure 4. Sketch of the triaxial cell

3.5 Experimental procedure

This section describes the experimental procedures followed for wettability alteration, wettability determination, geomechanical tests, ion chromatography on the effluent samples, oil volume measurements, and density and specific surface area determination.

3.5.1 Initial saturation and wettability alteration procedure

3.5.1.1 Cores used in wettability determination program by chromatographic separation technique and triaxial tests

The water-wet samples were saturated by 1.1 M NaCl brine. The wettability-altered samples were prepared according to the following procedure:

i) Saturation by 1.1 M NaCl brine;
ii) Mounted in Hassler cell and heated to 50°C;
iii) Flooded two PVs of the oil mixture in each direction at 0.7 MPa back pressure and 1.6 MPa confining pressure during

which the produced brine was collected and measured to estimate the irreducible water saturation S_{wi}.

iv) Submerged the samples in the same oil mixture in aging containers and left for 21 days at 90°C.

3.5.1.2 Cores used in wettability determination program by contact angle, United States Bureau of Mines (USBM) and Scanning Electron Microscope – Mineral Liberation Analysis (SEM-MLA) methods

3.5.1.2.1 Centrifuge for Primary Drainage

Seven cylindrical core samples of 38.1 mm diameter and 50 mm length, and 5 mm length end pieces from both ends (top and bottom, 14 in total) were saturated by 1.1 M NaCl brine. The brine saturated cores, including the 14 top and bottom end pieces with filter paper in between, were mounted into the core holders of the centrifuge (*Rotosilenta 630RS* centrifuge from Vinci Technologies). An overburden of 1.38 MPa was used, and the centrifuge was operated in drainage mode to displace the brine with oil to S_{wi}. Drainage was performed in seven steps from 500 rpm to 3500 rpm in increments of 500 rpm with three hours of equilibration time for each step. The capillary pressure was calculated at any position, r, along the core length using the Hassler-Brunner equation (Hassler and Brunner 1945):

$$P_c(r) = \frac{1}{2}\Delta\rho\omega^2(r_1^2 - r^2) \tag{29}$$

where $\Delta\rho = \rho_{out} - \rho_{in}$ is the density difference between the fluid expelled from the core (ρ_{out}) and the fluid entering the core (ρ_{in}), ω is the angular rotation speed of the centrifuge, and $r_1 \simeq 22.1$ cm (for drainage mode of centrifuge) and 16.5 cm (for imbibition mode of centrifuge) and r (varying from 0 to 5 cm) are the distances from the rotational axis to the outlet face and any point along the core length, respectively.

After reaching an equilibrium between the oil / water saturation and capillary pressure, i.e. when no more brine was being produced, the brine expelled from the core was measured and the average water saturation for each rotation speed was obtained. This water saturation was plotted against the capillary pressure estimated from equation (29) to produce the capillary pressure curve.

3.5.1.2.2 Aging

After the centrifuge the overburden was reduced to 0.7 MPa and the core holders with cores and end pieces inside were placed in the oven to age at 90°C for aging time ranging from 6 to 30 days (Table 3).

Table 3. Aging time for different cores

Core No.	**Saturation porosity (%)**	**Aging Time (days)**
1	38.6	6
2	38.5	9
3	37.8	12
4	36.9	15
5	38.0	18
6	38.1	21
7	37.6	30

After aging, the seven full sized cores were used for USBM wettability measurement, and the seven top and seven bottom end pieces were used for the contact angle measurements and SEM-MLA analyses, respectively.

3.5.2 Establishing wettability

3.5.2.1 Chromatographic separation technique

The chromatographic separation procedure is based on the idea that the water wet areas of the chalk surface attract SO_4^{2-} ions that are present in the injected brine, i.e. SO_4^{2-} ions adsorb on the calcite surfaces that are in contact with water. Therefore, when a brine containing SO_4^{2-} and SCN^- tracer is injected (into a sample saturated by non-sulfate and non-tracer brine) the sulfate is delayed compared to the non-affine tracer during frequent sampling of the effluent fluids. The key premise in this work is that the area spanned by the sulfate concentration curve compared to the tracer curve of the effluent samples is proportional to the surface area available for the sulfate ions to adsorb. The ratio of the area between curves for a mixed-wet sample divided by the reference area of a water-wet sample defines the wetting index (W_i),

$$W_i = \frac{A_{mw}}{A_{ww}} \tag{30}$$

where A_{mw} and A_{ww} are the areas between the SO_4^{2-} and SCN^- curves for mixed-wet and water wet samples, respectively. The areas under the SO_4^{2-} and SCN^- curves were determined using the trapeze method in this study.

The wettability determination could not be performed on the cores used in the triaxial test program since the flow of fluids used in the wettability determination could alter the wettability, as sulfate is a wettability modifier (Strand et al. 2006; Zhang and Austad 2006; Zhang et al. 2007). It would also displace oil from the core prior to the mechanical test. Therefore, several wettability tests were performed in order to check the repeatability and obtain confidence that all cores had similar wettability. Hence, the assumption that the wettability determined from the wettability determination program also applies to the wettability-altered cores in the triaxial test program held strong ground.

Wettability determination was performed in Hassler (**Paper I** and **Paper III**) and triaxial (**Paper II**) cells by (i) flooding four PVs of SW0T brine, (ii) injecting SW1T brine for 500 minutes with a flow rate of 0.2 ml/min. During the SW1T brine injection, 36 to 40 samples were collected using a Gilson fraction sampler. Each sample contained 2 ml of fluids collected over 10.0 minutes, with 2.5 minutes waste time between each sample.

For each fluid sample, the thiocyanate and sulfate concentrations were determined using ion chromatography (IC). The concentration c_k of each species k (SCN^- and SO_4^{2-}) is rescaled by the SCN^- and SO_4^{2-} concentrations of SW0T c_{k0} (in this case zero) and SW1T $c_{k1} = 0.024$ mol/liter, such that a reduced concentration $\widehat{C_k}$ could be obtained,

$$\widehat{C_k} = \frac{c_k - c_{k0}}{c_{k1} - c_{k0}} \tag{31}$$

This reduced concentration varies between zero and one, and when the effluent concentration equals the inlet concentration it gives $\widehat{C_k} = 1$. This enables the thiocyanate and sulfate curves to be plotted together. The area between these curves was estimated by integration using the trapeze method. Further, larger cores will have a larger total surface area than the smaller ones, so the areas are reported in per gram of the core for accurate comparison.

3.5.2.2 Contact angle method

The top end pieces of the aged core samples were mounted in a *Vinci IFT 700* instrument to measure the contact angle by sessile drop method. The same NaCl brine, used to saturate the samples initially, was used as the droplet fluid and each droplet was of size $\sim 5 \cdot 10^{-4}$ ml (radius of 0.5 mm). 8-10 photographs were acquired over two minutes each enabling us to observe how the droplet obtained a stable geometry over time. The top end pieces were at the oil front during the primary imbibition process and hence, it was assured that the saturation was uniform. Contact angle was measured at multiple spots (about 10 to 12) on the surface of the piece and an average value was taken as the contact angle for that sample. The generally accepted contact angle wettability classification is given in Table 4.

Table 4. Contact angle wettability classification (McPhee et al. 2015).

	Water Wet	**Neutral Wet**	**Oil Wet**
Minimum	0°	60-75°	105-120°
Maximum	60-75°	105-120°	180°

3.5.2.3 USBM method

After the primary drainage and aging, the NaCl brine was forcibly imbibed (primary imbibition) into the cores using the centrifuge in imbibition mode to obtain residual oil saturation (S_{or}) before a secondary drainage was performed to reach S_{wi} (Donaldson et al. 1969, 1980; Donaldson 1981; McPhee et al. 2015). The receiving tubes, coupling cups to core holders, were saturated by the same fluid as the cups holding the fluid that enters the cores. A confining pressure of 1.38 MPa and seven centrifugal steps from 500 to 3500 rpm, with 500 rpm increments and three hours equilibration time, were used. The trapezoidal method was used to estimate the area under the secondary drainage (A_1) and primary imbibition (A_2) capillary pressure curves, and the wettability index W_i was calculated from the following equation,

$$W_i = \log \frac{A_1}{A_2} \tag{32}$$

In conjunction to equation (32), the wettability index W_i is greater than 0 for water-wet, smaller than 0 for oil-wet and around 0 for neutral-wet systems.

3.5.2.4 SEM-MLA analysis

The bottom end pieces of the aged core samples were used for SEM-MLA analysis (Sripal and James 2016, 2018).

A *FEI Quanta 650 Field Emission Gun (FEG) Scanning Electron Microscope (SEM)* equipped with Bruker high throughput energy dispersive X-ray (EDX) system and backscattered electron detectors was used. Imaging on the flat sample surfaces was carried out at very low vacuum conditions (0.6 Torr). Additionally, the samples were not subjected to any metallic or carbon coating on the surface, except for a liquid graphite coating on the sample holder. Instrument conditions and parameters included a high voltage of 25 kV, spot size of 5.75, working distance of 13.5 mm, 10 nA beam current, 16 µs BackScattered Electron (BSE) dwell time, 10 pixel minimum size (400 pixel frame resolution for 1-mm high full well (HFW)), and 12-ms spectrum dwell for EDX. Each of these Mineral Liberation Analysis (MLA) acquisitions was completed using version 3.1.4.683 MLA software and took between 3 and 4 hours per sample.

Prior to testing the individual aged end pieces, two pure chalk pieces, one with a drop of the oil mixture and another with a drop of 1.1M NaCl-brine on it, were analyzed to determine the oil and NaCl-brine (termed 'halite') signatures and added to the SEM mineral database. The aged end pieces were, then, analyzed to determine the relative quantity of oil, halite and carbonate in percent. The results for individual samples were acquired as a digital map of the minerals and a data table listing their mineral composition. The mineralogy was determined using GXMAP measurement mode within FEI mineral liberation analyzer software, equipped on the SEM. Each mineral identified was within an 80% match to a known standard X-ray. The premise was to link the oil/halite concentrations to the overall wetness of the mineral surface, which in this study was controlled by the aging time.

3.5.3 Hydrostatic tests in a triaxial cell

The $MgCl_2$ flow-through experiments in **Paper I** and **Paper III** were conducted according to the following stages:

1. Mounted the cores in the triaxial cell (K1 to K4 in **Paper I**, and M1 to M4 in **Paper III**); kept the bypass valve open with no flow-through the cores.
2. Increased confining pressure (σ_{rad}) to 1.2 MPa and pore pressure (P_f) to 0.7 MPa simultaneously.
3. Increased temperature to 130°C.
4. σ_{rad} increased to approximately 1.5 times above yield at a loading rate of 0.045 MPa/min with bypass open. The onset of yield stress was determined when the hydrostatic stress - volumetric strain curve deviated by more than 0.7 MPa for Kansas chalk and more than 0.5 MPa for Mons chalk from the straight elastic line used to determine the bulk modulus (K).
5. Observed creep; for the first 15 days of creep period bypass valve was kept open.
6. Afterwards bypass valve was closed and $MgCl_2$ brine flooding was commenced through cores at a flow rate of 0.010 ml/min.
7. Increased $MgCl_2$ brine flooding rate to 0.040 ml/min for all tests after a certain number of days.
8. Decreased flow rate back to 0.010 ml/min for some of the cores.
9. Cleaned the cores with four PVs of DW at the end of the test.
10. Used toluene to remove the leftover oil from wettability-altered cores, followed by flooding methanol to remove toluene. Toluene was flooded till the effluent became completely transparent in color. Afterwards, DW was used to remove methanol from these cores.
11. Chromatographic separation tests were performed on all Mons samples after mechanical tests (**Paper III**). These tests were not performed on Kansas samples.
12. Demounted all cores from triaxial cell.

After demounting, the wet mass, dry mass, length and diameter were measured. Afterwards, the samples were cut into six sections of almost equal length and tested for density and specific surface area using gas pycnometer and Brunauer–Emmett–Teller (BET) theory, respectively (see sections 3.5.7 and 3.5.8).

Flow-through experiments were also performed on Kansas chalk samples with SSW (K5 to K8 in **Paper I**). The procedure followed was the same as with $MgCl_2$ brine, except that the cores were flooded only at 0.010 ml/min flow rate. For details, the reader is referred to **Paper I**. Flow-through experiments with SSW were not performed on Mons chalk samples in this study.

3.5.4 Triaxial tests at low effective stresses with frequent tracer tests to evaluate chalk surface area evolution with time

Tracer tests were performed in triaxial cells at frequent intervals of time on a separate set of Kansas chalk samples, drilled from the same chalk block as for the hydrostatic tests, to evaluate the extent to which chemical interactions induced by the continuous $MgCl_2$ brine injection modify the water wetness of the chalk samples. One water wet (KA1) and three mixed wet (KA2 to KA4) samples were flooded by $MgCl_2$ brine at low effective stresses and tracer tests were performed after 7 days each for KA1 and 10 days each for KA2 to KA4 using chromatographic separation technique.

Readers are advised to refer to **Paper II** for the detailed experimental procedures followed for the water wet sample KA1 and the mixed wet samples KA2, KA3 and KA4.

3.5.5 Measurement of oil production

During the hydrostatic tests (**Paper I** and **Paper III**) and the triaxial tests at low effective stresses (**Paper II**), the oil produced was collected in a burette / separator placed on the downstream side of the experimental setup and read by eye at frequent intervals.

3.5.6 Ion Chromatography (IC)

The effluent samples acquired were diluted 500 times with de-ionized water to meet the linear regime of the *Dionex IC S-5000+ Ion Chromatography* system. The samples were diluted using the *Gilson GX-271* liquid handler operated by the *Trilution* software. Once the analysis finished, a series of peaks, corresponding to each ion in the effluent sample, was obtained. The area under each peak was assumed to be proportional to the ion concentration in the fluid when compared to known standards with known concentrations.

3.5.7 Mineral density determination

Samples were cut into six sections of almost equal length after mechanical tests. These sections were kept in the oven at 110°C overnight. Next morning these sections were taken out and placed in a vacuum sealed container to cool down. Each section was, then, weighted and inserted, one-by-one, into the *Micromeritics AccuPyc II 1340 Gas Pycnometer* (using helium) to measure the solid volume. With mass and solid volume known, the mineral density of each section was estimated.

3.5.8 Specific surface area (SSA) determination

The SSA was estimated by Brunauer–Emmett–Teller (BET) theory, which works on the principle of physical adsorption of gas molecules on a solid surface (Brunauer et al. 1938). The SSA measurements were carried out on *Micromeritics TriStar II* instrument using liquid nitrogen, as it does not chemically react with the chalk. Two grams of powdered chalk were added to the sample glass tube and degassed for 5 hours at 110°C on *Micromeritics VacPrep 061 Sample Degas System*. A stable vacuum pressure of 20-30 mTorr was attained for all tested samples before the sample tubes were attached to the BET apparatus. The specific surface area was measured automatically by the *TriStar II 3020* software.

4 Results and Discussion

This section presents the results from the experimental studies performed on both Kansas and Mons chalks, followed by a detailed discussion of these results.

4.1 Results of wettability determination

4.1.1 Impact of aging time on qualitative analysis of wettability using contact angle method

It was not possible to obtain a stable and time-independent contact angle measurement for samples with 6 and 9 aging days as the droplet initially had a maximal contact angle of around 65° and 66°, but within only a few seconds, it spread out and got sucked into chalk developing into a contact angle of 0° with time. Samples aged 12 and 15 days formed sessile droplets enabling stable contact angle measurements of 78° and 85°, respectively. Increasing the aging time to 18, 21 and 30 days the contact angle increased to 102°, 110°, and 108°, respectively (Figure 5 and Figure 6 (left), Table 5). Hence, as the aging time was increased to 18 days and beyond, the contact angle reached a plateau of more than 100° which is in-line with oil wet characteristics, said to be greater than 105° (Anderson 1986; Cuiec et al. 1994).

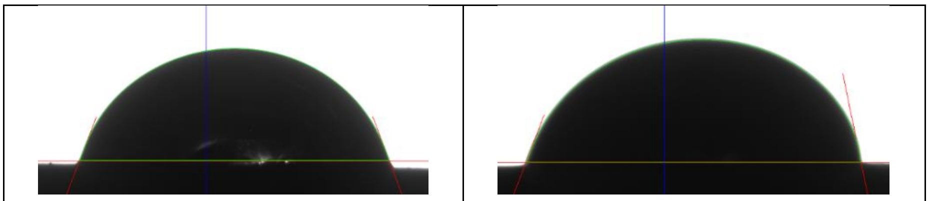

Sample 1 (θ = 65°) Age time: 6 days

Sample 2 (θ = 66°) Age time: 9 days

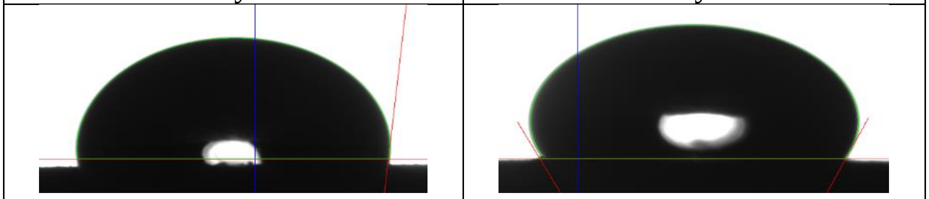

Sample 3 (θ = 78°) Age time: 12 days

Sample 4 (θ = 85°) Age time: 15 days

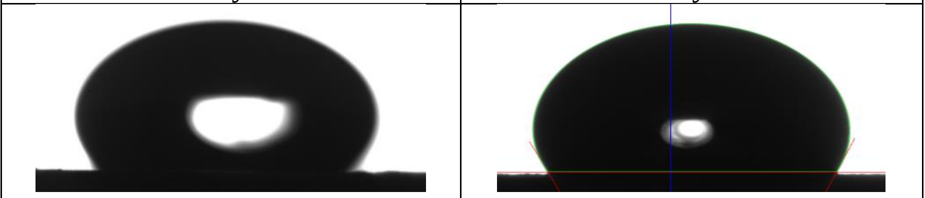

Sample 5 (θ = 102°) Age time: 18 days

Sample 7 (θ = 108°). Age time: 30 days

Figure 5. Brine droplet of size $\sim 5 \cdot 10^{-4}$ ml placed onto the aged top end piece. The contact angle is shown for differently aged chalk samples (see **Paper IV**).

4.1.2 Impact of aging time on quantitative analysis of wettability using USBM method

After the samples were aged they were imbibed by NaCl brine (primary imbibition) from S_{wi} to the residual oil saturation (S_{or}, Figure 7 and Table 5). The area under the P_c vs S_w curve during primary imbibition is termed A_2. The cores were, then, taken out of the core holders which were switched to drainage mode before secondary drainage was performed (in which oil expelled brine). The area under the P_c vs S_w curve during secondary drainage is termed A_1.

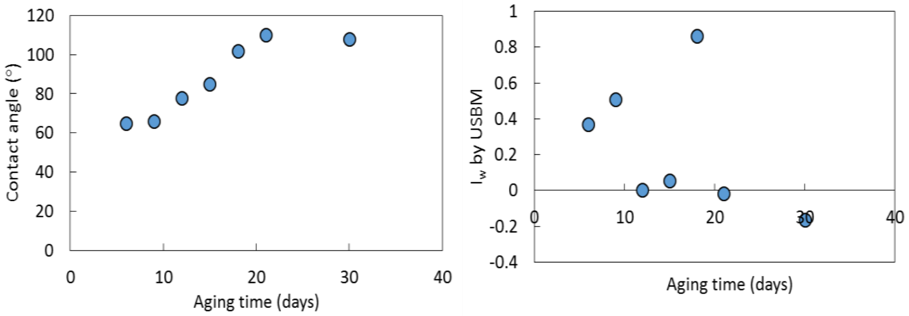

Figure 6. Left: Contact angle on the top end piece of aged chalk cores as a function of aging time. Right: Wettability index measurement using USBM method as a function of aging time (see **Paper IV**).

The wettability index I_w from USBM method was estimated using the log10 of the ratio A_1 by A_2 in equation (32). From the I_w reported in Table 5, it can be seen that, except from core number 5 (18 days), an increasing aging time leads to a lowered wettability index, ranging from 0.37 and 0.51 for 6 and 9 days aging to around zero for 12, 15 and 21 days, and -0.16 for 30 days aging. Figure 6 (right) gives a plot of wettability index estimated by USBM method as a function of aging time. The abnormality with result from sample aged 18 days is quite uncertain and is likely caused by either excess confining pressure or due to the presence of natural fractures within chalk, which led to further disintegration during the primary imbibition and secondary drainage tests.

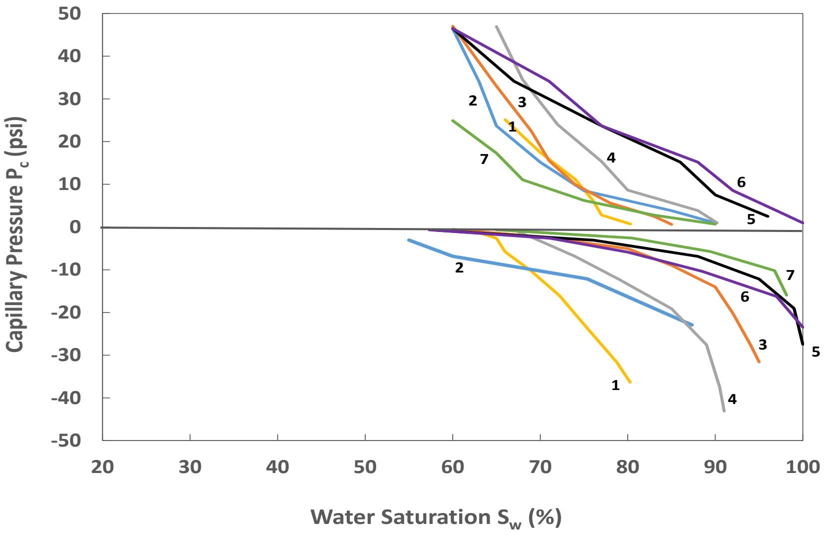

Figure 7. Primary imbibition (brine displacing oil, $P_c < 0$) and secondary drainage (oil displacing brine, $P_c > 0$) for Kansas chalk samples 1 to 7, number of aging days in parenthesis: 1 (6-yellow), 2 (9-blue), 3 (12-orange), 4 (15-grey), 5 (18-black), 6 (21-purple) and 7(30-green) (see **Paper IV**).

Note: For samples 5 and 6, the primary imbibition data was adjusted to 100% maximum saturation as the experiments overestimated the saturations to beyond 100%. The S_{or} reported for samples 5 and 6 in Table 5 are assumed to be the penultimate points after the saturations were adjusted to 100%.

4.1.3 Impact of aging time on qualitative analysis of wettability using SEM-MLA analysis

The lower end pieces were analyzed using SEM–MLA in which the oil/brine content of the surface of the samples was determined (Table 5). Based on the individual surface measurements (reported in Table 6) for the amount of oil/brine/calcite of the aged chalk samples, the SEM-MLA wettability estimates are reported in Table 5. Figure 8 provides two examples of mineral/fluid MLA maps and SEM images of samples aged for 6 days and 30 days showing how an increasing aging time results in an increased oil signature on the chalk samples. Standnes and Austad

(2000a, 2000b) also concluded that the increase in aging time increased the affinity of oil towards the chalk surface.

Table 5. Experimental measurements for Kansas chalk (see **Paper IV**)

Core No.	**Aging Time (days)**	**S_{wi} (%)**	**Contact Angle (°)***	**SEM-MLA oil %**	**I_w (USBM)**
1	6	64.71	65 (29.4)	10	0.368
2	9	54.32	66 (26.8)	19	0.510
3	12	58.10	78 (9.1)	27	0.005
4	15	62.61	85 (7.5)	37	0.053
5	18	54.15	102 (6.2)	37	0.864
6	21	54.33	110 (4.2)	39	-0.018
7	30	58.64	108 (4.5)	46	-0.165

*150 to 300 data points were collected with average value reported and standard deviation presented in brackets

Table 6. Mineral list from the SEM-MLA analysis for Kansas chalk samples 1 to 7, number of aging days in parenthesis: 1(6), 2(9), 3(12), 4(15), 5(18), 6(21) and 7(30) (see **Paper IV**).

Color	Mineral	% Area coverage by sample						
		#1	#2	#3	#4	#5	#6	#7
🟪	Carbonate	8	21	61	3	57	50	31
🟨	Halite	82	60	12	60	6	11	23
🟧	Oil	10	19	27	37	37	39	46
⬛	Others	0	3	3	4	3	1	2

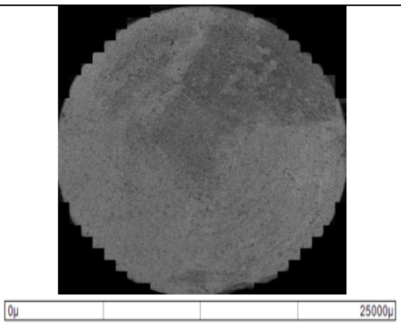	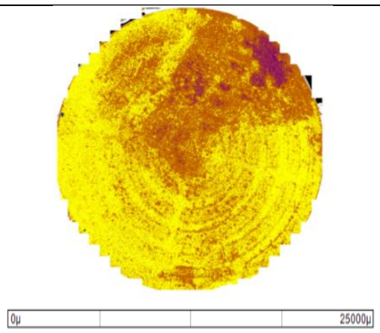
Chalk sample 1 (aged 6 days) SEM	Chalk sample 1 (aged 6 days) MLA
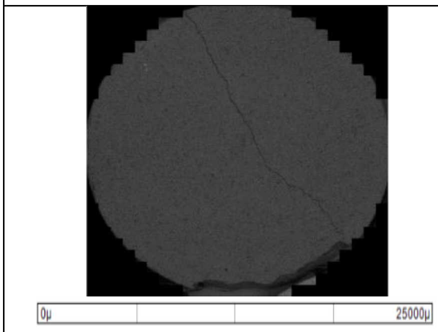	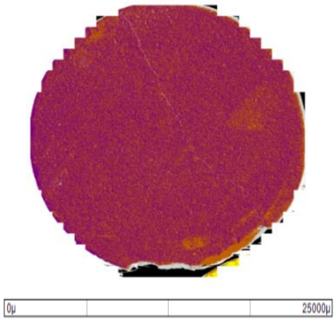
Chalk sample 7 (aged 30 days) SEM	Chalk sample 7 (aged 30 days) MLA

Figure 8. SEM and MLA images of different aged chalk samples (see **Paper IV**).

Comparison of results from contact angle, USBM and SEM-MLA methods

The wettability measurements reported here, from the three methods, imply that an aging time exceeding 21 days was enough to ensure that the Kansas chalks are oil wet when the samples were saturated by 1.1 M NaCl brine and 2.12 mg KOH/g oil and aged at 90°C. The results from these methods, especially contact angle and USBM methods, show that the cores attained neutral wet state and were on the oil wet side.

Similar work had been carried out previously on Rørdal chalk samples (Graue et al. 1999), wherein the chalk samples were submerged into crude oil for wettability alteration, and then after aging the crude oil was flushed out by decahydronapthalene, which subsequently was flushed out by decane for imbibition tests. Graue et al. (1999) reported that a stable wettability was obtained for cores aged more than 14 days using this set of fluids.

4.1.4 Results of wettability estimation from chromatographic separation technique

Chromatographic separation technique was applied to both Kansas (**Paper I**) and Mons (**Paper III**) chalk types.

4.1.4.1.1 Initial wettability of Kansas chalk

For Kansas chalk, the average area for water-wet and wettability-altered cores was found to be $(1.59 \pm 0.07) \cdot 10^{-3}$ PV/g and $(0.88 \pm 0.05) \cdot 10^{-3}$ PV/g, respectively. This corresponds to an average W_i of 0.55 ± 0.05 for the wettability-altered samples, meaning they are close to neutral-wet condition but on the water-wet side. An example of two chromatographic separations of a completely water-wet (Kww7) and a wettability-altered sample (Kmw3) is shown in Figure 9(a) and (b), respectively. Here, the reduced ion concentration is plotted against PVs of SW1T flooded. Each dot reflects a single effluent water sample and the separation between the sulfate ion and thiocyanate tracer ion can be visualized. Figure 9(c) displays the difference between the measured thiocyanate and sulfate concentrations for the water-wet core (Kww7) and wettability-altered core (Kmw3).

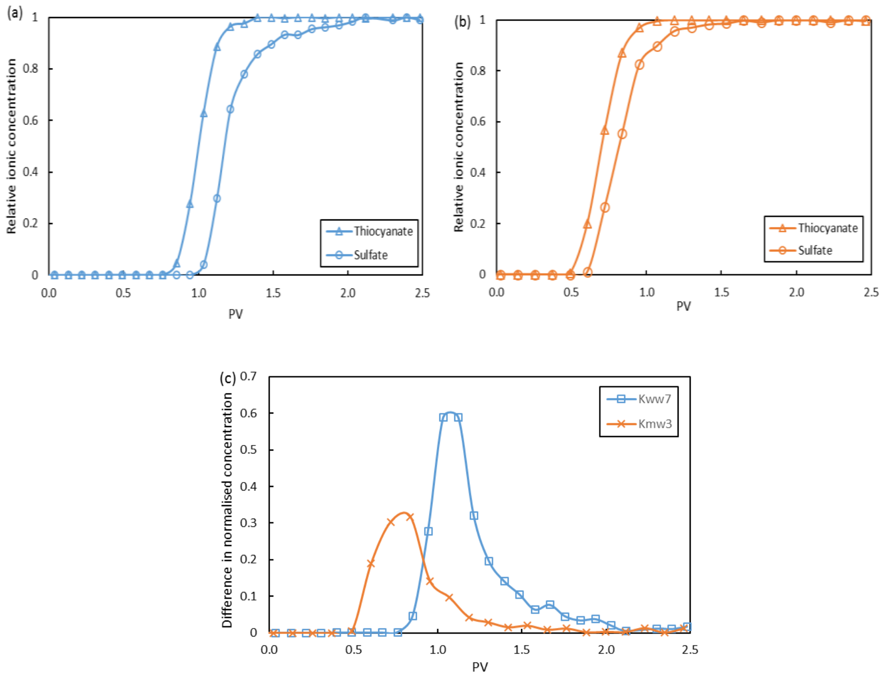

Figure 9. Chromatographic separation on (a) water-wet core (Kww7, blue) and (b) wettability-altered core (Kmw3, orange). The plots (a) and (b) show how the increase in sulfate concentration is delayed compared to the thiocyanate concentration after SW1T is injected. The plot (c) shows the difference in normalized concentrations between the thiocyanate and sulfate curves for the water-wet (blue) and wettability-altered cores (orange). The integrated separation area for Kww7 and Kmw3 was 1.71×10^{-3} PV/g and 0.92×10^{-3} PV/g, respectively (see **Paper I)**.

4.1.4.1.2 Initial wettability of Mons chalk

Similarly, for Mons chalk, the average area for water-wet and wettability-altered samples was estimated to be 1.48 ± 0.08 PV/g and 0.93 ± 0.04 PV/g, respectively. This corresponds to an average W_i of 0.63 ± 0.07 for the wettability-altered samples, which also means that they are close to neutral-wet condition but on the water wet side. Figure 10(a) and (b) shows two chromatographic separation tests performed on a completely water-wet sample (Mww2) and a wettability-altered sample (Mmw3). Figure 10(c) displays the difference between the measured thiocyanate and sulfate concentrations for the water-wet sample (Mww2, blue) and wettability-altered sample (Mmw3, green).

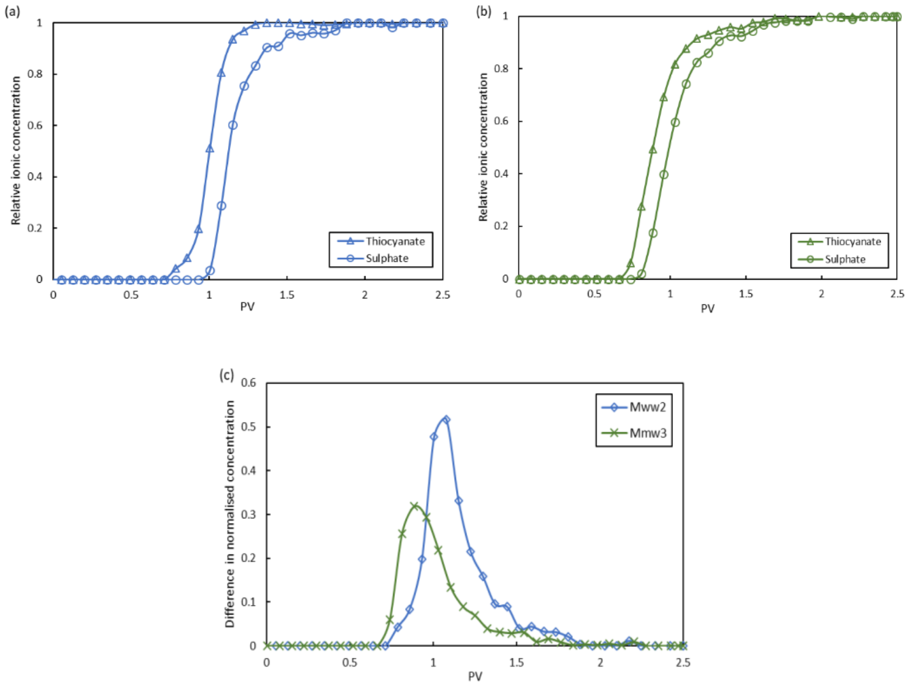

Figure 10. Chromatographic separation on (a) water-wet core (Mww2, blue) and (b) wettability-altered core (Mmw3, green). The plots (a) and (b) show how the increase in sulfate concentration is delayed compared to the thiocyanate concentration after SW1T is injected. The plot (c) shows the difference in normalized concentrations between the thiocyanate and sulfate curves for the water-wet (blue) and wettability-altered cores (green). The integrated separation area for Mww2 and Mmw3 was 1.43×10^{-3} PV/g and 0.98×10^{-3} PV/g, respectively (see **Paper III**).

Readers are advised to refer to **Paper I** and **Paper III** for the estimated individual areas for the Kansas and Mons water-wet and wettability-altered samples.

Comparison of wettability determination results from Kansas and Mons chalks

It is observed that these two chalk types differ in their wettability values with the same aging procedure. The wettability for the wettability-altered Kansas chalk was found to be 0.55 ± 0.05, whereas wettability-altered Mons chalk gave the wetting index of 0.63 ± 0.07, which shows that Mons chalk was more water wet compared to Kansas chalk at the start of the hydrostatic loading at 130°C. This shows that the mineralogy of the two chalks play a role in determining how wettability of the two types is changed after aging at same temperature for the same period of time with same brine and oil compositions. It is likely that the presence of silicates and clay in Kansas chalk make it more oil wet compared to Mons chalk which is very pure. It may also be due to the higher initial water saturation for Mons chalk that they were left more water wet to start with after aging at similar conditions.

Standnes and Austad (2000a) reported that the wettability induced by crude oils on chalk surfaces is related to the number of acidic components in the crude oil, i.e. crude oils with high acid numbers have a greater potential to turn the chalk oil-wet. Zhang and Austad (2005) also showed that the acid number affect the wetting state. Hence, a deviation in the AN from 2.12 mg KOH/g used in this study to any other value may change the wetness of the chalk cores for the same aging time.

Comparison of results from contact angle and USBM methods with the results from chromatographic separation technique

The results from contact angle and USBM methods show that the cores were neutral wet, but on the oil wet side, after aging for 21 days at 90°C. The chromatographic separation technique also showed that the cores were neutral wet state, but on the water wet side, with same aging conditions. This small difference in the wettability determination between these methods is likely within the margin of error, but further studies are needed using contact angle, USBM and SEM-MLA methods to check for the repeatability of the results.

4.2 Impact of wettability on fluid flow in porous media and mechanical response in chalk

Wettability affects the flow and distribution of reservoir fluids in the rock and plays a significant role in determining how immiscible fluids move through reservoirs, deciding production rates of oil and water and the ultimate oil recovery. Consider an oil wet reservoir rock, where oil is bonded to the mineral surfaces, flooded by water. The injected water flows through the center of the pores, expelling the mobile oil here. This behavior subsequently leads to a rapid water breakthrough, and a high water cut later on leaving significant immobile oil volumes behind. The immobile oil volumes would further depend upon the specific surface area and the oil film thickness. If the same reservoir rock was water-wet, i.e. oil being the non-wetting phase, the oil will occupy the center of the larger pores. During waterflooding the injected water will tend to imbibe into the smaller pores, moving oil into the larger pores where it can be displaced. Oil, then, moves ahead of the waterfront, which results in increased primary oil recovery before water breakthrough occurs. After water breakthrough, almost all the remaining oil becomes immobile. The disconnected residual oil is in the form of oil droplets trapped by capillary forces, arising from the surface energy between oil, water and mineral surface, where the curvature of the oil droplet is larger than the pore throat diameter.

Wettability may also be important to the mechanical behavior of rock. The mechanical response of the material to imposed stress is dictated by the load bearing structure. In a water-wet system, the grains have a larger affinity to water, hence water weakening of chalk has been observed due to chemical reactions occurring between the minerals constituting chalk and reactive brines. In an oil wet system where oil coat the chalk surface, it is envisioned that oil prevents the water phase to get in contact and react with mineral grains, thereby keeping the chalk rock strong and stiff. In a wettability-altered system, however, it is expected that the detailed spatial distribution of oil and water along the pore walls will control the link between wettability index and sample stiffness and strength. In this study, the work has been performed on outcrop chalk samples and the effect of wettability on chalk mechanics at hydrostatic conditions has been quantified.

4.2.1 Impact of wettability on elastic stiffness and plastic strength

The stress-strain curve during loading and the position of yield stresses for Kansas cores K1 to K8 and Mons cores M1 to M4 are shown in Figure 11 and Figure 12, respectively. The bulk moduli, and the yield and creep stresses used further in the experiments are reported in Table 7 and Table 8, respectively, for both chalk types.

During hydrostatic loading from 1.2 MPa to approximately 1.5 times the yield at 130°C and 0.7 MPa pore pressure, the inlet was closed, NaCl brine was bypassed and the initial saturation fluids only moved towards the outlet due to compaction. The elastic stiffness (bulk modulus) and plastic strength (onset of yield) were observed to be affected by the oil/water saturation and wetness of the cores (Figure 11 and Figure 12). Further on, the wettability-altered Kansas samples were found to be 33% stiffer and 35% stronger than the water-wet Kansas samples (Figure 11), meaning that the stiffness and strength are correlated with each other resulting in stiffer wettability-altered cores to be stronger than the water-wet samples. Similar correlations between stiffness and strength were also shown for 100% water saturated chalk at both 30°C and 130°C (Nermoen et al. 2018a) and for Stevns Klint chalk at ambient temperature (Katika et al. 2015). For Mons chalk, on the other hand, the water-wet and the wettability-altered samples showed similar stiffnesses and strengths (Figure 12).

Table 7. Bulk modulus of both Kansas and Mons cores during hydrostatic loading used in the triaxial test program.

Chalk Type	Injection brine*	Core	Wetting state	S_{wi} (-)	Bulk modulus (GPa)
Kansas	$MgCl_2$ flow	K1	Water wet	1	1.3±0.005
		K2		1	1.9±0.008
		K3	Wettability-altered	0.28	2.6±0.006
		K4		0.29	2.2±0.008
	SSW flow	K5	Water wet	1	2.2±0.007
		K6		1	1.9±0.020
		K7	Wettability-altered	0.27	2.5±0.007
		K8		0.28	2.3±0.005
Mons	$MgCl_2$ flow	M1	Water wet	1	1.3±0.008
		M2		1	1.8±0.034
		M3	Wettability-altered	0.34	1.0±0.006
		M4		0.36	1.1±0.009

*Note: During hydrsostatic loading, the inlet was closed and the initial saturation fluids (NaCl brine for water wet and NaCl brine + oil mixture for wettability altered) were only allowed to move towards the outlet due to compaction. The injection brines are given here just to distininguish between the samples that were flooded by $MgCl_2$ and SSW later on.

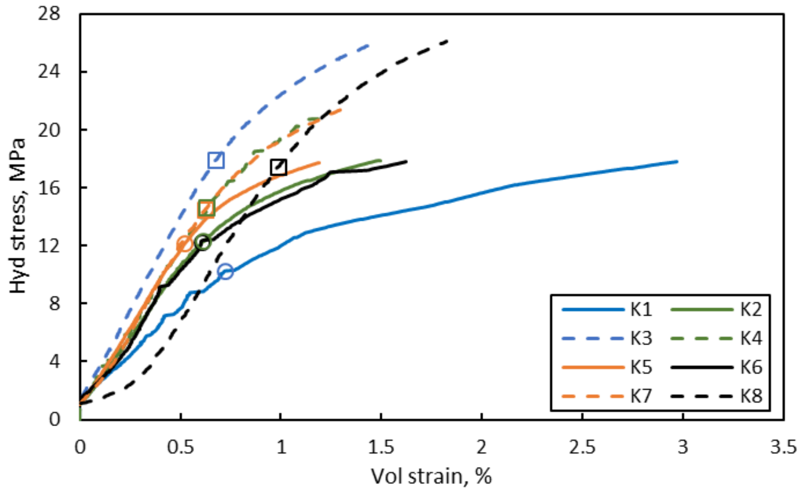

Figure 11. Hydrostatic stress versus volumetric strain for Kansas cores used in the triaxial test program. Solid and dashed lines represent water-wet and wettability-altered cores, respectively. Yield stresses for these cores are displayed in their corresponding curves (circles for water-wet and squares for wettability-altered cores) (see **Paper I**).

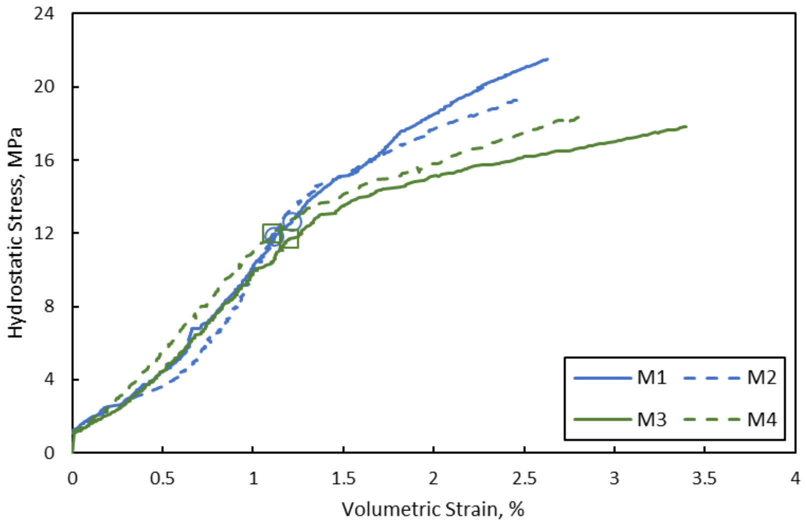

Figure 12. Hydrostatic stress versus volumetric strain for Mons cores used in the triaxial test program. Blue solid and dashed lines represent water-wet cores and green solid and dashed lines represent wettability-altered cores. Yield stresses for these cores are displayed in their corresponding curves (circles for water-wet and squares for wettability-altered cores) (see **Paper III**).

Table 8. Onset of yield stresses and creep stresses are given for Kansas and Mons cores used in the triaxial test program.

Chalk Type	**Injection brine***	**Core**	**Wetting state**	**Onset of yield stress (MPa)**	**Creep stress (MPa)**
Kansas	$MgCl_2$ flow	K1	Water wet	10.3	17.9
		K2		12.9	17.9
		K3	Wettability-altered	17.9	26.1
		K4		14.6	20.8
	SSW flow	K5	Water wet	12.5	17.8
		K6		12.4	17.9
		K7	Wettability-altered	14.5	21.6
		K8		17.7	26.1
Mons	$MgCl_2$ flow	M1	Water wet	14.4	21.5
		M2		13.3	19.3
		M3	Wettability-altered	12.4	17.8
		M4		12.3	18.3

*Note: During hydrsostatic loading, the inlet was closed and the initial saturation fluids (NaCl brine for water wet and NaCl brine + oil mixture for wettability altered) were only allowed to move towards the outlet due to compaction. The injection brines are given here just to distininguish between the samples that were flooded by $MgCl_2$ and SSW later on.

A significant difference in the loading stiffness and yield strength, beyond the experimental uncertainty, was not observed in Mons chalk. The initial soft behavior at low stresses, i.e. the initial large strains of the water-wet samples, can be caused by closure of micro-cracks and fractures formed due to the sample handling. Further experiments are required to identify if the mechanical parameters for Mons samples can be altered by aging, e.g. with a more acidic oil, higher aging temperature/time, or by lowering S_{wi} even more before oil is injected (a lower value of S_{wi} could make the core more oil-wet).

Oil adsorption impact particle-particle contact forces

The thickness of the charged diffusive layer on calcite surfaces is characterized by the Debye length (Lyklema 2005; Megawati et al. 2013; Voake et al. 2019) that increases with increasing temperature (Andreassen and Fabricius 2010). A thickening of the layer (Debye length) increases the repulsive area between particles causing further weakening of water-saturated samples. Voake et al. (2019) further reported a Debye length of around 200 nm at 130°C using Debye-Huckel theory.

The force between particles in the presence of water is dictated by the sum of attractive van der Waals forces and repulsive electrostatic forces from the overlapping diffusive layer. When oil replace water on surface areas where the double layers would otherwise interact (regions with electrostatic repulsion), the disjoining pressure would reduce and the overall force balance between particles would change. When the normal force between two grains increase (in the case of oil adsorption), it becomes harder for particles to re-organize. This seems to have occurred in Kansas, which has a Biot coefficient of 0.91 (Voake et al. 2019) and smaller pore size (characterized by the lower relaxation time T_2 estimated from the NMR studies, Voake et al. 2019) than Mons with a Biot coefficient of 0.95 (Figure 13(a) and Table 13 in Appendix). If oil adsorbs on mineral surfaces but not on nearby particle contacts, the geomechanical parameters would remain un-affected. This seems to have occurred in Mons (Figure 13(b)).

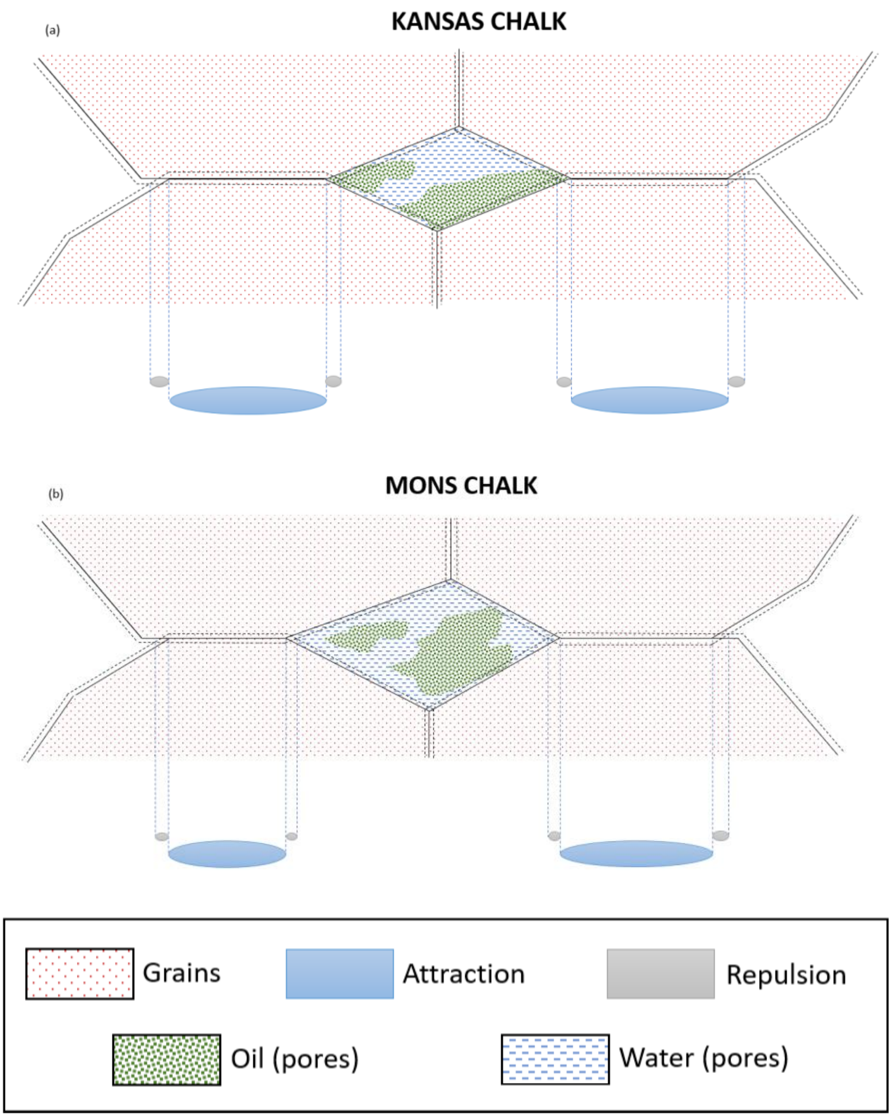

Figure 13. Partitioning of oil and water in pores for (a) Kansas and (b) Mons chalks. Attractive van der Waals and repulsive electrostatic forces present between calcite grains are also shown. Mons chalk has larger pore size and Biot coefficient compared to Kansas chalk (Voake et al. 2019) (see **Paper III**).

With the same oil, brine composition and aging temperature, it has been reported that Kansas chalk remains water-wet if the aging time is less than 6 days, and aging for 21 days was enough to obtain a stable neutral-wettability (**Paper IV**). It remains to be tested how mechanical parameters change for the same oil/water saturation for unaged samples. If the aging conditions were modified, the Mons chalk may become more mixed/oil wet thereby affecting stiffness and strength differently than in this study.

4.2.2 Impact of wettability on creep behavior

The creep stress for all eight Kansas cores and four Mons cores was set to be 1.5 times yield stress so that the development could be compared to each other. Since the yield stress was determined with the naked eye during hydrostatic loading, the creep stress chosen deviated from the factor 1.5 times yield stress (Table 8). The actual creep stresses (in Figure 14, Figure 15 and Figure 16) varied between a factor of 1.4 and 1.7 times yield stress for Kansas cores, and 1.4 and 1.5 times yield stress for Mons cores.

During the first 15 days of creep period, the inlet valve was kept closed and NaCl brine was bypassed. The initial resident fluids were able to flow through core due to compaction only and could leave the core on the downstream side. NaCl brine weakly interacts with the mineral surfaces in chalk and leads to minor calcite dissolution. Madland et al. (2011) showed the effect of flooding NaCl brine through water-wet Liège chalk and observed that the calcium concentration in the effluent was as low as 0.004 mol/l throughout the experiment. Andersen et al. (2018) showed negligible mineral precipitation effects for both water-wet Kansas and Mons chalks flooded by NaCl brine. In the hydrostatic tests performed in this work, the cores were only initially saturated by NaCl, and not flooded. The interactions between chalk and stagnant NaCl brine were observed to be negligible as the amount of dissolved calcite, due to interaction of chalk with NaCl brine, amounted to less than 0.01% in mass compared to the initial dry mass of the samples.

4.2.2.1 Kansas chalk

The volumetric creep strain for the four water-wet (100% NaCl brine saturated) and four wettability-altered cores (with initial NaCl brine saturation ranging from 27% to 29%) during the first 15 days followed approximately the same creep trend when stress was set to 1.5 times the yield (Figure 14 and Figure 15). The samples were not flooded during this time interval, and the fluid movement was controlled by pore volume reduction. The observation that how creep is evolving for both water-wet and wettability-altered chalks may imply that oil wetness is not affecting the way in which the grains re-organize. These observations exemplify how different mechanical parameters correlate to each other.

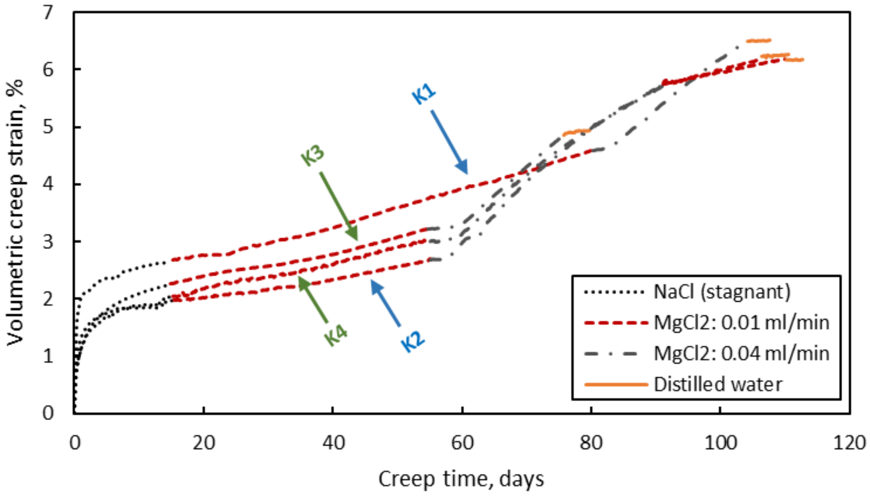

Figure 14. Volumetric creep strain with time during $MgCl_2$ flow through water-wet Kansas cores K1 and K2 (blue arrows), and wettability-altered Kansas cores K3 and K4 (green arrows) (see **Paper I**).

From 16th day the injection of $MgCl_2$ and SSW started. The injection of $MgCl_2$ brine has shown to induce chemical reactions leading to additional creep rates, and more chemical reactions taking place during a time interval leads to an increased creep rate (Nermoen et al. 2015). When $MgCl_2$ brine was injected at the lower rate of 0.010 ml/min (approx. 0.5 initial PVs (PV_i) per day), the strain curve went from having a negative second derivative to a straight line with a more-or-less constant strain rate. Quadrupling the flow rate to 0.040 ml/min, after a certain number of days, increased the linear creep rate by a factor of 2.5 to 4. This is in line with the analysis of the effluent fluids (Figure 17) that display how the loss rate (in grams per day) of Ca and gain rate of Mg also increased by a factor of 2 to 4 after the flow rate was quadrupled. This shows how chemical reactions drive reduction in the solid volume by reducing the overall mass and increasing the mineral density, and how this behavior is linked to the creep rate with time (Nermoen et al. 2016; Andersen et al. 2018). As shown in the presented data, the presence of oil in the pores does not alter the dissolution/precipitation driven water weakening dynamics, neither qualitatively nor quantitatively.

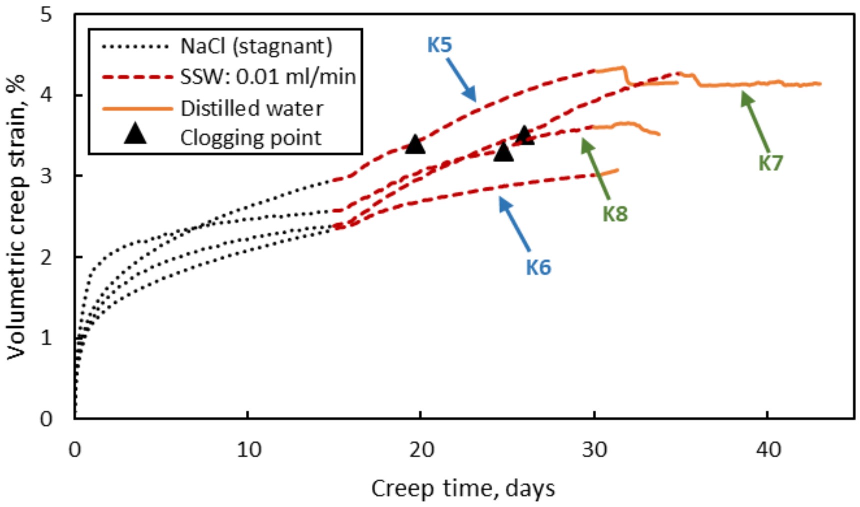

Figure 15. Volumetric creep strain with time during SSW flow through water-wet Kansas cores K5 and K6 (blue arrows), and wettability-altered Kansas cores K7 and K8 (green arrows) (see **Paper I**).

The chalk samples that were flooded with SSW (i.e. K5 to K8, Figure 15) displayed a qualitatively similar behavior as the $MgCl_2$ samples (K1 to K4, Figure 14). Injecting SSW induced chemical reactions and adsorption of surface-active ions leading to immediate additional creep rates. All cores showed comparable volumetric strain curves, irrespective of the initial wettability and oil/water saturation. After clogging (in the water-wet K5 and wettability-altered K7 and K8 samples) after a certain period, the strain rate declined because of reduced effective stress due to pore pressure buildup. The clogging did not occur inside the samples but in the steel tubing on the outlet side, so opening the bypass valve reduced the pore pressure and the strain rate regained its pre-clogging values.

4.2.2.2 Mons chalk

The volumetric creep strain at constant creep stresses (given in Table 8) for different wettability cores followed a comparable trend for all Mons samples throughout the creep period (Figure 16). They showed a similar trend during the stagnant fluid creep period. After the start of $MgCl_2$ injection at 0.010 ml/min flow rate, the strain rate curve stayed negative for around 15 days, after which it stayed constant for the rest of the flooding period at this flow rate (depicted by a zero slope curve, see Figure 16). This is similar to previous observations with clean chalks such as Mons and Stevns Klint (Andersen et al. 2018).

All samples showed an accelerated strain, irrespective of the initial wettability, when the flow rate of $MgCl_2$ injection was increased to 0.040 ml/min (Figure 16). The strain rate increased by a factor of 3 to 8 at the starting of injection period at higher rate. Nonetheless, the strain rate showed fluctuations and decreased by a factor of 1.5 to 2.5 times by the end of the higher rate injection phase. This shows how chemical reactions are independent of the oil/water saturation and the initial wetness of the Mons chalk cores but depend on the chalk mineralogy as these fluctuations were not observed for Kansas cores. During DW flooding to clean the cores, the strain rate dropped down to zero instantly depicting that no major interactions took place between DW and the rock, and that there was negligible precipitation of any secondary phases.

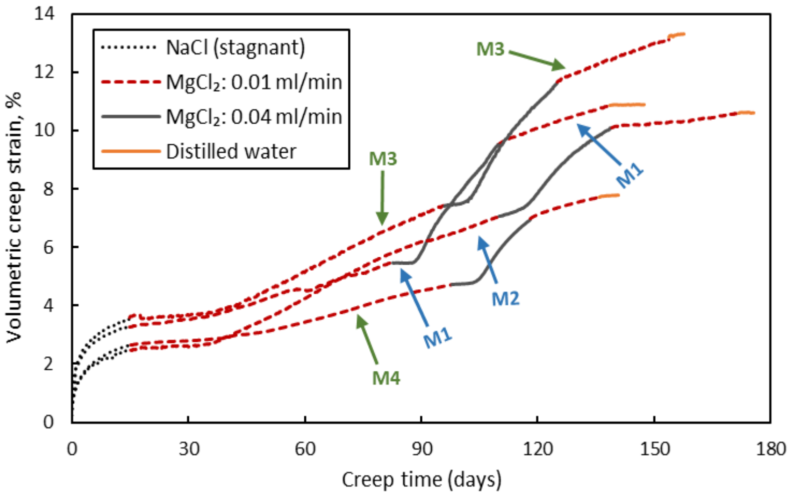

Figure 16. Volumetric creep strain with time during $MgCl_2$ flow through water-wet Mons cores M1 and M2 (blue arrows), and wettability-altered Mons cores M3 and M4 (green arrows) (see **Paper III**).

Impact of DW injection during cleaning of cores

During DW injection to clean the cores of any salts, the strain rate dropped significantly for all cores flooded by $MgCl_2$ brine (Figure 14 and Figure 16), even though the temperature and stress level were the same. The solubility of calcite in DW at 25°C is reported to be 0.013 g/l (Voake et al. 2019) and it decreases with increase in temperature (Coto et al. 2012). This means that 0.00039 g of calcite dissolved per PV of DW flooded through cores (approximate PV of 30 ml) at 25°C. As four PVs of DW were flooded to clean the cores at 130°C, the calcite dissolved amounts to approximately 0.001 % in mass compared to the initial dry mass of the cores (average initial dry mass of 135 g). Hence, it may be concluded that the interactions of DW with calcite are minor in nature.

For SSW flooded cores, a decrease in the strain rate is observed for the cores where clogging occurred due to pore pressure increase (K5, K7 and K8) during flooding by DW to clean the cores. For core K6 (without clogging), an increase in the volumetric creep strain is observed. This was also observed by Korsnes et al. (2006b).

These observations further exemplify how chemical reactions that undergo during the continuous flow of reactive fluids affect the rate of deformation, thereby displaying the link between chemical reactions and the quantitative amount of water weakening. Of special importance to emphasize is that all these observations are insensitive to the initial wettability and brine/oil saturation of the chalks.

4.2.3 Impact of wettability on rock-fluid interactions

4.2.3.1 Rock-fluid interactions during $MgCl_2$ flow

Figure 17 and Figure 18 display the effluent calcium and magnesium ion concentrations for Kansas and Mons chalk, respectively, during $MgCl_2$ brine flow through the two water-wet (a and b) and two wettability-altered (c and d) cores. Since the dominating chemical reactions are attributed to the precipitation of magnesium-bearing minerals and the dissolution of calcium carbonate, the focus is on the calcium and magnesium ions. Besides, magnesium ions can also adsorb on the calcite surface on the expense of calcium desorption. In all, dissolution/precipitation and adsorption/desorption lead to a decrease in the magnesium concentration in the sampled effluent compared to the injected brine concentration and an increase in the calcium concentration.

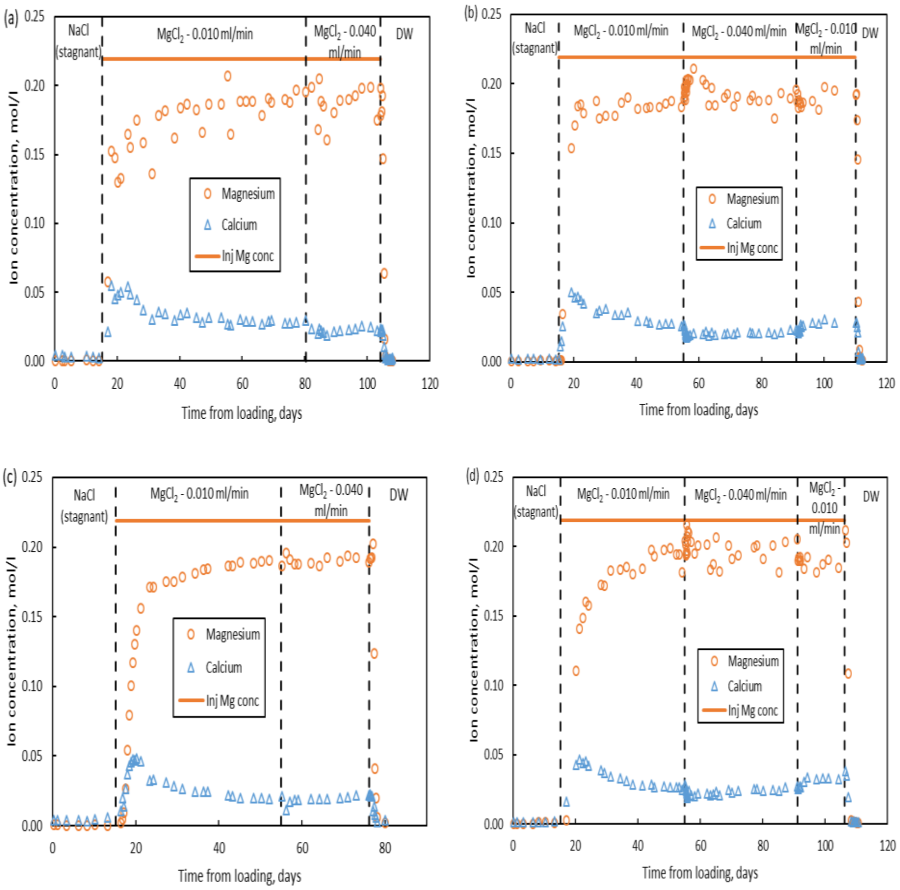

Figure 17. Kansas chalk samples flooded by $MgCl_2$ brine. Effluent ion concentrations of calcium and magnesium ions, and the injected magnesium ion concentration over time are shown for water-wet cores (a) K1 and (b) K2 and wettability-altered cores (c) K3 and (d) K4 (see **Paper I**).

The effluent analyses (Figure 17 and Figure 18) of Kansas and Mons chalks show that the calcium production and magnesium retention rates (in g/day) changed by a factor of 2 to 6 (rates estimated by multiplying the ion concentration in mol/l, flow rate in l/day and molecular weight of calcium and magnesium in g/mol) when the flow rate quadrupled – irrespective of the wettability and oil/water saturation. This shows how chemical reactions may drive reduction in solid volume by reducing the overall mass and increasing the mineral density, and how this behavior links to the bulk creep strain rate (Nermoen et al. 2016; Andersen et al. 2018).

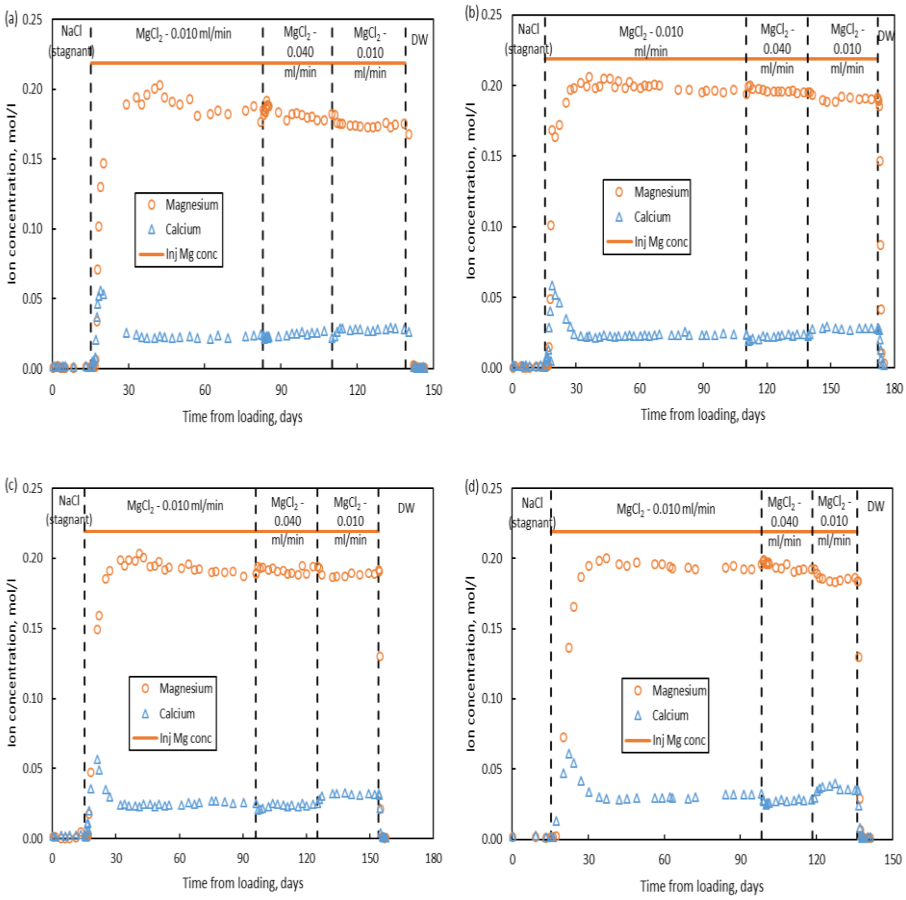

Figure 18. Mons chalk samples flooded by $MgCl_2$ brine. Effluent ion concentrations of calcium and magnesium ions, and the injected magnesium ion concentration over time are shown for water-wet cores (a) M1 and (b) M2, and wettability-altered cores (c) M3 and (d) M4 (see **Paper III**).

The effluent analyses on Kansas and Mons chalks have shown that interactions took place between the pore fluid and the mineralogical surfaces during $MgCl_2$ brine flooding.

At least two water weakening mechanisms are required to understand how the change in fluid composition in the effluent analysis (Figure 17 and Figure 18) and strain rate depend on each other: (i) Chemical reactions between brine and chalk related to dissolution and precipitation, and (ii) the adsorption of surface-active divalent ions (magnesium and sulfate ions) on the chalk surface and desorption of calcium ions. This adsorption changes the electrostatic repulsion thereby changing the inter-particle forces governing grain movements (Megawati et al. 2013). In all cases irrespective of the brine composition, the oil/brine saturation and wettability, the calcium concentration increased and the magnesium concentration decreased in the effluent. This is related to the production of calcium ions resting on the mineral surface and dissolution of calcite as well as precipitation of magnesium carbonate (Madland et al. 2011; Nermoen et al. 2015; Zimmermann et al. 2015; Minde et al. 2017, 2018a, 2018b; Andersen et al. 2018) and adsorption of magnesium ions onto and desorption of calcium ions from the calcite surface (Ahsan and Fabricius 2010; Alam et al. 2010; Nermoen et al. 2018a; Liu et al. 2018). However, only a limited number of surface sites are available, so the adsorption/desorption contribution to the changes in the ion concentrations will not prevail indefinitely. Adsorption/desorption dynamics could only occur within the first few pore volumes of the reactive brine injection in these cases. Afterwards the dissolution/precipitation processes dominate the calcium and magnesium effluent dynamics. Secondary minerals can be identified using SEM. Qualitatively, the mineral replacement seems to be insensitive to the initial water wetness and oil/brine saturation. The described behavior is in-line to what was indicated by X-ray diffraction and SEM studies carried out on chalk after $MgCl_2$ brine flow-through experiments by Madland et al. (2011) and Megawati et al. (2015).

4.2.3.2 Rock-fluid interactions during SSW flow

The chemical interactions between the core and the injected fluid are more complicated when SSW is injected compared to $MgCl_2$ brine. This is because there are additional ions other than Mg ions present in SSW that interact with chalk leading to more complex chemical interactions. The effluent ion concentrations of sulfate, magnesium and calcium are reported in Figure 19 for the two water-wet (K5 and K6) and one wettability-altered (K8) cores. The effluent analysis of the wettability-altered core K7 is not shown due to lack of data.

In the same way as during $MgCl_2$ flow, magnesium ions are retained in the cores and calcium ions are produced when SSW is injected through Kansas chalk. In addition, sulfate ions are retained in the cores. During the first 15 days of creep period (bypass), magnesium and sulfate concentrations in the effluents are observed to be zero, while a small production of calcium ions can be seen for K5 and K6 (Figure 19(a) and (b)). This may imply that calcite dissolution has taken place within the core, and that these ions are transported *either* by advection together with fluids expelled as the core is compacted *or* by diffusion through the tubing to the bypass valve and then transported along with the fluids from there.

The bypass valve was closed and SSW was flooded through the cores from the 16th day, after which a transient period is observed (Figure 19). In this period the calcium, magnesium and sulfate concentrations increase until 17-18 days after which a stable concentration is reached for core K6 (Figure 19(b)). The concentration of these three ions did not stabilize for cores K5 and K8 (Figure 19(a) and (c)). After a certain period, the system clogged due to precipitation in the steel tubing on the outlet side of the cores (K5, K7 and K8) and the bypass had to be opened to avoid pore pressure buildup.

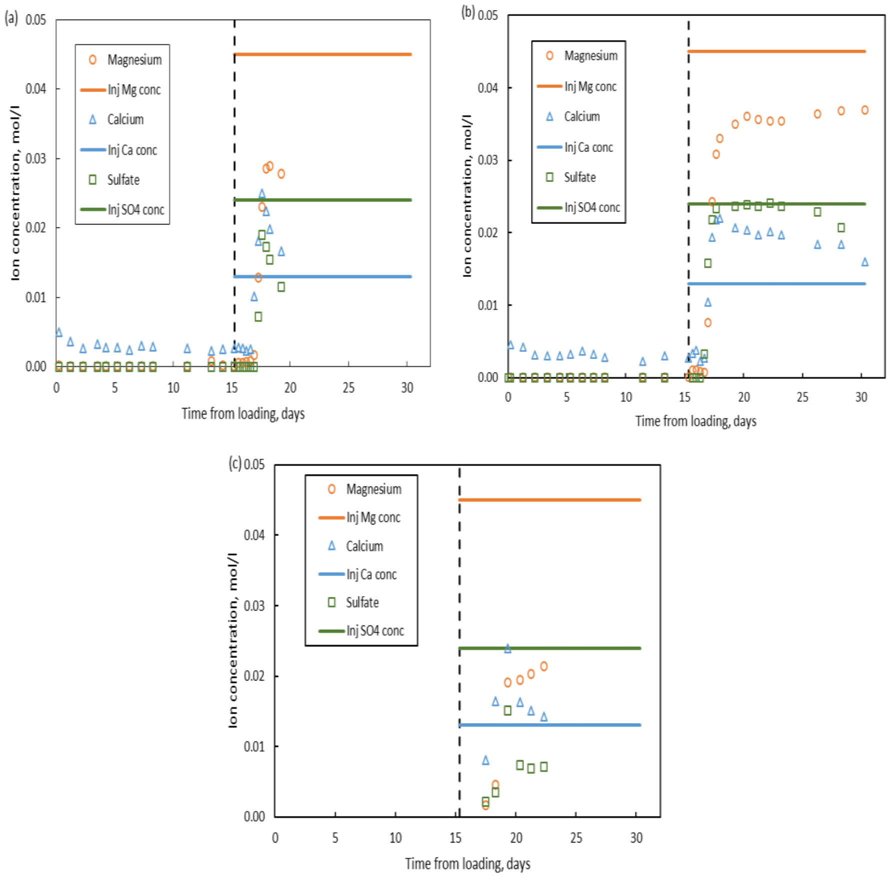

Figure 19. Kansas chalk samples flooded by SSW brine. Injected and effluent ion concentrations of calcium, magnesium and sulfate ions over time are shown for water-wet cores (a) K5 and (b) K6, and wettability-altered core (c) K8. The effluent analysis of the wettability-altered core K7 is not shown due to lack of data. The black dashed vertical line in the plots depict the start of SSW flooding (see **Paper I**).

4.2.4 Impact of wettability on chalk surface area evolution during $MgCl_2$ flow

The initial tracer test was performed on the Kansas water wet sample KA1 before the injection process started, thereafter tracer tests were performed after NaCl brine had been injected for 7.5 days, and after two injection periods of $MgCl_2$ brine for 7 days each. All the tracer tests were performed at ambient temperature, whereas the temperature during injection of $MgCl_2$ and NaCl was 130°C such that chemical reactions could occur. The aim was to quantify how the two brines affected the area spanned by the sulfate-thiocyanate concentration curves. Figure 20(a) displays the normalized concentration data along y-axis and PV_i of SW1T injected along x-axis. It can be seen how thiocyanate concentration increases ahead of the sulfate concentration and the rise in sulfate concentration is delayed in comparison. The area spanned between the thiocyanate and sulfate curves is displayed in Figure 20(b), whereas the area per gram of the core is reported in Table 9. The integrated area between the curves are given in units of PV per gram to capture the sample size effect.

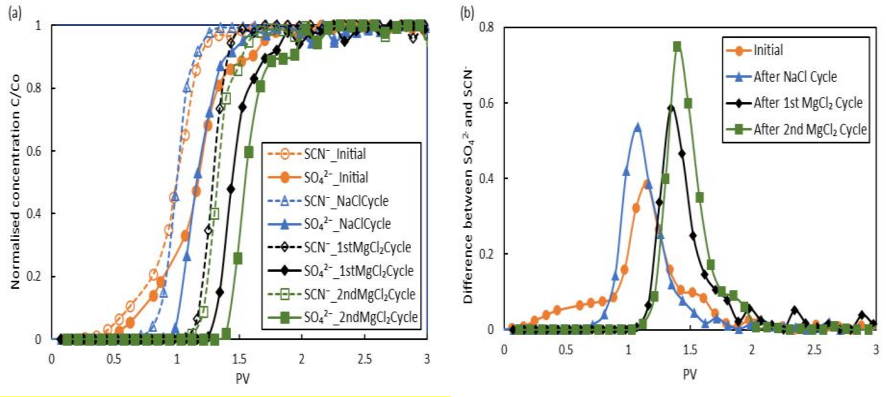

Figure 20. (a) Chromatographic separation during SW1T injection at ambient temperature on KA1. The normalized concentrations for thiocyanate (dashed curves) and sulfate (solid curves) ions are shown for initial tracer test (orange), after 7.5 days of NaCl injection (blue), after 7 days of 1st $MgCl_2$ injection (black) and after 7 days of 2nd $MgCl_2$ injection (green). The integrated areas between thiocyanate and sulfate are given in Table 9. (b) Difference between SCN^- and SO_4^{2-} as a function of PVs injected for each tracer test (see **Paper II**).

The initial tracer test yielded an area (orange curve in Figure 20(b)) of 1.45×10^{-3} PV/g, while after NaCl injection for 7.5 days the curve changed its shape, but the area increased insignificantly to 1.46×10^{-3} PV/g, i.e. an increase of 0.7%. After $MgCl_2$ brine was injected for 7 days, the area (black curve) increased to 1.60×10^{-3} PV/g, i.e. an increase of 10.3%. After a second $MgCl_2$ brine injection phase for another 7 days, the area increased to 1.75×10^{-3} PV/g, i.e. 20.7% increase compared to the initial tracer test and 9.4% compared to the first $MgCl_2$ injection phase. These results show how the surface area that plays a role in sulfate adsorption increases with time. Figure 20(b) also displays how the difference evolve through time, where the curves shift towards the right, and the maximal difference between the thiocyanate and sulfate tracer increases each time.

Three Kansas mixed wet samples KA2 to KA4 were used to test the hypothesis that $MgCl_2$ brine could modify the wetting state of mixed wet chalk. For the three samples, one, two and four tracer tests were performed. Each tracer test was performed after $MgCl_2$ brine was injected for 10 days in each phase at a rate of $1PV_i$/day at 130°C.

For KA2, KA3 and KA4, the initial tracer test yielded areas of 0.81×10^{-3} PV/g, 0.86×10^{-3} PV/g and, 0.86×10^{-3} PV/g, respectively. This implies a water wetness of 0.56, 0.59 and 0.59 for the three cores (using equation (30)), respectively, by using the area estimated for the water wet reference sample KA1 (1.45×10^{-3} PV/g).

For the three cores after 10 days $MgCl_2$ injection at 130°C, the area between thiocyanate and sulfate concentration curves changed to 1.41×10^{-3} PV/g, 1.38×10^{-3} PV/g, and 1.35×10^{-3} PV/g, respectively. The corresponding wetting indices changed to 0.97, 0.95 and 0.93 for KA2, KA3 and KA4, respectively, which corresponds to an increase in the water wet surface area by a factor of 1.73, 1.61 and 1.57 compared to the surface area before $MgCl_2$ injection started. Then, KA2 was dismantled while further $MgCl_2$ injection of KA3 and KA4 continued.

After another 10 days of $MgCl_2$ injection at 130°C, the water wet surface area of KA3 and KA4 increased to 1.50×10^{-3} PV/g and 1.55×10^{-3} PV/g, namely an increase of the water wet surface available for sulfate adsorption by a factor 1.74 and 1.80 compared to initial measurement. Both these values are greater than the KA1 reference of 1.45×10^{-3} PV/g, implying that the water wet surface area increased to more than the surface area of 100% water wet core. After this second $MgCl_2$ injection phase, the KA3 sample was dismantled.

A third and fourth $MgCl_2$ injection phases of 10 days each were conducted for KA4. Here, the integrated area between the thiocyanate and sulfate curves increased to 1.62×10^{-3} PV/g and 1.71×10^{-3} PV/g, which corresponds to an increase by a factor of 1.88 and 1.99 compared to the initial value. The left column of Figure 21((a), (c) and (e)) displays normalized sulfate and thiocyanate concentrations and the right column ((b), (d) and (f)) displays the difference between sulfate and thiocyanate concentrations as function of number of PVs of SW1T injected for different tracer tests performed on mixed wet samples KA2, KA3 and KA4, respectively.

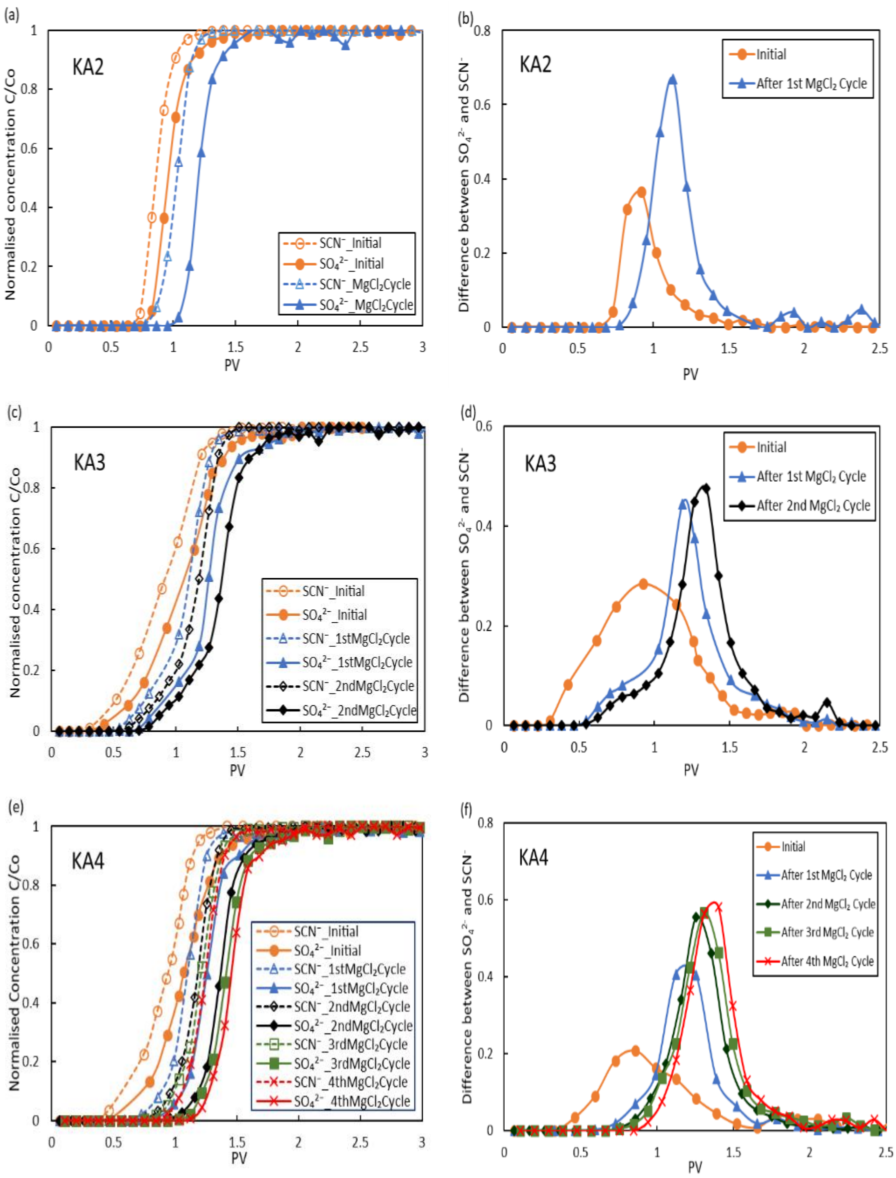

Figure 21. Chromatographic separation test at ambient temperature for the mixed wet samples KA2, KA3 and KA4. The left column ((a), (c) and (e)) displays normalized concentrations for thiocyanate (dashed curves) and sulfate (solid curves) and are shown for the initial tracer test (orange), and after 1st (blue), 2nd (black), 3rd (green), and 4th (red) injection phases of $MgCl_2$ brine each lasting 10 days. The right column ((b), (d) and (f)) displays the difference

between sulfate and thiocyanate. Clear trends in the difference are seen, the area increases, the peak increases and the curve is shifted to the right for each curve, see Table 9 and Figure 22 (see **Paper II**).

The plots (Figure 20 and Figure 21) show how the increase in sulfate concentration is delayed compared to the thiocyanate concentration when SW1T brine is injected. Table 9 summarizes the values of the area obtained between the sulfate and thiocyanate ions during tracer tests for all samples.

Table 9. Estimated integrated areas per gram of the sample for water and mixed wet samples, and the corresponding wettability indices. NaCl and $MgCl_2$ were injected at 130°C for chemical reactions to occur while tracer tests were conducted at ambient temperature.

Sample	**Timing of tracer test**	**Number of injection days at 130°C**	**Integrated sulfate – tracer area per gram sample (10^{-3}PV/g)**	**Wetting index (W_i)**
KA1 Water wet	Initial tracer test	0	1.45	1.00
	NaCl inj.	7.5	1.46	1.01
	1st $MgCl_2$ inj.	14.5	1.60	1.10
	2nd $MgCl_2$ inj.	21.5	1.75	1.21
KA2 Mixed wet	Initial tracer test	0	0.81	0.56
	$MgCl_2$ inj.	10.0	1.41	0.97
KA3 Mixed wet	Initial tracer test	0	0.86	0.59
	1st $MgCl_2$ inj.	10.0	1.38	0.95
	2nd $MgCl_2$ inj.	20.0	1.50	1.03
KA4 Mixed wet	Initial tracer test	0	0.86	0.59
	1st $MgCl_2$ inj.	10.0	1.35	0.93
	2nd $MgCl_2$ inj.	20.0	1.55	1.07
	3rd $MgCl_2$ inj.	30.0	1.62	1.12
	4th $MgCl_2$ inj.	40.0	1.71	1.18

The evolution in the areas spanned by the SCN^- and SO_4^{2-} curves per gram of the water wet KA1 sample in Figure 20(b) and the mixed wet samples KA2, KA3 and KA4 in Figure 21(b), (d) and (f) are displayed together in Figure 22. Here in Figure 22(a), it can be seen how the continuous $MgCl_2$ injection at 1 PV_i per day evolved the water wet area available for sulfate adsorption.

Further on, the estimated wetting index, when compared to the initial surface area of the 100% water wet core, evolved with increased amount of $MgCl_2$ injection (Figure 22(b)). After 20 days of $MgCl_2$ injection both KA3 and KA4 had a surface area exceeding the initial area of KA1, implying that the amount of water wet area in the core has increased. This is an indication that new mineral phases were growing from nucleation seeds within the cores which is in line with what has been observed for water wet chalk samples flooded by $MgCl_2$ brine previously (Andersen et al. 2018).

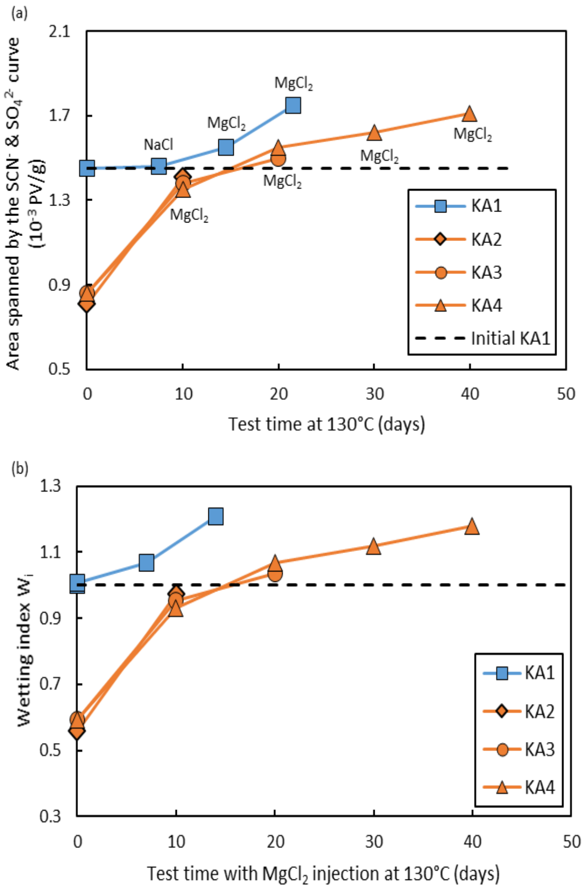

Figure 22. (a) Area spanned by the thiocyanate and sulfate concentration curves for water wet sample KA1 (blue) and mixed wet samples KA2, KA3 and KA4 (orange) as a function of test time at 130°C. (b) Evolution of wetting index as a function of $MgCl_2$ brine injection days at 130°C for all samples. The black dashed line in (b) gives the wetting index of a completely water wet core (equal to one) (see **Paper II**).

For the water wet sample KA1, the area obtained between the thiocyanate and sulfate curves remained the same after flooding NaCl brine as before the flooding, supporting the notion that Na^+ and Cl^- ions are inert to weakly reactive to the mineral surfaces in chalk. This is in-line with Madland et al. (2011). Later when the same sample was flooded by $MgCl_2$ brine, an increase in this area was observed with time (Table 9). The time-dependent chemical reactions between the brine and calcite minerals displayed in Figure 23 for the water wet sample KA1 are interpreted as a) magnesium adsorption on available surface sites, and b) dissolution of calcite and precipitation of secondary magnesium-bearing minerals, where the effluent magnesium concentration never reaches the injected concentration and triggers mineralogical changes in the chalk framework. The same behaviour has been reported in other similar experimental studies (Madland et al. 2009, 2011; Megawati et al. 2011; Nermoen et al. 2015; Zimmermann et al. 2015; Wang et al. 2016; Minde et al. 2017, 2018a; Andersen et al. 2018).

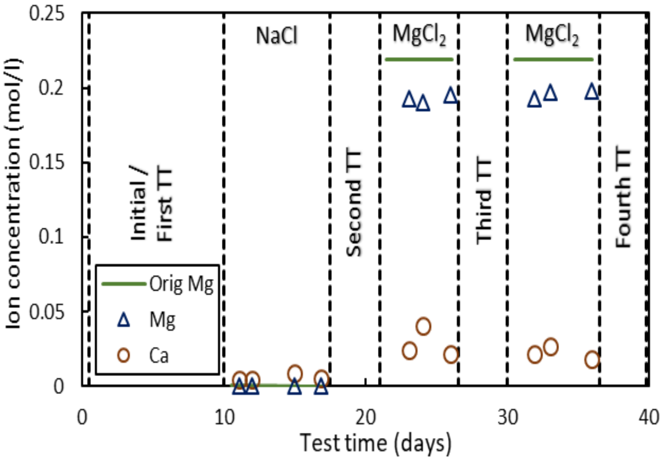

Figure 23. Effluent ion concentrations of calcium and magnesium ions, and the injected magnesium ion concentration over time are shown for the water wet sample KA1. The abbreviation TT stands for tracer test (see **Paper II**).

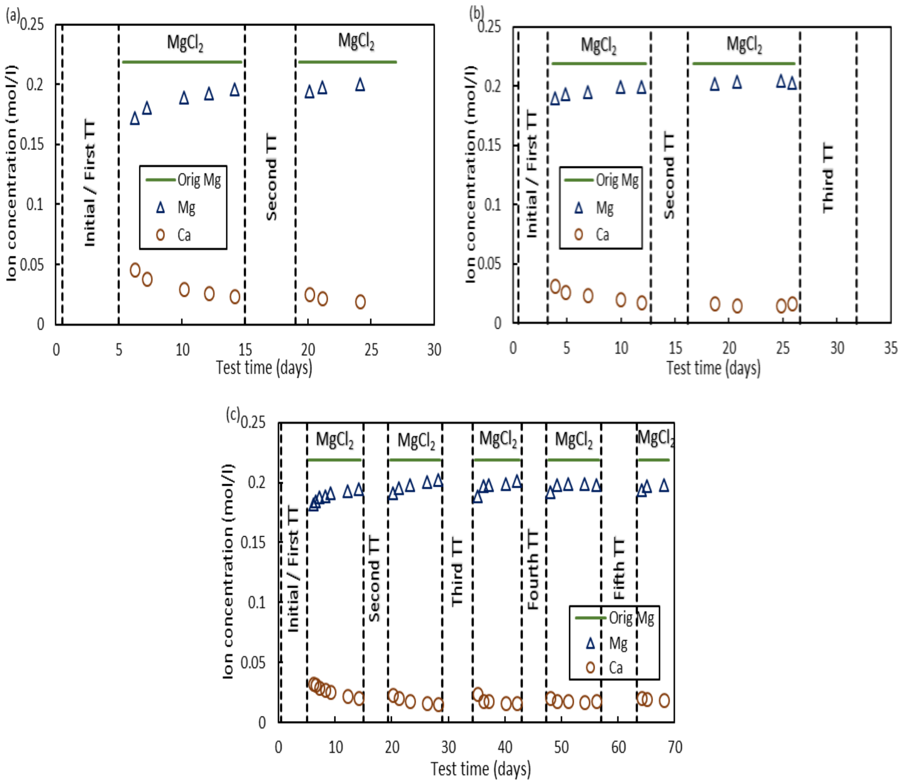

Figure 24. Effluent ion concentrations of calcium and magnesium ions, and the injected magnesium ion concentration over time are shown for the mixed wet samples (a) KA2, (b) KA3 and (c) KA4. The abbreviation TT stands for tracer test (see **Paper II**).

The mixed wet samples KA2, KA3 and KA4, which were also flooded by $MgCl_2$ brine, showed similar results in both IC data and evolution of water wet area where the brine flow increased the water wetness of the cores, as the water wet surface area increased after each 10 day $MgCl_2$ flooding cycle (Table 9). The wettability index of samples KA3 and KA4 exceeded 1 after the second $MgCl_2$ injection phase, implying that the available water wet surface area in these samples exceeded the total mineral area available for the water wet reference sample KA1. From the effluent analysis of these mixed wet samples (Figure 24), it is observed that calcium is produced and magnesium is retained in the samples throughout the injection period, in-line with the continuous dissolution/precipitation processes taking place in water saturated samples. Precipitated minerals have been documented to grow using Field Emission Gun Scanning Electron Microscopy (FEG-SEM) and EDX studies (Madland et al. 2011; Megawati et al. 2011; Nermoen et al. 2015; Zimmermann et al. 2015; Wang et al. 2016; Minde et al. 2017, 2018a, 2018b; Andersen et al. 2018).

4.2.5 Observations of oil volume development for the wettability-altered cores

The produced oil volume during flow and compaction was measured in a vertical column on the downstream side of the experimental setup and read off by eye at frequent time intervals. The results of the oil production are reported in Table 10. Based on the difference between the pore volume and measured oil volume, the water volumes were estimated through time.

Table 10. Initial and final oil and water volumes in wettability-altered Kansas cores K4 and K7 and Mons core M4.

Chalk type	**Kansas**		**Mons**
Wettability-altered core	**K4**	**K7**	**M4**
Injection brine	**$MgCl_2$**	**SSW**	**$MgCl_2$**
Irreducible water volume before test, ml	8.3	8.0	12.0
Irreducible water saturation S_{wi}, %	28.5	27.4	36.4
Initial oil volume, ml	20.8	21.2	21.0
Total produced oil at the end of the test, ml	8.8	9.8	11.2
Oil volume after test, ml	12.0	11.4	9.8
Oil saturation after test, %	49.4	45.2	41.4
Pore volume before and after test, ml	29.1 and 24.3	29.2 and 25.2	33.0 and 23.7

4.2.5.1 Oil volume development during $MgCl_2$ flow

4.2.5.1.1 Through Kansas chalk

Figure 25(a) shows the oil and water volumes and (b) the change in the saturation of oil inside the core with time from the start of hydrostatic loading for the wettability-altered Kansas core K4.

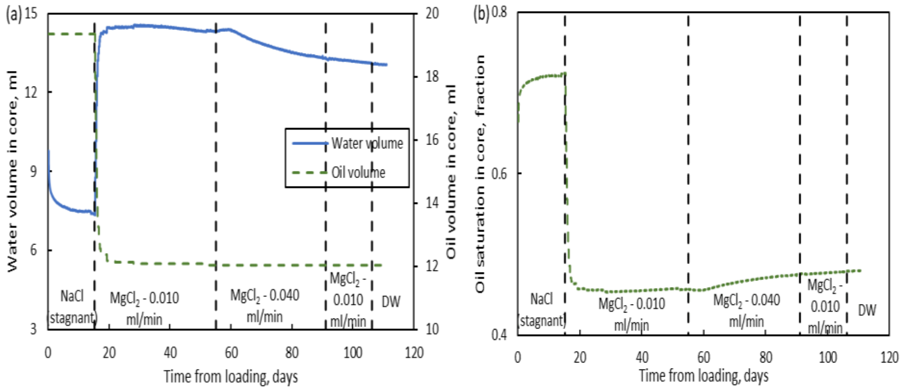

Figure 25. Wettability-altered Kansas sample K4. (a) Oil and water volumes in the core obtained from measurements of the oil volume produced, bulk volume from compaction and solid volume from chemical reactions and (b) oil saturation in the core with time from the start of hydrostatic loading. Black dashed vertical lines depict the time when brine composition and/or flow rate changed (see **Paper I**).

The heating of the cells led to production of oil interpreted to be caused by thermal expansion of oil. However, during loading and subsequent compaction without flow-through (stagnant NaCl brine in the pores), no additional oil was produced implying that, within the error of measurement, only water was expelled during compaction. When $MgCl_2$ flooding started, oil was produced immediately. After a certain time, however, the oil production ceased even though compaction and chemical reactions continued.

The increase in flow rate of $MgCl_2$ brine to 0.04 ml/min on the 56th day did not lead to additional oil production even though more than 57% of the initial oil was left inside the core. The additional dissolution of calcium and precipitation of magnesium triggered by the four-fold increase in flow rate (see Figure 17), and the four-fold increase in pressure drop across the core, did not have any effects on oil production. As observed from Figure 25(b), the oil saturation increases from 60 days and onwards. This is because compaction prevailed with time, but no more oil was recovered from the core. Therefore, the compaction occurred by reducing the water volume, whilst the oil volume remained constant.

Volumetric compaction by pore volume reduction only contributed to the expulsion of the free moving fluids in the pores, namely water. Even though the core deforms, and the pore volume decreases, neither compaction nor $MgCl_2$ brine induced chemical reactions lead to additional tail-end oil production. Two main reasons are used to interpret this: (1) oil is bonded and trapped on mineral surfaces in 50 nm to 0.1 μm thick oil films (calculated by dividing the immobile residual oil volume to the surface area of the sample), and (2) the oil droplets surrounded by water split up in smaller ganglia in which the pressure difference across is insufficient to overcome the capillary forces halting oil production.

4.2.5.1.2 Through Mons chalk

Figure 26(a) shows the oil and water volumes, and (b) the oil saturation inside the core throughout the duration of the test from the start of hydrostatic loading for the Mons wettability-altered core M4.

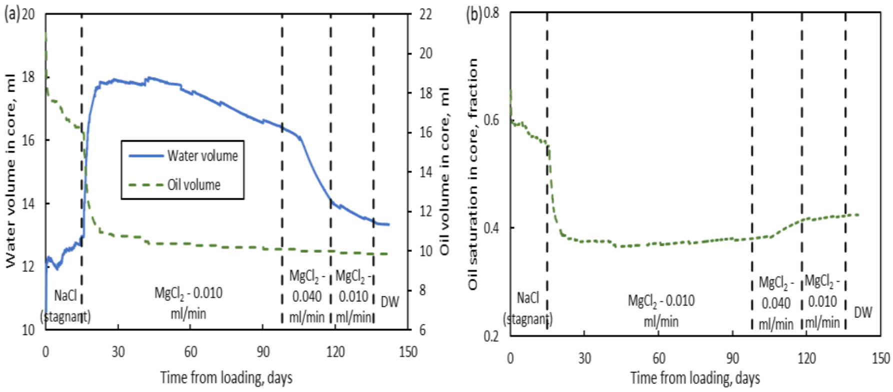

Figure 26. Wettability-altered Mons sample M4. (a) Oil and water volumes in the core obtained from measurements of the oil volume produced, bulk volume from compaction and solid volume from chemical reactions and (b) oil saturation in the core with time from the start of hydrostatic loading. Black dashed vertical lines depict the time when brine composition and/or flow rate changed (see **Paper III**).

During hydrostatic loading and no-flow creep period (up to 15th day), 4.7 ml oil was produced from wettability-altered Mons M4 core. Hence, deformation contributed to 43% of the total oil recovered after the initial thermal expansion. This value is comparable to the bulk volume loss of the sample (i.e. $\Delta V_s = \Delta V_p = \Delta V_{oil}$). Given that the water was not mobilized implies that oil was the mobile phase during compaction. After the first 15 days of creep, $MgCl_2$ was injected. In this phase, all the oil was produced during the initial 2-3 PVs, and after which despite the ongoing chemical reactions and compaction, negligible oil was produced from the core. This shows that the non-equilibrium rock-fluid interactions between the calcite surface and $MgCl_2$ brine did not contribute to any tail-end recovery after the initial displacement.

The increase in flow rate of $MgCl_2$ brine to 0.04 ml/min on the 98th day did not lead to any significant additional oil production. Therefore, the additional dissolution of calcium and precipitation of magnesium triggered by the four-fold increase in flow rate did not have any significant effect on the oil recovery. Even though pore volume decreased with time, the compaction caused by the imposed stresses led to expelling of only water from the core. Hence, oil saturation increased from 90 days and onwards (Figure 26(b)).

On the other hand, no oil was produced during the loading and the creep phase due to compaction and further no oil was recovered during $MgCl_2$ injection through wettability-altered Kansas chalk after the initial displacement. The recovery of oil from Mons chalk due to compaction is likely due to the fact that it is more water-wet (W_i of 0.63 ± 0.07) to start with compared to the wettability-altered Kansas chalk (W_i of 0.55 ± 0.05). Wettability-altered Mons M4 core also has a larger volumetric strain during loading and creep in the stagnant phase compared to the Kansas wettability-altered cores, which could also have resulted in production of oil. Kansas chalk also has a smaller pore size than Mons (Voake et al. 2019) and due to the capillary forces, they need the extra flow energy from the injection brine to produce oil. However, it remains to be tested how compaction-driven multiphase flow and geomechanical properties are changed for unaged oil/water saturated Kansas and Mons chalk samples.

4.2.5.2 Oil volume development during SSW flow

4.2.5.2.1 Through Kansas chalk

Similar observations were made for SSW flooded K7 core as for $MgCl_2$ flooded K4 sample. Figure 27(a) shows the oil and water volumes with time, and (b) displays the oil saturation inside the wettability-altered Kansas K7 core from the start of hydrostatic loading. No oil was observed during loading and insignificant amount of oil was obtained during the subsequent compaction in the course of the 15 days of bypass period. When SSW flooding started on the 16th day, oil was produced immediately but ceased after a certain time even though compaction and chemical reactions continued.

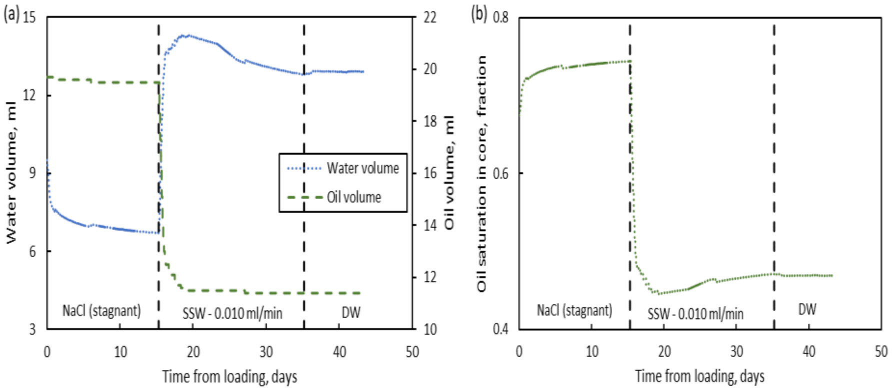

Figure 27. Wettability-altered Kansas sample K7. (a) Oil and water volumes in the core obtained from measurements of the oil volume produced, bulk volume from compaction and solid volume from chemical reactions and (b) oil saturation in the core with time from the start of hydrostatic loading. Black dashed vertical lines depict the time when brine composition changed (see **Paper I**).

The oil recovery observations showed that SSW flood gave 4% more oil recovery than $MgCl_2$ flood during the initial displacement of oil (46.2% oil recovery for K7 and 42.3% oil recovery for K4). This may indicate that SSW alters wettability favorably for oil recovery. However, after the initial displacement of oil during the flooding of these brines, the pore volume reduction did not change the volume of oil in the cores and only water was expelled. Combined observations of oil production during compaction and non-equilibrium flow imply that (a) $MgCl_2$ and SSW brines do not mobilize oil adsorbed on the rock surface, and (b) compaction do not contribute to oil production after the initial displacement. This observation is opposite to the interpretations of the Ekofisk production by Sulak and Danielsen (1989) where they concluded that compaction drive results in increased hydrocarbon recovery.

4.2.6 *Observations of specific surface area after tests for all cores*

The cores were cut into six equal sections after mechanical tests and tested for SSA using BET technique.

4.2.6.1 Specific surface area changes in Kansas chalk after tests

Measurements of the SSA of unaltered and unflooded Kansas chalk are reported in Table 11 where the untested end pieces are the ones that are left on each side during the cutting of the cylindrical cores. The untested SSAs are compared to six sections of the tested and flooded cores where section 1 represent the sample material placed close to the inlet and section 6 represent the outlet part. SSA measurements were not obtained on SSW flooded samples.

Table 11. Specific surface area measurements of unflooded core material from both sides of the core, and for sections along the core for K1 to K4 after test ($MgCl_2$ flooded samples).

Core	**K1**	**K2**	**K3**	**K4**
Core section	**Water-wet**		**Wettability-altered**	
	SSA, m^2/g	**SSA, m^2/g**	**SSA, m^2/g**	**SSA, m^2/g**
Outlet end-piece (Unflooded)	2.91	2.68	1.80	2.30
6	2.23 & 2.26	3.15 & 3.12	3.56 & 3.56	1.12 & 1.14
5	3.11	3.04	3.17	1.17
4	3.47 & 3.47	2.64	2.43 & 2.45	1.19 & 1.21
3	3.89	2.95 & 2.92	2.26	1.17
2	3.41	2.87	2.25	1.05
1	3.31 & 3.32	3.27 & 3.24	1.97 & 2.01	1.09 &1.04
Inlet end-piece (Unflooded)	3.20	2.98 & 2.99	1.57	2.50
Test time (days)	108.2	112.9	80.2	110.8

The non-homogenous chemical replacement dynamics are observed in the SSA measurements of Kansas cores (Table 11). The change in SSA was non-uniform through the cores. The trends were not clear, except that the SSA of cores K1, K3 and K4 increased from the inlet towards the middle of the samples. This may be because of the initial spatial variability in grain size through the core, and inherent uncertainty in the measurements themselves, so firm conclusions cannot be drawn. Andersen et al. (2018) also observed the non-homogeneous chemical replacement dynamics in $MgCl_2$ brine flooded water wet Kansas samples. They observed that the SSA decreased from the inlet towards the outlet of the samples.

4.2.6.2 Specific surface area changes in Mons chalk after tests

Measurements of the SSA of unaltered and unflooded Mons chalk are reported in Table 12 where the untested end pieces are the ones that are left on each side during the cutting of the cylindrical cores.

Table 12. Specific surface area measurements of unflooded core material from both sides of the core, and for sections along the core for Mons samples M1 to M4 after test ($MgCl_2$ flooded samples).

Core	**M1**	**M2**	**M3**	**M4**
Core section	**Water-wet**		**Wettability-altered**	
	SSA, m^2/g	**SSA, m^2/g**	**SSA, m^2/g**	**SSA, m^2/g**
Outlet end piece (unflooded)	1.82	1.98	2.11	1.96
6	2.33	2.26	2.20	2.02
5	2.47	2.43	2.14	2.08
4	2.45	2.49	2.39	2.44
3	2.45	2.46	2.55	2.45
2	2.47	2.49	3.05	2.82
1	2.18	2.40	3.35	3.02
Inlet end piece (unflooded)	2.13	2.05	2.22	2.17

The non-homogeneous chemical replacement dynamics were also observed in the SSA of Mons samples (Table 12). The SSA of water-wet Mons cores increase towards the middle of the core and then decrease towards the outlet, whereas the SSA of the wettability-altered cores decrease towards the outlet with the highest value observed at the inlet of the samples. Andersen et al. (2018) demonstrated that the SSA of the water-wet Mons chalk decreased from the inlet to the outlet sections of the samples. This difference in our results may be linked to the initial spatial variability in grain size through the cores, the number of pore volumes flooded through the cores or the flow rates of the injection fluids.

4.3 Implications on the industry

The chalk samples used in this study are analogues to the North Sea chalk reservoirs. The experimental results on both Kansas and Mons outcrop chalks have shown that the compaction rates, during the injection of reactive brines, are independent of the initial wettability and hence the initial oil/water saturation in the cores. This has been further confirmed by the ion chromatography carried out on effluent samples, which gave the observations on the rock-fluid interactions. This shows that the oil present in the pore spaces do not obstruct and block the path of the brine injected during waterflooding to contact the grain-grain contacts. Hence, the results obtained from the wettability-altered cores are similar to those from water-wet cases. Therefore, it is concluded that the results from the water-wet cores obtained from the experimental studies carried out in the past three decades are applicable to the real reservoir systems.

It is further expected that deeply buried and more diagenetically overprinted chalks, such as Ekofisk and Valhall chalk reservoirs in the Norwegian Continental Shelf, are predicted to behave very similar to Kansas outcrop chalk, and thereby show similar strength and stiffness response to injection brines as shown by Kansas chalk.

5 Conclusions and scope of future work

5.1 Conclusions

This study deals with the impact of initial wettability and reactive flow on chalk mechanics and oil recovery. Two different outcrop chalks from Kansas (USA) and Mons (Belgium) quarries were used as model materials in this study. The whole study was divided into two test programs: (a) Wettability determination program to determine the wetting state of the wettability-altered chalk, and (b) Triaxial test program in which the cores were hydrostatically loaded to 1.5 times yield stress and tested for their mechanical response to the applied external stress.

Impact of aging time
A study was performed to deduce the aging time required to obtain a stable wettability in Kansas chalk at the aging temperature of 90°C with 1.1M NaCl brine and oil mixture of 60% - 40% (by volume) Heidrun crude oil - heptane as the saturation fluids. The methods used to determine wettability were contact angle, USBM and SEM-MLA. The results showed that atleast 21 days of aging time is required to obtain a stable wettability at the specified aging conditions. Similar investigations are needed to deduce the aging time for obtaining stable wettability in Mons chalk.

Determining wettability
The wettability of all chalk cores used in the triaxial test program was altered in the same way at the specified conditions and aged for 21 days at 90°C. The wettability was determined using the chromatographic separation method. The wettability-altered Kansas and Mons samples gave a wetting index of 0.55 ± 0.05 and 0.63 ± 0.07, respectively. Even though both obtained a neutral wet state, the wetting indices obtained were still different for the two chalk types. This shows that the mineralogy of the two chalks play a role in determining their wettability

at the same aging conditions. It is likely that the presence of silicates and clay in Kansas chalk make it more oil wet compared to Mons chalk which is very pure.

Elastic and plastic parameters

During loading with no flow-through of NaCl brine and at 130°C, the water-wet and wettability-altered Mons samples showed similar stiffnesses and strengths. On the other hand, the wettability-altered Kansas samples showed 33% higher stiffnesses and 35% higher strengths compared to the water-wet Kansas samples. This is likely due to oil replacing water on surface areas where electrical double layers would interact if only water was found in the pores. This leads to reduced disjoining pressure, and thereby increased normal force between particles, which makes particles re-organizing by sliding more difficult. This is an interpretation for why geomechanical parameters for Kansas chalk are affected by wettability alteration, while they remain unaffected for Mons. The importance of the overlapping double layers is more pronounced for Kansas chalk because of its smaller Biot coefficient and smaller pore size than Mons chalk.

Time dependent deformation

During the creep phase, the strain rates followed a comparable trend independent of wetting state for both Kansas and Mons chalk types. This observation was found to be the same during both the bypass period (first 15 days) and the flow of reactive brines. Injection of reactive brines induced chemical reactions leading to additional creep rates in both chalk types.

Geochemical interactions – on the impact of oil

Geochemical effects (shown by IC of the effluent samples) are also not found to be affected by the presence of oil and the initial wetness of the cores. In all cases irrespective of the brine composition, the initial oil/brine saturation and wettability, the calcium concentration increases and the magnesium concentration decreases in the effluent (in $MgCl_2$

flooded samples). This is linked to the dissolution of calcite as well as precipitation of magnesium carbonate and adsorption of magnesium ions onto and desorption of calcium ions from the calcite surface. Effluent analysis also showed a reduction in the sulfate concentration in the effluents from SSW flooded samples. This is linked to the adsorption of sulfate ions on the charged calcite surfaces. As shown in the presented evidence, the presence of oil in the pores does not alter the dissolution/precipitation driven water weakening dynamics, neither qualitatively nor quantitatively. It is also shown how chemical reactions drive reduction in the solid volume by reducing the overall mass for $MgCl_2$ flooded samples and increasing the mineral density, and how this behavior is linked to the creep rate with time.

Hence, it was shown that as wettability has minimal to no effect on the compaction rates and geochemical effects during the injection of reactive brines through both water-wet and wettability-altered chalk samples, the results from the water-wet cores (obtained from the experimental studies in the past three decades) are applicable to the real reservoir systems.

Multiphase transport – oil production with time

The oil recovery from the wettability-altered Kansas and Mons samples was continuously monitored during the loading and creep periods. The results from Kansas chalk showed that after the initial displacement of mobile oil during injection of $MgCl_2$ and SSW brines, there was no additional oil recovery due to ongoing compaction or non-equilibrium brine flow. On the other hand, wettability-altered Mons samples showed 43% oil recovery through compaction even before the injection of $MgCl_2$ brine started. This oil production may be linked to the partitioning of oil and water in Mons samples after aging, which probably differs from Kansas samples as wettability-altered Mons samples were more water wet to start with compared to Kansas samples. After the displacement of oil during the first 2-3 PVs of $MgCl_2$ injection, no tail-end oil recovery was observed in the later stages. This is likely due to the fact that the injected brines are not able to mobilize the oil bonded on the walls or the pressure difference across the oil ganglia is insufficient to overcome capillary forces.

Petrophysical changes
The non-homogenous chemical replacement dynamics were observed in the SSA measurements of both Kansas and Mons cores. The trends were not clear for Kansas chalk and further investigations are required to draw any firm conclusion. However, the SSA measurements of Mons chalk after tests have shown to be clearly affected by the wetting state. The wettability-altered Mons cores showed the highest value of SSA at the inlet decreasing towards the outlet whereas the SSA of water-wet Mons cores increased towards the middle and then decreased towards the outlet of the samples.

Overall, the results have shown that although the injection of reactive brines through chalk lead to enhanced compaction, which is found to be insensitive to the wetness of the samples, it does not lead to any tail-end oil recovery.

5.2 Scope of future work

This study opens the scope for a detailed future work which can include:

a) Geochemical analysis of the flooded core samples to compare the changes in the solid framework of water-wet and wettability-altered samples.
b) Tuning wettability in lab since wettability impacts how oil and water are partitioned within the pores, followed by measuring if compaction and chemical reactions would mobilize oil either at lower or higher wettability indexes.
c) Hydrostatic loading of the wettability-altered samples to check for the reproducibility of the geomechanical results in this study at different aging conditions.

d) Hydrostatically loading to different stress levels above yield to check if a similar response in the creep rates is observed with both $MgCl_2$ and SSW brines.
e) Injecting brines with different compositions to optimize the oil recovery and minimize chalk compaction.
f) The wettability impacts how oil and water are partitioned within the pores. Hence, it would be important to check for the effect of this spatial partitioning of oil and water on the enhanced oil recovery by compaction.
g) Analytical and numerical modeling to define strain partitioning in the geomechanical experiments performed on chalk.

6 References

Ahsan, R. and Fabricius, I.L., 2010. Sorption of magnesium and sulfate ions on calcite. In 72nd EAGE Conference and Exhibition incorporating SPE EUROPEC 2010, Extended Abstracts, SP13.

Alam, M.M., Ahsan, R., Shaik, A.K., and Fabricius, I.L., 2010. Surface charge of calcite and its influence on the electrical conductivity in chalk. In 80th Annual International Meeting, Society of Exploration Geophysicists, Expanded Abstracts, 2686-2691.

Andersen, M.A., Foeged, N., and Pedersen, H.F., 1992. The Link between Waterflood-Induced Compaction and Rate-Sensitive Behavior in a Weak North Sea Chalk. In: *Proceedings of the Fourth North Sea Chalk Symposium*, Deauville, France, September.

Andersen, P.Ø., Wang, W., Madland, M.V., Zimmermann, U., Korsnes, R.I., Bertolino, S.R.A., Minde, M., Schulz, B., and Gilbricht, S., 2018. Comparative Study of Five Outcrop Chalks Flooded at Reservoir Conditions: Chemo-mechanical Behaviour and Profiles of Compositional Alteration. *Transport in Porous Media*, **121**(1), 135-181.

Anderson, W.G., 1986. Wettability Literature Survey - Part 1: Rock/Oil/Brine Interactions and the Effects of Core Handling on Wettability. *Journal of Petroleum Technology*, **38**(10), 1125-1144.

Andreassen, K.A. and Fabricius, I.L., 2010. Biot critical frequency applied to description of failure and yield of highly porous chalk with different pore fluids. *Geophysics*, **75**(6), E205-E213.

Borromeo, L., Egeland, N., Minde, M.W., Zimmermann, U., Andò, S., Madland, M.V. and Korsnes, R.I., 2018. Quick, Easy, and Economic Mineralogical Studies of Flooded Chalk for EOR Experiments Using Raman Spectroscopy. *Minerals*, **8**(6), 221. ISSN 2075-163X. https://doi.org/10.3390/min8060221.

Brunauer, S., Emmett, P.H., and Teller, E., 1938. Adsorption of gases in multimolecular layers. *Journal of the American chemical society*, **60**(2), 309-319.

Burchette, T.P., 2012. Carbonate Rocks and Petroleum Reservoirs: A Geological Perspective from the Industry. *Geological Society,* London, Special Publications, **370**(1), 17-37.

Coto, B., Martos, C., Peña, J. L., Rodríguez, R., and Pastor, G., 2012. Effects in the solubility of $CaCO_3$: Experimental study and model description. *Fluid Phase Equilibria*, **324**, 1-7.

Cuiec, L., Bourbiaux, B., and Kalaydjian, F., 1994. Oil recovery by imbibition in low-permeability chalk. *SPE Formation Evaluation (Society of Petroleum Engineers); (United States)*, **9**(3).

Donaldson, E.C., 1981. Oil-water-rock wettability measurement. *Am. Chem. Soc., Div. Pet. Chem., Prepr.; (United States)*, *26*(CONF-810308-(Vol. 1)).

Donaldson, E.C., Kendall, R.F., Pavelka, E.A., and Crocker, M.E., 1980. Equipment and procedures for fluid flow and wettability tests of geological materials (No. DOE/BETC/IC-79/5). Department of Energy, Bartlesville, OK (USA). Bartlesville Energy Technology Center.

Donaldson, E.C., Thomas, R.D., and Lorenz, P.B., 1969. Wettability Determination and Its Effect on Recovery Efficiency. *SPE Journal*, **9**(1), 13–20.

Doornhof, D., Kristiansen, T.G., Nagel, N.B., Pattillo, P.D., and Sayers, C., 2006. Compaction and Subsidence. *Oilfield Review*, **18**, 50-68.

Fan, T. and Buckley, J.S., 2007. Acid number measurements revisited. *SPE Journal*, **12**(04), 496-500.

Fathi, S.J., Austad, T., and Strand, S., 2010. "Smart Water" as a Wettability Modifier in Chalk: The Effect of Salinity and Ionic Composition. *Energy & Fuels,* **24**(4), 2514-2519. http://dx.doi.org/10.1021/ef901304m.

Fjær E., Holt, R.M., Horsrud, P., Raaen, A.M., and Risnes, R., 2008. *Petroleum related rock mechanics*, 2nd Ed., Amsterdam: Elsevier.

Flügel, E., 2004. *Microfacies of Carbonate Rocks: Analysis, Interpretation and Application*. Springer Science & Business Media.

Gauer, P.R., Sylte, J.E., and Nagel, N.B., 2002. Ekofisk Field Well Log Decompaction. Paper SPE/ISRM 78177 presented at the Rock Mechanics Conference, Irving, Texas, October 20-23.

Graue, A., Viksund, B.G., and Baldwin, B.A., 1999. Reproducible wettability alteration of low-permeable outcrop chalk. *SPE Reservoir Evaluation & Engineering,* **2**(02), 134-140.

Hassler, G.L., and Brunner, E., 1945. Measurement of capillary pressures in small core samples. *Trans. AIME*, **160**,114-123.

Hattin, D.E., and Cobban, W.A., 1977. Upper Cretaceous stratigraphy, paleontology, and paleoecology of western Kansas. *The Mountain Geologist* **14**(3-4):175–217

Heggheim, T., Madland, M.V., Risnes, R., and Austad, T., 2005. A Chemical Induced Enhanced Weakening of Chalk by Seawater. *Journal of Petroleum Science and Engineering*, **46**, 171-184.

Hellmann, R., Renders, P.J.N., Gratier, J.P., and Guiguet, R., 2002a. Experimental pressure solution compaction of chalk in aqueous solutions. Part 1. Deformation behavior and chemistry. *Water-Rock Interactions, Ore Deposits, and Environmental Geochemistry: A Tribute to David A. Crerar,* **7**(7), 129–152.

Hellmann, R., Gaviglio, P., Renders, P.J.N., Gratier, J.P., Bekri, S., and Adler, P., 2002b. Experimental pressure solution compaction of chalk in aqueous solutions. Part 2. Deformation examined by SEM, porosimetry, synthetic permeability, and X-ray computerized tomography. *Water-Rock Interactions, Ore Deposits, and Environmental Geochemistry: A Tribute to David A. Crerar*, **7**(7), 153–178.

Hermansen, H., Landa, G.H., Sylte, J.E., and Thomas, L.K., 2000. Experiences after 10 years of waterflooding the Ekofisk field, Norway. *Journal of Petroleum Science and Engineering*, **26**, 11–18.

Hermansen, H., Thomas, L.K., Sylte, J.E., and Aasbøe, B.T., 1997. Twenty Five Years of Ekofisk Reservoir Management. Paper SPE 38927 presented at the SPE Annual Technical Conference and Exhibition, San Antonio, Texas, USA, October 5-8.

Heugas, O. and Charlez, P., 1990. Mechanical effect of the water injection on Ekofisk chalk. In: Third North Sea Chalk Symposium, Copenhagen, Denmark.

Hiorth, A., Cathles, L.M., and Madland, M.V., 2010. The impact of pore water chemistry on carbonate surface charge and oil wettability. *Transport in porous media*, **85**(1), 1-21.

Hiorth, A., Jettestuen, E., Cathles, L.M., and Madland, M.V., 2013. Precipitation, Dissolution, and Ion Exchange Processes Coupled with a Lattice Boltzmann Advection Diffusion Solver. *Geochimica et Cosmochimica Acta*, **104**, 99–110. http://dx.doi.org/10.1016/j.gca.2012.11.019.

Hjuler, M.L., and Fabricius, I.L., 2009. Engineering properties of chalk related to diagenetic variations of Upper Cretaceous onshore and offshore chalk in the North Sea area. *Journal of Petroleum Science and Engineering*, **68**(3-4), 151-170.

Johnson, J.P. and Rhett, D.W., 1986. Compaction Behavior of Ekofisk Chalk as a Function of Stress. Paper SPE 15872 presented at the European Petroleum Conference, London, United Kingdom, October 20-22. doi: 10.2118/15872-MS.

Katika, K., Addassi, M., Alam, M.M., and Fabricius, I.L., 2015. The effect of divalent ions on the elasticity and pore collapse of chalk evaluated from compressional wave velocity and low-field Nuclear Magnetic Resonance (NMR). *Journal of Petroleum Science and Engineering*, **136**, 88-99.

Korsnes, R.I., Madland, M.V., and Austad, T., 2006a. Impact of Brine Composition on the Mechanical Strength of Chalk at High Temperature. *Eurock 2006: Multiphysics Coupling and Long Term Behaviour in Rock Mechanics*, Taylor and Francis, London, 133-140.

Korsnes, R.I., Strand, S., Hoff, O., Pedersen, T., Madland, M.V., and Austad, T., 2006b. Does the Chemical Interaction between Seawater and Chalk affect the Mechanical Properties of Chalk? *Eurock 2006: Multiphysics Coupling and Long Term Behaviour in Rock Mechanics*, Taylor and Francis, London, 427-434.

Korsnes, R.I., Madland, M.V., Austad, T., Haver, S., and Røsland, G., 2008. The Effects of Temperature on the Water Weakening of Chalk by Seawater. *Journal of Petroleum Science and Engineering*, **60**, 183-193.

Kristiansen, T.G., Barkved, O.I., Buer, K., and Bakke, R., 2005. Production-Induced Deformations Outside the Reservoir and Their Impact on 4D Seismic. Paper IPTC 10818 presented at the International Petroleum Technology Conference, Doha, Qatar, November 21-23. http://dx.doi.org/10.2523/IPTC-10818-MS.

Liteanu, E., Spiers, C.J., and de Bresser, J.H.P., 2013. The influence of water and supercritical CO_2 on the failure behavior of chalk, *Tectonophysics*, **599**, 157–169. doi: 10.1016/j.tecto.2013.04.013.

Liu, J., Wani, O.B., Alhassan, S.M., and Pantelides, S.T., 2018. Wettability Alteration and Enhanced Oil Recovery Induced by Proximal Adsorption of Na^+, Cl^-, Ca^{2+}, Mg^{2+}, and SO_4^{2-} Ions on Calcite. *Physical Review Applied*, **10**(3), 034064.

Longman, M.W., B.A. Luneau, and S.M. Landon, 1998. Nature and Distribution of Niobrara Lithologies in the Cretaceous Western Interior of the Rocky Mountain Region. *The Mountain Geologist*, **35**, 137-170.

Lord, C.J., Johlman, C.L., and Rhett, D.W., 1998. Is capillary suction a viable cohesive mechanism in chalk? In: SPE/ISRM Rock Mechanics in Petroleum Engineering, Trondheim, Norway.

Lucia, F.J., 1992, Carbonate Reservoir Models: Facies, Diagenesis, and Flow Characterization: Part 6. Geological Methods, *ME 10: Development Geology Reference Manual*, AAPG Spec. Pub. Type: Methods in Exploration, A095, 269-274.

Lyklema, J., 2005. *Fundamentals of interface and colloid science: soft colloids*, **5**. San Diego, USA: Elsevier, Academic Press.

MacDonald, G.J., 1956. Experimental determination of calcite-aragonite equilibrium relations at elevated temperatures and pressures. *American Mineralogist: Journal of Earth and Planetary Materials*, **41**(9-10), 744-756.

Madland, M.V., Hiorth, A., Korsnes, R.I., Evje, S., and Cathles, L., 2009. Rock Fluid Interactions in Chalk Exposed to Injection of Seawater, $MgCl_2$, and NaCl Brines with Equal Ionic Strength. Paper A22 presented at the 15th European Symposium on Improved Oil Recovery, Paris, France, April 27-29.

Madland, M.V., Hiorth, A., Omdal, E., Megawati, M., Hildebrand-Habel, T., Korsnes, R.I., Evje, S., and Cathles, L.M., 2011. Chemical Alterations Induced by Rock-Fluid Interactions when Injecting Brines in High Porosity Chalks. *Transport in Porous Media*, **87**, 679-702.

Madland, M.V., Midtgarden, K., Manafov, R., Korsnes, R.I., Kristiansen, T.G., and Hiorth, A., 2008. The Effect of Temperature and Brine Composition on the Mechanical Strength of Kansas Chalk. Paper SCA2008-55 presented at the International Symposium of the Society of Core Analysts, Abu Dhabi, UAE, October 29-November 2.

Maury, V., Piau, J.M., and Halle, G., 1996. Subsidence induced by water injection in water sensitive reservoir rocks: The example of Ekofisk. Paper SPE 36890 presented at the SPE European Petroleum Conference, Milan, Italy, October 22-24.

McPhee, C., Reed, J., and Zubizarreta, I., 2015. *Core Analysis: A Best Practice Guide,* **64**, 313-345, Amsterdam: Elsevier.

Megawati, M., Andersen, P.Ø., Korsnes, R.I., Evje, S., Hiorth, A., and Madland, M.V., 2011. The effect of aqueous chemistry pH on the time-dependent deformation behavior of chalk experimental and modelling study. In: Pore2Fluid International Conference. 16–18 Nov, Paris, France.

Megawati, M., Hiorth, A., and Madland, M.V., 2013. The Impact of Surface Charge on the Mechanical Behaviour of High-Porosity Chalk. *Rock Mechanics and Rock Engineering*, **46**(5), 1073-1090.

Megawati, M., Madland, M.V., and Hiorth, A., 2015. Mechanical and Physical Behavior of High-Porosity Chalks Exposed to Chemical Perturbation. *Journal of Petroleum Science and Engineering*, **133**, 313-327.

Minde, M.W., Haser, S., Korsnes, R.I., Zimmermann, U., and Madland, M.V., 2017. Comparative Studies of Mineralogical Alterations of Three Ultra-long-term Tests of Onshore Chalk at Reservoir Conditions. In: 19th European Symposium on Improved Oil Recovery/IOR Norway 2017. European Association of Geoscientists and Engineers. ISBN 978-94-6282-209-2.

Minde, M.W., Zimmermann, U., Madland, M.V., Korsnes, R.I., Schulz, B. and Gilbricht, S., 2018a. Mineral Replacement in Long-Term Flooded Porous Carbonate Rocks. Submitted to *Geochimica et Cosmochimica Acta*, publication under review.

Minde, M.W., Wang, W., Madland, M.V., Zimmermann, U., Korsnes, R.I., Bertolino, S.R., and Andersen, P.Ø., 2018b. Temperature effects on rock engineering properties and rock-fluid chemistry in opal-CT-bearing chalk. *Journal of Petroleum Science and Engineering*, **169**, 454-470.

Nagel, N.B., 1998. Ekofisk Field Overburden Modelling. Paper SPE 47345 presented at the SPE/ISRM Rock Mechanics in Petroleum Engineering, Trondheim, Norway, July 8-10.

Nermoen, A., Korsnes, R.I., Haug, S., Hiorth, A., and Madland, M.V., 2014. The dynamic stability of chalks during flooding of non-equilibrium brines and CO_2, Stavanger: Fourth EAGE CO_2 Geological Storage Workshop, Demonstrating Storage Integrity and Building Confidence in CCS.

Nermoen, A., Korsnes, R.I., Hiorth, A. and Madland, M.V., 2015. Porosity and Permeability Development in Compacting Chalks during Flooding of Non-Equilibrium Brines: Insights from Long-Term Experiment. *Journal of Geophysical Research: Solid Earth*, **120**. https://doi.org/10.1002/2014JB011631

Nermoen, A., Korsnes, R.I., Aursjø, O., Madland, M.V., Kjørslevik, T.A.C., and Østensen, G., 2016. How Stress and Temperature Conditions Affect Rock-Fluid Chemistry and Mechanical Deformation. *Frontiers in Physics*. http://dx.doi.org/10.3389/fphy.2016.00002.

Nermoen, A., Korsnes, R.I., Storm, E.V., Stødle, T., Madland, M.V., and Fabricius, I.L., 2018a. Incorporating electrostatic effects into the effective stress relation – insights from chalk experiments. *Geophysics*, **83**(3), 1-13.

Nermoen, A., 2018b. Porosity Evolution during Chemo-Mechanical Compaction. doi: 10.5772/intechopen.72795.

Neveux, L., Grgic, D., Carpentier, C., Pirnon, J., Truche, L., and Girard, J.P., 2014a. Influence of hydrocarbon injection on the compaction by pressure solution of a carbonate rock: An experimental study under triaxial stresses. *Marine and Petroleum Geology*, **55**, 282–294.

Neveux, L., Grgic, D., Carpentier, C., Pironon, J., Truche, L., and Girard, J.P., 2014b. Experimental simulation of chemomechanical processes during deep burial diagenesis of carbonate rocks. *Journal of Geophysical Research: Solid Earth*, **119**(2), 984–1007. https://doi.org/10.1002/2013JB010516

Overview Greater Ekofisk Area, ConocoPhillips Norway, 2019, http://www.conocophillips.no/our-norway-operations/greater-ekofisk-area/overview/ (viewed on 11.05.2019).

Piau, J.M. and Maury, V., 1994. Mechanical effects of water injection in chalk reservoirs. In: SPE/ISRM Rock Mechanics in Petroleum Engineering, Delft, Netherlands.

Richard, J., Sizun, J.P., and Machhour, L., 2005. Environmental and diagenetic records from a new reference section for the Boreal realm: the Campanian chalk of the Mons basin (Belgium). *Sedimentary Geology*, **178**(1-2), 99-111.

Risnes, R., 2001. Deformation and Yield in High Porosity Outcrop Chalk. *Phys. Chem. Earth* (A), **26**, 53-57.

Risnes, R., Haghighi, H., Korsnes, R.I., and Natvik, O., 2003. Chalk-Fluid Interactions with Glycol and Brines. *Tectonophysics*, **370**, 213-226.

Roehl, P.O. and Choquette, P.W. (Eds.), 1985. *Carbonate Petroleum Reservoirs*. New York: Springer.

Runnels, R.T., and Dubins, I.M., 1949. Chemical and petrographic studies of the Fort Hays Chalk in Kansas. *Kansas Geological Survey Bulletin*, **82**, 1-36.

Schroeder, C. and Shao, J., 1996. Plastic deformation and capillary effects in chalks. In: *Proceedings of the 5th North Sea Chalk Symposium*, Reims, France.

Sripal, E. and James, L.A., 2016. Application of an Optimization Method for Restoration of Core Samples for SCAL Experiments. Paper SCA2016-002 presented at the International Symposium of the Society of Core Analysts, Snowmass, Colorado, USA, August 22–26.

Sripal, E. and James, L.A., 2018. Application of an Optimization Method for the Restoration of Core Samples for SCAL Experiments. *Petrophysics*, **59**(1), 72-81.

Standnes, D.C. and Austad, T., 2000a. Wettability alteration in chalk: 1. Preparation of core material and oil properties. *Journal of Petroleum Science and Engineering*, **28**(3), 111-121.

Standnes, D.C. and Austad, T., 2000b. Wettability alteration in chalk: 2. Mechanism for wettability alteration from oil-wet to water-wet using surfactants. *Journal of Petroleum Science and Engineering*, **28**(3), 123-143.

Strand, S., Standnes, D.C., and Austad, T., 2006. New Wettability Test for Chalk Based on Chromatographic Separation of SCN^- and SO_4^{2-}. *Journal of Petroleum Science and Engineering*, **52**, 187-197.

Strand, S., Hjuler, H.L., Torsvik, R., Pedersen, J.I., Madland, M.V., and Austad, T., 2007. Wettability of chalk: Impact of silica, clay content and mechanical properties. *Petroleum Geoscience*, **13**(1), 69-80.

Sulak, R.M., 1991. Ekofisk Field: The First 20 Years. *Journal of Petroleum Technology*, **43**(10), 1-265.

Sulak, R.M. and Danielsen, J., 1989. Reservoir Aspects of Ekofisk Subsidence. *Journal of Petroleum Technology*, **41**(7), 709-716, SPE 17852-PA.

Sylte, J.E., Thomas, L.K., Rhett, D.W., Bruning, D.D., and Nagel, N.B., 1999. Water Induced Compaction in the Ekofisk Field. Paper SPE 56426 presented at the SPE Annual Technical Conference and Exhibition, Houston, Texas, October 3-6.

Tang, G. and Firoozabadi, A., 2001. Effect of pressure gradient and initial water saturation on water injection in water-wet and mixed-wet fractured porous media. *SPE Reservoir Evaluation & Engineering* **4**(6): p. 516-524.

Teufel, L.W., Rett, D.W., and Farrell, H.E., 1991. Effect of reservoir depletion and pore pressure drawdown in in-situ stress and deformation in the Ekofisk field, North Sea. In: *Proceedings of the 32nd U.S. Rock Mechanics Symposium*, p. 63-72, Norman, Oklahoma, July 10-12.

Thomas, L.K., Dixon, T.N., Evans, C.E., and Vienot, M.E., 1987. Ekofisk Waterflood Pilot. *Journal of Petroleum Technology*, **39**(02), 221-232.

Voake, T., Nermoen, A., Ravnås, C., Korsnes, R.I., and Fabricius, I.L., 2019. Influence of temperature cycling and pore fluid on tensile strength of chalk. *Journal of Rock Mechanics and Geotechnical Engineering*, **11**(2), 277-288.

Wang, W., Madland, M.V., Zimmermann, U., Nermoen, A., Korsnes, R.I., Bertolino, S.R.A., and Hildebrand-Habel, T., 2016. Evaluation of porosity change during chemo-mechanical compaction in flooding experiments on Liège outcrop chalk. *Geological Society, London, Special Publications,* **435**(1), 26 October. https://doi.org/10.1144/SP435.10.

Wiborg, R., and Jewhurst, J., 1986. Ekofisk subsidence detailed and solutions assessed. *Oil & Gas Journal*, **84**(7), 47-51.

Zhang, P. and Austad, T., 2005. The Relative Effects of Acid Number and Temperature on Chalk Wettability. Paper SPE 92999 presented at SPE International Symposium on Oilfield Chemistry, Houstan, Texas, USA, February 2-4.

Zhang, P. and Austad, T., 2006. Wettability and oil recovery from carbonates: Effects of temperature and potential determining ions. *Colloids and Surfaces A: Physicochemical and Engineering Aspects*, **279**(1-3), 179-187.

Zhang, P., Tweheyo, M.T., and Austad, T., 2006. Wettability Alteration and Improved Oil Recovery in Chalk: The Effect of Calcium in the Presence of Sulfate. *Energy & Fuels*, **20**, 2056-2062.

Zhang, P., Tweheyo, M. T., and Austad, T., 2007. Wettability alteration and improved oil recovery by spontaneous imbibition of seawater into chalk: Impact of the potential determining ions Ca^{2+}, Mg^{2+}, and SO_4^{2-}. *Colloids and Surfaces A: Physicochemical and Engineering Aspects*, **301**(1-3), 199-208.

Zimmermann, U., Madland, M.V., Nermoen, A., Hildebrand-Habel, T., Bertolino, S.A.R., Hiorth, A., Korsnes, R.I., Audinot, J.N., and Grysan, P., 2015. Evaluation of the compositional changes during flooding of reactive fluids using scanning electron microscopy, nano-secondary ion mass spectrometry, x-ray diffraction and whole rock geochemistry. *AAPG (Am. Assoc. Pet. Geol.) Bulletin*, **99**(5), 791–805. http://dx.doi.org/10.1306/12221412196.

Appendix

Comparison of Kansas and Mons chalk types.

Table 13. Comparison of Kansas and Mons chalk types.

	Kansas	**Mons**
Carbonate content, %	95-97	> 99
Initial wettability index	0.55 ± 0.05	0.63 ± 0.07
Biot coefficient (Voake et al. 2019)	0.91	0.95
Initial porosity, %	35-38	42-44
Initial water saturation, %	26-29	31-38
Relaxation time T_2 from NMR studies, ms (Voake et al. 2019)	15-80	35-200

Paper I

Sachdeva, J.S., Nermoen, A., Korsnes, R.I., and Madland, M.V. (2019). Impact of Initial Wettability and Injection Brine Chemistry on Mechanical Behaviour of Kansas Chalk. *Transport in Porous Media*, **128**(2), 755-795. https://doi.org/10.1007/s11242-019-01269-z.

Paper II

Sachdeva, J.S., Muriel, H., Nermoen, A., Korsnes, R.I., and Madland, M.V. (2019). Chalk Surface Area Evolution during Flow of Reactive Brines: Does Oil Play a Role? *Energy & Fuels*, **33**(6), 4890-4908. https://doi.org/10.1021/acs.energyfuels.9b00515.

Paper III

Sachdeva, J.S., Nermoen, A., Korsnes, R.I., and Madland, M.V. (2019). Effect of Initial Wettability on Rock Mechanics and Oil Recovery: Comparative Study on Outcrop Chalks. Submitted to *Transport in Porous Media*, publication under review.

Effect of Initial Wettability on Rock Mechanics and Oil Recovery: Comparative Study on Outcrop Chalks

Jaspreet S. Sachdeva*[1,2], Anders Nermoen[1,3], Reidar I. Korsnes[1,2], Merete V. Madland[1,2]

[1]The National IOR Centre of Norway, University of Stavanger, Stavanger, Norway
[2]Department of Energy Resources, University of Stavanger, Stavanger, Norway
[3]Norwegian Research Centre AS, Oslo, Norway
*Corresponding author: Jaspreet Singh Sachdeva (jaspreet.s.sachdeva@uis.no)

Keywords:

- Improved Oil Recovery
- Water flooding
- Chalk compaction
- Wettability
- Geomechanics
- Oil production measurements

ABSTRACT

Brines containing surface-active divalent ions such as Ca^{2+}, Mg^{2+} and SO_4^{2-} impact the stiffness, strength and time-dependent deformation of water wet outcrop chalk from various locations. This study documents how stiffness and strength of wettability-altered oil and water saturated (mixed wet) chalk compares to water saturated samples during hydrostatic loading. During hydrostatic creep, the strain rate response to magnesium chloride ($MgCl_2$) brine injection is compared for water wet and mixed wet samples. For the mixed wet samples, the oil production was estimated during compaction and $MgCl_2$ flow. The results presented here were then compared to a similar test series on Kansas outcrop chalk. The differences were interpreted in terms of difference in physical parameters such as porosity and pore size.

The samples were wettability altered and tested in parallel at hydrostatic conditions and 130°C. It was found that the initial wettability controlled the plastic strength measurements of Mons chalk with initial resident fluids inside the pores but to a lesser extent than the corresponding Kansas chalk. Afterwards, when Mons cores were hydrostatically loaded to a stress level approximately 1.5 times yield, both water wet and wettability-altered Mons chalk samples gave comparable trends during a stagnant phase and a following $MgCl_2$ injection phase at varying flow rates. Similar observations were reported for water wet and wettability-altered Kansas chalk as well. It was also shown that the non-equilibrium chemical reactions were insensitive to the initial wettability for both Kansas and Mons chalks. The oil production observations, however, showed that 43% of the total oil was recovered during early-stage compaction from Mons chalk with no flow, whereas Kansas chalk did not produce any oil. No tail-end oil production was observed due to compaction or non-equilibrium brine flow in any of the two chalk types.

INTRODUCTION

The physico-chemical interactions between resident fluids and reservoir rock have an impact on the mechanical rock properties. This has led to considerable investigations towards searching for more optimal injection fluids. Chalk is a highly porous and a low permeable rock. Due to the large surface area in chalk, surface processes (dissolution/precipitation and adsorption/ desorption) dominate the bulk mechanical behaviour. Studies have shown that the injection of seawater into chalk lead to enhanced compaction of the reservoir rock and hence acts as an important driving mechanism to mobilise pore fluids towards production facilities, thereby leading to improved oil recovery rates (Sulak and Danielsen 1989; Sulak 1991; Hermansen et al. 2000). The enhanced reservoir compaction has also shown to induce seafloor subsidence which raises serious concerns related to the safety of personnel on the platforms and the equipment in the wellbore (Sulak and Danielsen 1989; Maury et al. 1996; Nagel 1998; Sylte et al. 1999; Gauer et al. 2002). This compaction has been found to be caused by both pore pressure depletion early in the field life and water weakening induced by seawater injection during the later stages (Gauer et al. 2002).

Research on how chalk mechanics was affected by pore fluid composition intensified after the detection of subsidence at Ekofisk field (Norwegian Continental Shelf). A key research question had been to find how the mechanical chalk properties were affected by aqueous chemistry, with focus on elastic stiffness, plastic strength and time-dependent creep deformation rates (Risnes 2001; Hellmann et al. 2002a, 2002b; Risnes et al. 2003; Korsnes et al. 2006a, 2006b, 2008; Madland et al. 2008, 2011; Megawati et al. 2011, 2013; Neveux et al. 2014a, 2014b). The relationship between chalk mechanics and pore fluid chemistry has been important to the petroleum industry (Hermansen et al. 2000; Nagel 2001; Fabricius and Borre 2007).

Until now, the rock-mechanical studies have concentrated mostly on water wet and water saturated systems. It has been shown that the surface-active divalent ions, such as magnesium (Mg^{2+}) and sulphate (SO_4^{2-}), have a huge effect on the mechanical behaviour. Heggheim et al. (2005) observed that sulphate ions in the injected synthetic seawater (SSW) brine led to a reduced yield and caused weakening of chalk. Korsnes et al. (2008) also observed the same effect by demonstrating that flooding SSW containing sulphate ions through chalk yielded at a significantly lower stress compared to the samples flooded by SSW without sulphate ions. Megawati et al. (2011) showed that the reduction in yield is due to its adsorption on the charged calcite surface, which leads to a disjoining pressure at the grain-grain contacts and causes pore collapse failure at lower stresses.

When magnesium chloride ($MgCl_2$) brine is injected through chalk, dissolution of calcite $CaCO_3$ and precipitation of magnesite $MgCO_3$ occur (Madland et al. 2011; Nermoen et al. 2015; Zimmermann et al. 2015; Minde et al. 2017, 2018a, 2018b; Andersen et al. 2018). These dissolution/precipitation processes lead to enhanced bulk volume creep rates in chalk compared to when flooded with weakly reactive sodium chloride (NaCl) brine (Madland et al. 2009, 2011). Further, Nermoen et al. (2015) showed that the compaction rate was sensitive to the injection rate. At higher flooding rates, the rate of dissolution of calcite and precipitation of Mg-bearing minerals increased. The solid volume changed because the sample lost mass and the mineral density increased (density of magnesite is 3.0 g/cm^3 and calcite 2.7 g/cm^3). Further, the solid volume changes led to a reduction in bulk volume and the grains unlocked and reorganised to reduce pore volume. Long-term $MgCl_2$ flooding tests (516 days and 1072 days) on Liège water wet chalk (Belgium) altered the mineralogy from calcite to Mg-bearing minerals dominated by magnesite (Nermoen et al. 2015; Zimmermann et al. 2015; Minde et al. 2017; Borromeo et al. 2018). Mg^{2+} ions have also shown to adsorb on the calcite surface leading to desorption of calcium ions (Ahsan and Fabricius 2010; Alam et al. 2010; Nermoen et al. 2018). Nermoen et al. (2018) showed that adsorption of magnesium ions onto the charged calcite surface caused less weakening than when sulphates were present in the injection brine.

It has also been suggested that chemical reactions between the injected non-equilibrium brines and chalk surface lead to additional oil recovery (Hiorth et al. 2010) either due to rock dissolution or change in the surface charge during brine injection that affects rock wettability. For chemical reactions to be non-negligible, tens (or hundreds) of pore volumes are required. So, for chemical reactions to play a role in enhancing the oil recovery, it must be to mobilise oil after the initial displacement. This idea was tested in a recent study by Sachdeva et al. (2019). Here, however, no oil was produced during tail-end oil production through $MgCl_2$ flow even though chemical reactions and pore volume compaction occurred.

Megawati et al. (2015) and Andersen et al. (2018) studied five different chalk types and found a dependence of the non-carbonate content on how the mechanical creep behaviour was affected by $MgCl_2$ brine injection. Injecting this brine into impure chalks (Liège, Aalborg and Kansas) led to an immediate increased creep rate. However, in pure chalks (Mons and Stevns Klint) the creep response was delayed by a time lag of several weeks before a tertiary-like creep developed. These rock samples were never exposed to oil, which enabled the aqueous solution to contact the minerals directly. A question that has been raised is to what extent these results are applicable to actual chalk reservoirs. Chalk wettability has been studied extensively to understand how different wetting states affect multiphase fluid flow with focus on oil recovery (Standnes and Austad 2000a, 2000b; Zhang and Austad 2005; Strand et al. 2007). In the present study, we also focus on the mechanical stiffness, strength and creep rate dependencies upon brine injection into wettability-altered chalk, besides oil recovery.

Sachdeva et al. (2019) studied how wettability affected the mechanical behaviour of Kansas outcrop chalk saturated by oil-water mixture. It was found that the elastic stiffness and plastic strength were higher for mixed wet samples compared to water wet samples, and that when $MgCl_2$ brine was injected the on-going rock-fluid interactions led to enhanced creep rates, which was found to be applicable for both water wet and mixed wet samples. However, after the initial oil displacement during the first 2-3 pore volumes (PVs) injected, no additional oil was produced from the samples even though the chemical reactions from the rock-fluid interactions took place. Further, ongoing pore volume compaction also did not mobilise any additional oil from the samples.

This study shares the same objective as Sachdeva et al. (2019), but here we perform experiments on Mons chalk which is mineralogical purer than Kansas. The geochemical analyses carried out by Andersen et al. (2018) showed that the unflooded and untested chalk samples from these two quarries were dominated by CaO as expected. Kansas chalk samples were found to contain CaO between 54.2 and 55.1 weight percent (wt%) and relatively small amounts of non-carbonate phases such as SiO_2 (between 1.1 and 1.5 wt%), K_2O (0.1 wt%) and Al_2O_3 (0.3 to 0.5 wt%). Trace elements, such as Rb, Zr and Y, were also found to be in minute quantities with concentrations below 5 ppm. Mons chalk contained a slightly lower SiO_2 (0.98 wt%) than chalk cores from Kansas with CaO amounting to around 55 wt%. With Al_2O_3 as low as 0.2 wt% and even lower trace element concentrations, this chalk type was concluded to be cleaner than the Kansas chalk.

The premise of this study was to alter the wettability, test the reproducibility in the wettability alteration, document the relation between wettability and stiffness, strength and time-dependent mechanical behaviour, and finally to determine how tail-end oil recovery is affected by compaction and continuous flow of reactive brine. The wetting state of Mons chalk cores was altered to a mixed wet state prior to mechanical testing at high effective stresses and 130°C temperature. The results from how wettability-altered Mons chalk responded to $MgCl_2$ injection are compared to those carried out on Kansas chalk by Sachdeva et al. (2019).

This study emphasises on how differences in the initial pore fluid saturations and wettability affect the mechanical response of Mons chalk. It further highlights the effect of mineralogical changes on chalk mechanics. The bulk, solid and pore volumes as well as oil and water volumes are monitored continuously to observe how the volume dependencies are linked to deformations and injection of reactive $MgCl_2$ brine.

MATERIALS AND METHODS

Rock sample material

Chalk samples from a single block obtained from the Trivières Formation in Mons (Belgium) were used. This chalk belongs to Late Cretaceous age and is very pure (> 99 wt% calcite).

Ten cylindrical samples were cored, radially adjusted to 38.1 mm diameter, cut at desired lengths and dried at 110°C overnight before dry mass was measured. The samples were then vacuumed and saturated by distilled water (DW) to measure saturated mass. The mass difference between the dry and saturated sample was used to estimate pore volume and saturation porosity (Table 1).

The samples were divided into two test series:

- Six samples were used for wettability determination. Three samples were kept water wet and 100% water saturated (Mww) for reference, and the other three were wettability altered (Mmw), Table 1.
- Four samples were used in triaxial test program (M1 to M4). Two samples were kept water wet and 100% water saturated, and the other two were wettability altered, Table 1.

Table 1. Basic properties of samples used for wettability determination and triaxial tests.

	Core ID	**Wetting state**	**Core length (mm)**	**Core diameter (mm)**	**Dry mass (g)**	**Saturated mass (g)**	**Pore volume (ml)**	**Bulk volume (ml)**	**Saturation porosity ϕ (%)**
Wettability determination program	Mww1	Water wet	72.4	38.1	126.7	162.1	35.4	82.5	42.9
	Mww2		69.9	38.1	122.3	156.5	34.2	79.7	42.9
	Mww3		73.2	38.1	130.2	165.4	35.2	83.5	42.2
	Mmw1	Mixed wet	72.4	38.1	123.9	159.3	35.4	82.5	42.9
	Mmw2		68.9	38.1	122.1	156.3	34.2	78.6	43.5
	Mmw3		69.4	38.1	120.9	155.0	34.1	79.1	43.1
Triaxial test program	M1	Water wet	72.7	38.1	129.4	164.4	35.0	82.9	42.2
	M2		68.9	38.1	119.9	153.8	33.9	78.6	43.2
	M3	Mixed wet	68.9	38.1	119.7	153.7	34.0	78.6	43.3
	M4		68.8	38.1	122.0	155.0	33.0	78.4	42.1

Description of fluids

Four brine compositions were used. In the wettability determination program, two different versions of artificial seawater were used: SW1T brine contained sulphate (SO_4^{2-}) and thiocyanate (SCN^-) tracer while SW0T did not (Table 2). The total dissolved solids of SW1T and SW0T were equal to synthetic sea water (SSW). The two other brines used during the triaxial tests program (Table 2) were:

- 1.1 M NaCl brine for initial saturation to resemble resident formation fluids. NaCl brine moderately interacts with chalk (Madland et al. 2011; Ricci et al. 2013; Hofmann et al. 2016).
- 0.219 M $MgCl_2$ brine used as a flooding brine with equal ionic strength as seawater. This is injected to trigger dissolution/precipitation effects from the Ca-Mg exchange (Madland et al.

2009, 2011) and adsorption effects of magnesium ions on the calcite surface (Ahsan and Fabricius 2010; Alam et al. 2010; Nermoen et al. 2018; Liu et al. 2018).

A 60%-40% volume mixture of crude oil from the Heidrun field offshore Norway and heptane was used. The acid number of the Heidrun oil was measured to be 2.82 mg KOH/g, while the acid number of the oil mixture was 2.12 mg KOH/g measured according to the Fan and Buckley (2007) procedure.

Table 2. Composition of brines used in the wettability determination program and for core flooding in the triaxial test program.

	Wettability determination program		Triaxial test program	
Ions	**SW0T**	**SW1T**	**1.1 M NaCl**	**0.219 M $MgCl_2$**
	mol/l	**mol/l**	**mol/l**	**mol/l**
HCO_3^-	0.002	0.002	0	0
Cl^-	0.583	0.492	1.1	0.438
SO_4^{2-}	0	0.024	0	0
SCN^-	0	0.024	0	0
Mg^{2+}	0.045	0.045	0	0.219
Ca^{2+}	0.013	0.013	0	0
Na^+	0.460	0.393	1.1	0
Li^+	0	0.024	0	0
K^+	0.010	0.034	0	0
Ionic Strength	0.643	0.647	1.1	0.657
TDS (g/l)	33.39	33.39	64.28	44.52

Wettability alteration and fluid saturations

Five wettability-altered samples (three for wettability determination and two for triaxial tests) were treated according to the following procedure:

- Saturated by 1.1 M NaCl brine.
- Mounted in a Hassler cell and heated to 50°C. Flooded two pore volumes (PVs) of the oil mixture in each direction during which the produced brine was collected to estimate the initial water saturation S_{wi}.
- Submerged the samples in the same oil mixture in aging containers and left for 21 days at 90°C.

The wettability-altered samples were termed Mmw1 to Mmw3 in the wettability determination program and M3 & M4 in the triaxial test program. The water wet samples were simply saturated by 1.1M NaCl brine and were termed Mww1 to Mww3 in the wettability determination program and M1 & M2 in the triaxial test program.

Chromatographic separation for wettability determination

The chromatographic separation technique for wettability determination used here, and developed by Strand et al. (2006a), refers to how the effluent concentration profile of non-affine tracers differ from that of surface-active ions. The surface-active divalent sulphate anions (SO_4^{2-}) replace the monovalent anions on the positively charged calcite surface sites. Sulphate adsorption occur on mineral surface areas in contact with water, hence a key premise is that mineral surfaces covered by oil will not capture the injected sulphate ions. By co-injecting sulphate anions and non-affine thiocyanate (SCN^-) tracer, after being flooded by a brine stripped of these ions, the two effluent concentration profiles split as the increased concentration of the adsorbed ion is delayed compared to the non-affine tracer. The split, measured by the area spanned by the two concentration profiles, as a function of pore volumes (PVs) injected is proportional to the mineral surface in contact with water. When oil is bound to calcite mineral surfaces in mixed wet samples, the separation area is reduced compared to water wet samples if the specific surface area is the same. The ratio of areas for mixed wet sample (A_{mw}) and water wet sample (A_{ww}) defines the wettability index (W_i),

$$W_i = \frac{A_{mw}}{A_{ww}} \tag{1}$$

A wettability index of 1 imply that the sample has the same number of surface sites for sulphate adsorption as the reference case, making it 100% water wet. A W_i of zero (overlapping sulphate and tracer curves) imply no sulphate ions adsorption making the sample 100% oil wet. Other values of W_i imply that the minerals are partially covered by oil (mixed wet). Rock fluid interactions also changes the specific surface area. Dissolution and precipitation reactions can increase or decrease the specific surface area, thereby changing the number of surface sites even when oil is present, hence leading to a mixed wet state.

Quantifying the wettability alteration by aging

The wettability alteration procedure was equivalent for all samples in both the 'wettability determination program' and 'triaxial test program'. Wettability determination could not be done on samples for the triaxial tests because the flow of fluids used to determine wettability displaces oil and alters the wettability, since sulphate has shown to modify wettability (Strand et al. 2006b; Zhang and Austad 2006; Zhang et al. 2007). We assume that the wettability determined for the three aged cores in the wettability determination program is the same as the two aged cores in the triaxial test program.

Wettability determination was performed in a Hassler cell by (i) flooding four PVs of SW0T brine, (ii) injecting SW1T brine for 500 minutes with a flow rate of 0.2 ml/min. During the SW1T injection, 40 samples were collected using a Gilson fraction sampler. Each sample contained 2 ml of fluids collected over 10.0 minutes, with 2.5 minutes waste time between each sample. For each fluid sample, the thiocyanate and sulphate concentrations were determined using ion chromatography (IC). The concentration c_k of each species k (SCN^- and SO_4^{2-}) is rescaled by the SCN^- and SO_4^{2-} concentrations of SW0T c_{k0} (in this case zero) and SW1T $c_{k1} = 0.024$ mol/liter, such that a reduced concentration $\hat{C}_k$ could be obtained,

$$\widehat{C_k} = \frac{c_k - c_{k0}}{c_{k1} - c_{k0}} \tag{2}$$

This reduced concentration varies between zero and one, and when the effluent concentration equals the inlet concentration, $\widehat{c_k} = 1$ enabling the thiocyanate and sulphate curves to be plotted together. The area between the curves was estimated by integration using the trapeze method. Further, larger cores will have a larger *total* surface area than smaller ones, so the areas are reported in per gram of the core for accurate comparison (Table 3).

Ion Chromatography (IC)

The effluent samples acquired were diluted 500 times with nanopure water (of specific resistance 18.2 MΩ-cm at 25°C) to meet the linear regime of the Dionex IC S-5000+ Ion Chromatography System. The samples were diluted using the Gilson GX-271 liquid handler operated by the Trilution software. Once the IC analysis finalised, a series of peaks, corresponding to each ion in the effluent sample, was obtained. The area under each peak was assumed to be proportional to the ion concentration in the fluid, when compared to known standards with known concentrations.

The triaxial cell setup for mechanical flow-through tests

The samples were mounted into the triaxial cell allowing for continuous measurements of axial and radial strains at elevated stresses and temperature (Figure 1). The triaxial cell was equipped with a heating element and a regulating system with temperature control (0.1°C precision). Three pumps were used to control the axial piston pressure (P_{pist}), confining pressure (σ_{rad}) and flow rate (Q). The pore pressure (P_p =0.7 MPa), was controlled by a back-pressure regulator ensuring constant pore pressure on the downstream side. An external Linear Voltage Differential Transducer (LVDT), placed on top of the moving piston, monitored the change in sample length (L) and an internal extensometer monitored the change in diameter (D).

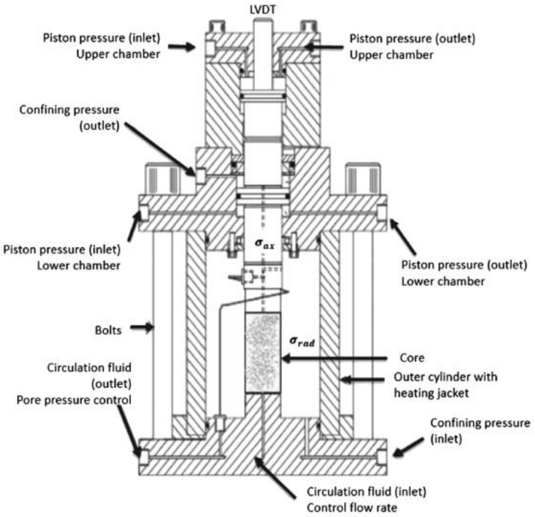

Figure 1. Sketch of the triaxial cell

The axial stress was calculated using radial stress, piston pressure, frictional pressure of the piston movement in the triaxial cell, and an area factor ($f_{area} = 1.28$) for the piston pressure chamber and the cross area of the plug,

$$\sigma_{\mathrm{ax}} = \sigma_{rad} + f_{area}\left(P_{pist} - P_{fric}\right) \qquad (3)$$

In the hydrostatic phase the stresses are equal in all directions, so the bulk modulus K is given by,

$$K = {}^{\Delta\sigma'_{ax}}\!/_{\Delta\varepsilon_{vol}} \qquad (4)$$

Here, $\Delta\sigma'_{ax}$ is the change in effective stress in axial direction and $\Delta\varepsilon_{vol}$ is the change in volumetric strain (see equation 7). The effective stress is given by the imposed stress in a spatial direction minus a fraction α times the pore pressure ($\sigma' = \sigma - \alpha P_{pore}$). We assume the Biot coefficient $\alpha = 1$ hereon.

Constitutive equations

The bulk, pore and solid volumes are linked through the constitutive equation $V_b = V_s + V_p$. During the test, the pore volume is not directly measured. Since porosity is determined by the ratio of pore volume (V_p) to bulk volume (V_b),

$$\phi = \frac{V_p}{V_b} = 1 - \frac{V_s}{V_b} \qquad (5)$$

the solid volume (V_s), estimated from the IC analysis, and the bulk compaction can be used to estimate porosity evolution using (Nermoen et al. 2015),

$$\phi(t) = \frac{\phi_o + \varepsilon_{vol} - \Delta V_s / V_{b,o}}{1 + \varepsilon_{vol}} \tag{6}$$

where ϕ_o is the original porosity, ε_{vol} is the volumetric strain and $V_{b,o}$ defines the original bulk volume.

Evolution in bulk volume with time

The radial strain was measured only at the middle of the core. Since radial deformation is non-equal along the length of the cores even in in hydrostatic tests (Nermoen et al. 2015), we introduced the factor X, assumed to be constant through the test, to improve the volumetric strain estimates from axial strain measurements,

$$\varepsilon_{vol} = X\varepsilon_{ax} \tag{7}$$

The factor X was determined from the ratio of length and volume changes measured with a sliding caliper directly on the core sample after test. As such, the bulk volume can be estimated via,

$$V_{b,t} = V_{b,o}(1 - \varepsilon_{vol}) = V_{b,o}(1 - X\varepsilon_{ax}) \tag{8}$$

Evolution in solid volume with time

The solid mass evolution over time $M_s(t)$ is calculated from the difference in the concentrations of the injected fluid and the produced effluent fluids (from ion chromatography) times the flow rate q_{in} and molar mass of Mg and Ca (n_{Mg}=24 g/mol and n_{Ca} = 40 g/mol),

$$M_s(t) = M_{s,0} + \eta \int_0^t q_{in}(n_{Mg}(c_{in,Mg} - c_{out,Mg}) - n_{Ca}(c_{in,Ca} - c_{out,Ca}))dt \tag{9}$$

This is used to interpolate between the measured mass before and after test, and η is a fitting parameter that makes the observed replacement of Ca by Mg from IC data match the observed mass loss (measured on a scale) in dry weight.

The solid density is measured before and after test, and we used the calcium produced from the sample $m_{Ca}(t)$, at time t to interpolate between the initial ($\rho_{s,o}$) and final ($\rho_{s,f}$) densities via,

$$\rho_s(t) = \rho_{s,o} + ((\rho_{s,f} - \rho_{s,o})(m_{Ca}(t)/m_{Ca,total})) \tag{10}$$

Using equations 9 and 10 the change in solid volume ΔV_s can be estimated,

$$\Delta V_s(t) = \frac{M_s(t)}{\rho_s(t)} - \frac{M_{s,o}}{\rho_{s,o}} \tag{11}$$

Evolution in porosity and pore volume with time: The pore volume is not directly monitored in the test, so it is estimated from the bulk volume (equation 8) minus the solid volume (equation 11) using,

$$V_p(t) = V_b(t) - V_s(t) = V_b(t) - V_{s,0} - \Delta V_s(t) \tag{12}$$

The water volume in the sample is not directly measured. So, to estimate the water volume as function of time we use,

$$V_b = V_p + V_s = V_w + V_o + V_s \tag{13}$$

where V_w and V_o are the volumes of water and oil. When this equation is re-shuffled for water volume, which is the unknown parameter in this experimental design, the measured quantities, namely the bulk volume, solid volume, and oil volume inside the sample, are used. The oil volume in the sample at any time is estimated from the initial oil volume minus the oil volume produced in a vertically oriented gravity glass separator. The oil (S_o) and water (S_w) saturations in the sample are then given by,

$$S_o(t) = \frac{V_o(t)}{V_p(t)} \text{ and } S_w(t) = \frac{V_w(t)}{V_p(t)} \tag{14}$$

These equations implicitly obey the requirement that $S_o + S_w = 1$.

Triaxial test program

The mechanical tests were performed according to the following procedure:

1. Mounted the cores in the triaxial cell with bypass valve open (no flow through the cores).
2. Simultaneously increased confining pressure (σ_{rad}) to 1.2 MPa and pore pressure (P_p) to 0.7 MPa.
3. Increased temperature to 130°C.
4. Increased hydrostatic stress to approximately 1.5 times yield at 0.045 MPa/min loading rate while observing volumetric strain to determine stiffness and strength. The stiffness measurements were carried out during loading conditions and hereon referred to as 'bulk modulus'.
5. Observed volumetric creep and oil production with constant pore pressure and hydrostatic stress with bypass valve open the first 15 days.
6. On the 16th creep day the bypass valve was closed and $MgCl_2$ brine was flooded at 0.010 ml/min flow rate.
7. Increased $MgCl_2$ brine flow rate to 0.040 ml/min after a certain number of days.
8. Decreased flow rate back to 0.010 ml/min.
9. Cleaned the cores with four PVs of DW at the end of the test.
10. Decreased temperature to room temperature. Used toluene to remove leftover oil from cores M3&M4, followed by methanol flooding to remove toluene. Multiple iterations of toluene and methanol flooding were performed till the effluent became completely transparent in colour.
11. Used DW to remove methanol from these cores.
12. Chromatographic separation tests were performed on all four samples.
13. Demount cores from the triaxial cell and measured saturated mass. Kept them in an oven at 110°C overnight.
14. Measured dry weights, lengths and diameters the day after.
15. Cut the cores into 6 sections of almost equal lengths. The density and specific surface area of these sections and of the unflooded end pieces were measured using gas pycnometer and Brunauer–Emmett–Teller (BET) theory, respectively.

Effluent samples were taken two to three times a week during steps 5 to 9. The ionic composition was estimated using ion chromatography. The oil production was measured for mixed wet cores M3 and M4 using a separator on the downstream side of the triaxial cell. Due to pore pressure fluctuations during the M3 test, the oil volume measurements were disregarded because of emulsification of the produced oil. Pore volume was estimated from the solid volume estimate and bulk volume measurement. With the oil production from core M4 known, the remaining oil volume inside the core was estimated.

Mineral density and specific surface area determination

The mineral density and specific surface area were estimated by Gas Pycnometry and Brunauer–Emmett–Teller (BET) technique, respectively.

Before the mineral density was measured, the cut sections for all samples were kept in the oven at 110°C overnight. Next morning these sections were taken out and placed in a vacuum sealed container to cool down. Each section was weighted and inserted, one-by-one, into the Micromeritics AccuPyc II 1340 Gas Pycnometer (using helium) to measure the solid volume. With mass and solid volume known, the mineral density of each section was estimated.

BET theory works by determining the adsorption of gas molecules on a solid surface (Brunauer et al. 1938). The specific surface area measurements were carried out on Micromeritics TriStar II instrument using liquid nitrogen, as it does not chemically react with the chalk. Two grams of powdered chalk was added to the sample glass tube and degassed for 5 hours at 110°C on Micromeritics VacPrep 061 Sample Degas System. A stable vacuum pressure of 20-30 mTorr was attained for all tested samples before the sample tubes were attached to the BET apparatus. The specific surface area was measured automatically by the TriStar II 3020 software.

RESULTS

The experimental results are presented in the following way: (i) Wettability determination program based on 3 reference water wet and 3 mixed wet samples, (ii) stiffness and strength measurements from the hydrostatic loading tests, (iii) volumetric deformation during creep, (iv) effluent sample analyses using ion chromatography, (v) oil volume development for the mixed wet samples, (vi) analyses of all cores used in the triaxial test program after tests, and (vii) wettability by chromatographic separation tests after triaxial tests on all samples.

Wettability determination based on 6 samples

Figure 2(a) and (b) show an example of two chromatographic separation tests performed on a completely water wet sample (Mww2) and a mixed wet sample (Mmw3). Here, the reduced ion concentration is plotted against PVs of SW1T flooded. Each dot represents a single effluent sample and the corresponding thiocyanate ion and sulphate ion concentrations. The separation between thiocyanate and sulphate ions can be seen. Figure 2(c) displays the difference between the thiocyanate and sulphate concentrations for the water wet sample (Mww2, blue) and mixed wet sample (Mmw3, green). The green curve has a smaller area and is shifted to the left of the blue. The integrated areas between the two curves were divided by the weight of the core to provide accurate comparison for differently sized cores. The average areas for water wet and mixed wet samples were 1.48 ± 0.08 PV/g and 0.93 ± 0.04 PV/g, respectively. This corresponds to an average W_i of 0.63 ± 0.07 for the wettability-altered samples. The estimated areas for all samples are reported in Table 3 displaying great repeatability. The initial irreducible water saturation ranged from 0.31 to 0.38.

Table 3. Estimated integrated areas per gram of the core for water wet and mixed wet samples, and the corresponding wettability indexes.

	Core	**Estimated area between sulphate and tracer (PV)**	**Integrated sulphate – tracer area per gram core (10^{-3} PV/g)**	**Wettability index (W_i)**	**Irreducible water saturation (S_{wi})**
Water wet	Mww1	0.201	1.59	1	1
	Mww2	0.175	1.43	1	1
	Mww3	0.184	1.41	1	1
	Average		1.48±0.08		
Mixed wet	Mmw1	0.112	0.88	0.60±0.03	0.31
	Mmw2	0.114	0.93	0.63±0.03	0.38
	Mmw3	0.118	0.98	0.66±0.04	0.37
	Average		0.93±0.04	0.63±0.07	

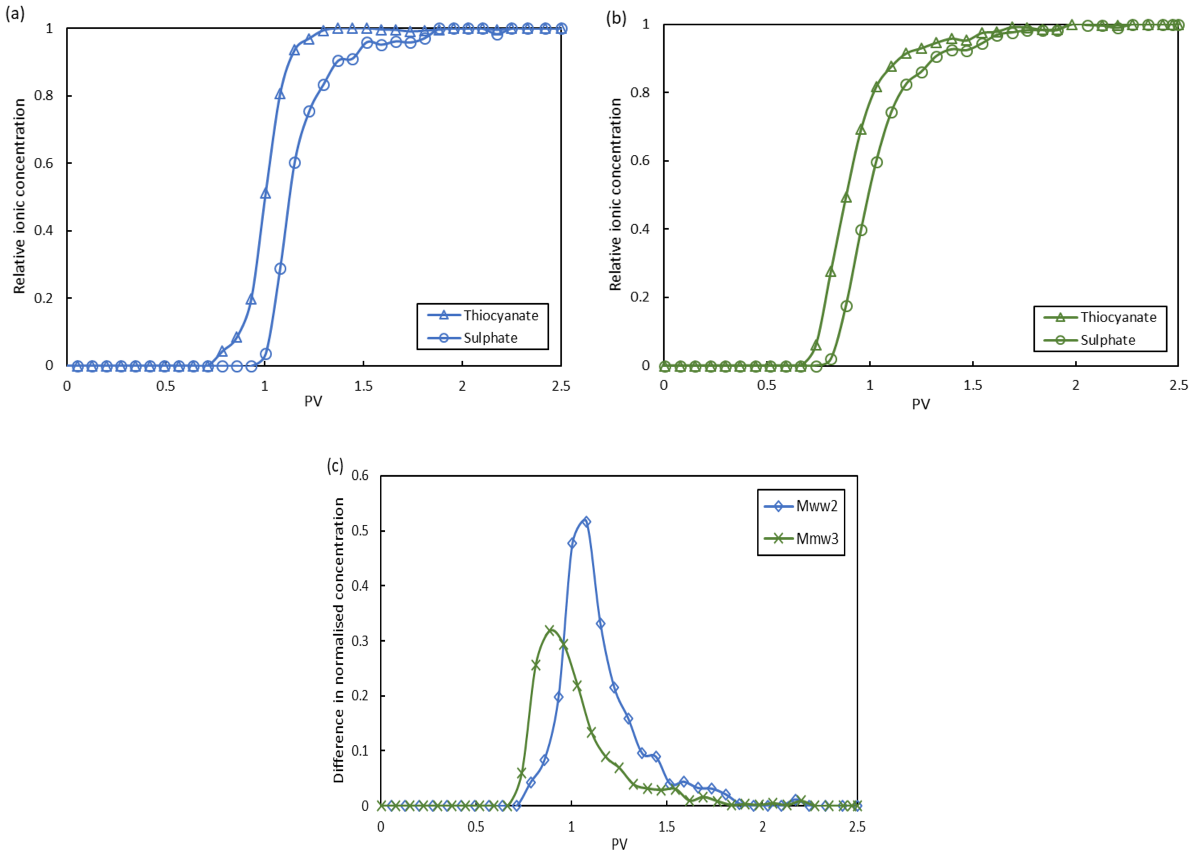

Figure 2. Chromatographic separation on (a) water wet core (Mww2, blue) and (b) mixed wet core (Mmw3, green). The plots (a) and (b) show how the increase in sulphate concentration is delayed compared to the thiocyanate concentration after SW1T is injected. The plot (c) shows the difference in normalised concentrations between the thiocyanate and sulphate curves for the water wet (blue) and mixed wet cores (green). The integrated separation areas for Mww2 and Mmw3 were 1.43×10^{-3} *PV/g and* 0.98×10^{-3} *PV/g, respectively, (Table 3).*

It is assumed that the W_i of the mixed wet samples used in the triaxial test program, drilled from the same block and altered in the same way, was also 0.63 ± 0.07.

Stiffness and strength determination from hydrostatic loading tests

The volumetric strain was measured during hydrostatic loading from 1.2 MPa to approximately 1.5 times the yield at 130°C and 0.7 MPa pore pressure. The onset of yield stress was determined at the point when the stress – strain curve deviated by more than 0.5 MPa from the initial straight elastic line used to determine the loading bulk modulus (K). The stress-strain curve during loading and the yield stresses for all four cores are shown in Figure 3(a), and the yield stress, bulk modulus and creep stress used further are reported in Table 4 that also display the initial water saturation.

Table 4. Bulk modulus, onset of yield stress and creep stress of M1 to M4 samples from hydrostatic loading at 130°C, 0.7 MPa pore pressure and with the bypass kept open.

Core	**Wetting state**	**Initial water saturation (fraction)**	**Onset of yield stress (MPa)**	**Creep stress (MPa)**	**Bulk modulus (GPa)**	**Uncertainty in bulk modulus (× 10^{-1} GPa)**	**Creep stress/yield stress factor**
M1	Water wet	1	14.4	21.5	1.3	0.08	1.49
M2		1	13.4	19.3	1.8	0.24	1.44
M3	Mixed wet	0.34	12.4	17.8	1.0	0.06	1.44
M4		0.36	12.3	18.3	1.1	0.09	1.49

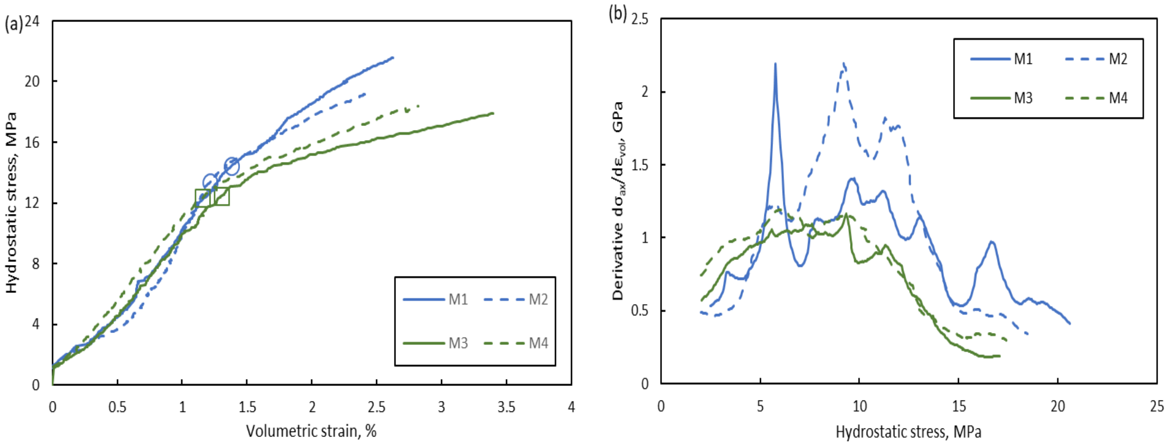

Figure 3. (a) Hydrostatic stress versus volumetric strain for all samples in the triaxial test program. Yield stresses are displayed on the curves. (b) Slope of stress-strain curve plotted as a function of stress. Blue and green lines represent water wet and mixed wet samples, respectively.

Stiffness observations

The loading bulk modulus was estimated from hydrostatic loading curves from 7 MPa to 11 MPa hydrostatic stress interval via equation 4 (reported in Table 4 and Figure 3(a)). The bulk moduli of the water wet samples (M1 and M2) were 1.3 GPa and 1.8 GPa, which were higher than the mixed wet samples (M3 and M4) that had stiffnesses of 1.1 GPa and 1.0 GPa, respectively. When the loading bulk modulus was measured in three other stress intervals, 2 - 10 MPa, 4 - 8 MPa and 4 - 10 MPa, the mixed wet samples M3 and M4 attained the same values (1.0 GPa and 1.1 GPa, respectively). However, the slopes in the stress-strain curves varied for the water wet samples, where M1 varied from 0.9 GPa to 1.8 GPa and M2 varied from 1.0 GPa to 1.3 GPa. Thus, it cannot be claimed that the stiffness is significantly altered by the aging procedure and wettability alteration. This is emphasised in Figure 3(b) where the slopes of the stress-strain curves obtained in +/- 0.5 MPa intervals is plotted against the hydrostatic stresses. Here, the variation in slope during loading is displayed. Stiffness estimates during simple loading are attributed with significant lack of imprecision and it has been discussed to what extent this is a valid method. The yield stress, however, can potentially be interpreted with greater certainty as seen in Figure 3(b) where the slope decreases systematically for all samples.

Strength observations

The yield stresses for all cores are reported in Table 4 and shown on the loading curves in Figure 3. The water wet cores (M1 and M2) yielded at 13.90 ± 0.50 MPa, while the mixed wet cores (M3 and M4) yielded at 12.35 ± 0.05 MPa. The yield stresses were also measured using the same elastic regions defined in the 'Stiffness observations' and were found to be varying in a range of ± 1 MPa. Even though the actual numbers obtained suggest that the water wet samples are stronger than the mixed wet samples, we cannot claim the differences observed to be significant since the certainty of the experimental method and interpretation is above or in the same range as the differences. Hence, the yield strength of water wet and mixed wet samples were found to be almost similar. Figure 4 shows the relationship between strength and stiffness based on the data reported in Table 4.

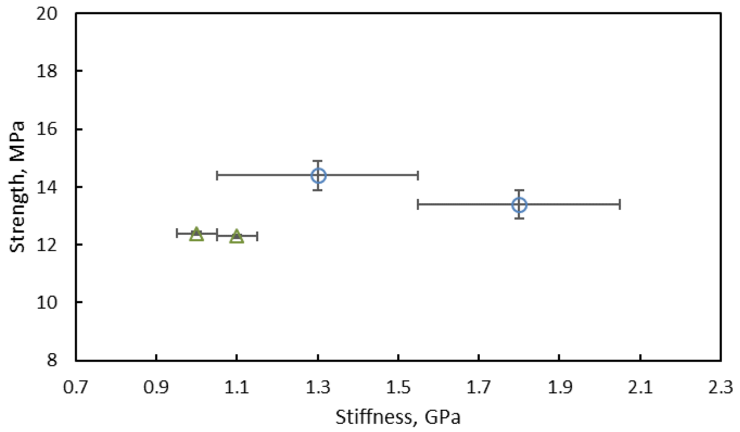

Figure 4. Plastic strength (onset of yield) versus stiffness (bulk modulus).

Volumetric deformation during creep

The creep stress was set to approximately 1.5 times yield stress. Since the yield stress was determined by naked eye during loading, the actual creep stresses deviated from the 1.5 factor when the yield stress was determined systematically. A variation between a factor of 1.44 and 1.49 times yield stress was used (Table 4). The creep strains and creep strain rates are shown in Figure 5 and Figure 6, respectively, for all four cores. The volumetric creep strain for different wettability cores followed a similar trend during the stagnant fluid creep period (black dotted lines in Figure 5 and all dotted lines in Figure 6). At the start of $MgCl_2$ flow at a rate of 0.010 ml/min, we observe that the strain rate decreased for approximately 15 days before an acceleration phase is observed for all cores (red dashed lines in Figure 5 and all solid lines in Figure 6). It is also observed that the creep curves obtained for the water wet core M2 and the mixed wet core M3 were almost parallel to each other (Figure 5). These two had a saturation porosity before test of 43.2% and 43.3%, respectively. The two other curves for the samples M1 and M4, with a porosity of 42.2% and 42.1% respectively, were also parallel. This may indicate how porosity can determine mechanical property, and further that the chalk mechanical behaviour is independent of the presence of oil in the cores but rather dependent on the solid framework and/or mineralogy of chalk. After increasing the flow rate four times to 0.040 ml/min in all cores, a flow rate induced accelerated strain (dark gray solid lines in Figure 5 and all dashed lines in Figure 6) is observed for all cores.

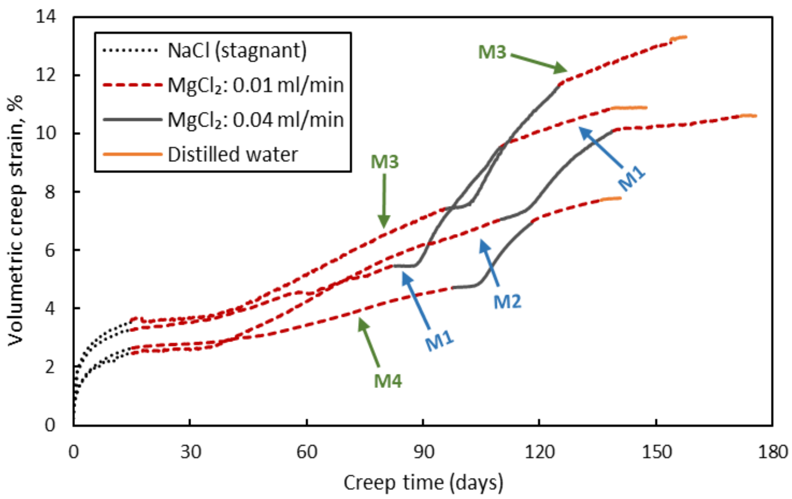

Figure 5. Volumetric creep strain with time for 100% brine saturated water wet cores M1 and M2 (blue arrows), and oil and brine saturated mixed wet cores M3 and M4 (green arrows).

Afterwards, the flow rate was reduced back to 0.010 ml/min leading to a rapid reduction in strain rate for all cores. The strain rate for all cores dropped to the original value obtained during the first flooding period at 0.010 ml/min. Before demounting, all cores were flooded by DW to remove salts from the pores and a sudden drop to almost zero in the creep strain rate for all cores was obtained (orange solid lines in Figure 5 and all dash-dotted lines in Figure 6). Hence, the slope of the creep curves was observed to be different for all cores, but the response to any changes in brine and flow rates was similar. The final volumetric creep strains at the end of the tests for cores M1 to M4 are 10.9% (after 147.5 creep days), 10.6% (after 175.7 creep days), 13.3% (after 157.7 creep days) and 7.8% (after 141.8 creep days), respectively.

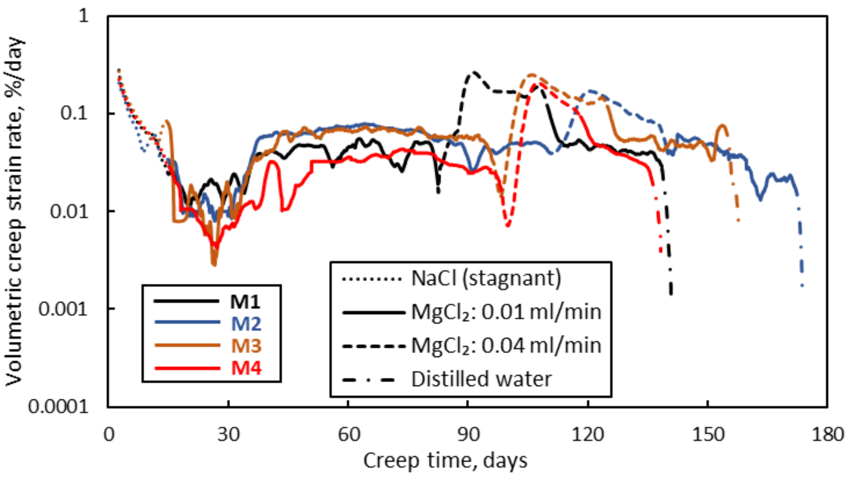

Figure 6. Volumetric creep strain rate with time for 100% brine saturated water wet cores M1 (black) and M2 (dark blue), and oil and brine saturated mixed wet cores M3 (brown) and M4 (red). The different brines are shown by (a) dotted lines for NaCl brine, (b) solid lines for $MgCl_2$ brine at a flow rate of 0.010 ml/min, (c) dashed lines for $MgCl_2$ brine at a flow rate of 0.040 ml/min, and (d) dash-dotted lines for DW.

Effluent ion concentration during $MgCl_2$ brine flow

Rock-fluid interactions changes the ion concentration of the effluent brine. Effluents were sampled two to three times per week during creep phase. The ion concentrations of the two most important ions, calcium and magnesium, for the water wet (M1 and M2) and mixed wet (M3 and M4) cores are shown in Figure 7.

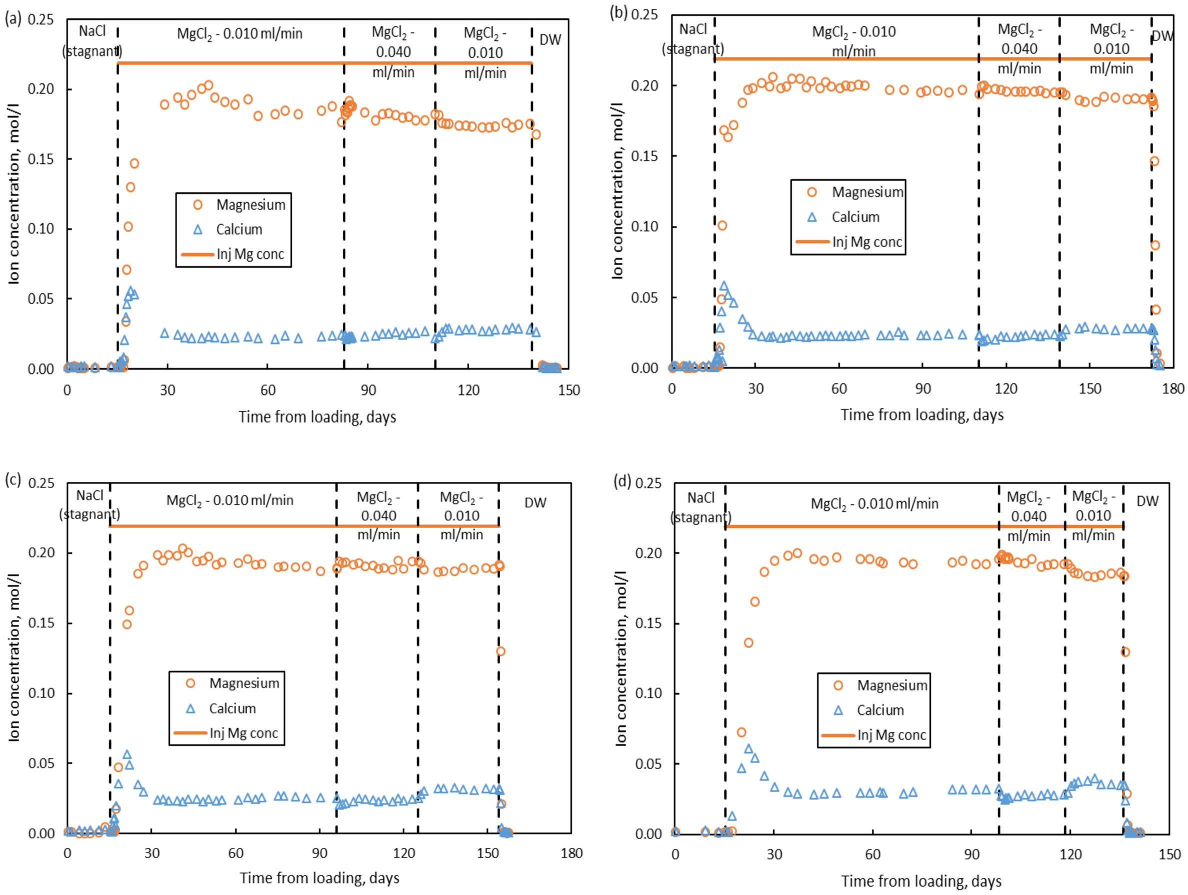

Figure 7. Samples flooded by 0.219M $MgCl_2$ brine. Effluent ion concentrations of calcium and magnesium and the injected magnesium concentration are shown for water wet cores (a) M1 and (b) M2, and mixed wet cores (c) M3 and (d) M4.

In all four plots in Figure 7, the magnesium concentration decrease compared to the injected concentration. This is a result of adsorption of magnesium ions on the mineral surface and desorption of calcium ions, and precipitation of magnesium-bearing mineral phases and dissolution of calcium carbonate (Madland et al. 2011; Nermoen et al. 2015; Zimmermann et al. 2015; Minde et al. 2017, 2018a, 2018b; Andersen et al. 2018; Sachdeva et al. 2019).

From 15 days onward when $MgCl_2$ brine flow started, a transient period in the calcium production and magnesium retention is seen until around 30 days, after which the production/retention stabilised. From 15 to 30 days the retention and production are interpreted to be a combination of dissolution/precipitation and adsorption/desorption processes. The retained magnesium concentration stabilised at 0.190-0.195 mol/l for all four samples irrespective of the wettability and initial saturations. The produced calcium concentration stabilised at 0.020-0.025 mol/l and 0.025-0.030 mol/l for water wet and mixed wet cores, respectively, i.e. the water wet samples displayed a slightly larger calcium production than the mixed wet samples. Further, in Figure 7(b), (c) and (d), when $MgCl_2$ flooding rate was increased four-fold to 0.040 ml/min, the produced calcium concentration decreased to around 0.020-

0.022 mol/l, whereas it remained almost unchanged for water wet sample M1 (Figure 7(a)). The change in magnesium concentration was found to be less sensitive to flow rate than for calcium and the flow rate sensitivity for magnesium ions was found to be similar for both water wet and mixed wet samples. Afterwards when the flow rate was decreased back to 0.010 ml/min, the magnesium concentration also decreased to around 0.180-0.185 mol/l for all four cores and the calcium concentration was found to have increased to a value around 0.025-0.030 mol/l and 0.033-0.038 mol/l for water wet and mixed wet cores, respectively. Same trends were seen for $MgCl_2$ flow through Kansas chalk (Sachdeva et al. 2019).

During cleaning, the calcium and magnesium concentrations fall drastically to almost zero for all cores, confirming that negligible to minor interactions occurred during DW flooding.

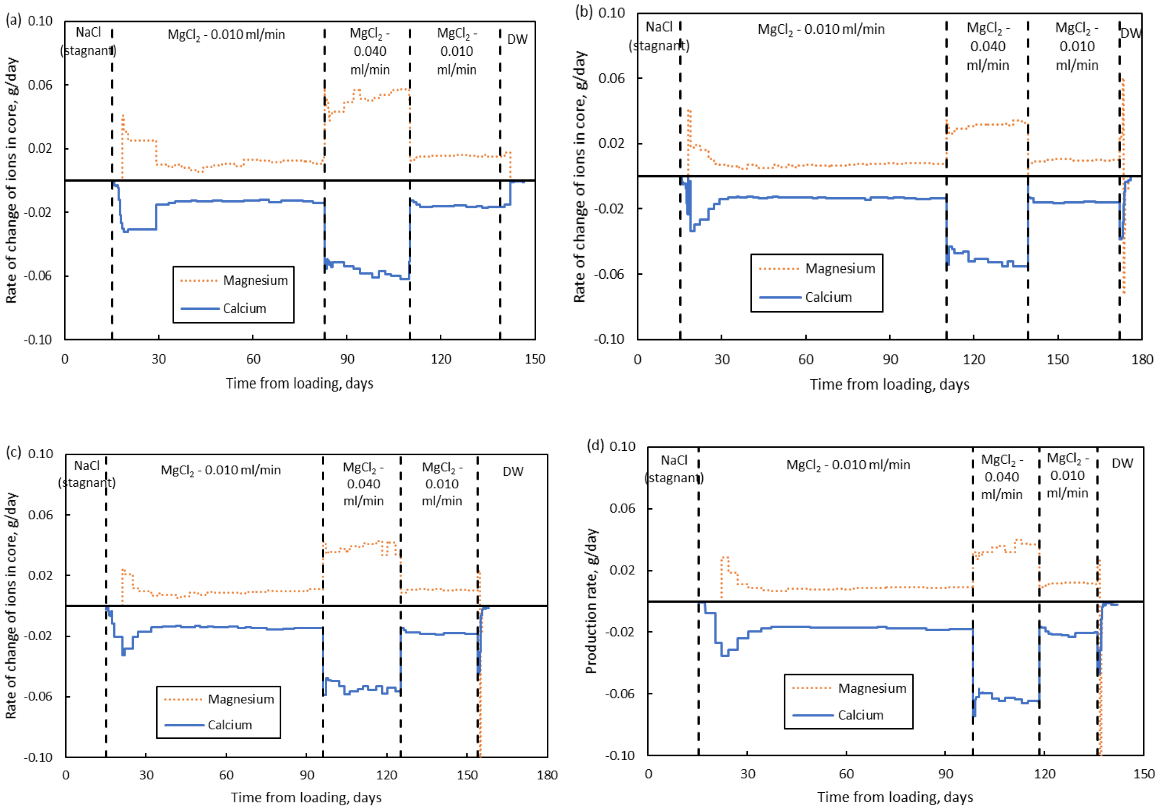

Figure 8. Samples flooded by 0.219M $MgCl_2$ brine. Evolution of rate of change of calcium and magnesium ions in the core (g/day) as a function of time is shown for 100% brine saturated water wet cores (a) M1 and (b) M2, and oil and brine saturated mixed wet cores (c) M3 and (d) M4.

The production rate of calcium and retention rate of magnesium, in units of gram per day shown in Figure 8, are obtained from a product of the ion concentration change, molar weight and flow rate. The analysis was done from the core perspective, hence the magnesium retained is positive and calcium produced is negative. For all cores, the rate of change of these two ions was zero during bypassing of NaCl brine for the first 15 days as the flow rate through the cores was zero. When $MgCl_2$ injection started through the cores at a rate of 0.010 ml/min, a peak in the retention and production rates of magnesium and calcium is seen. The magnesium retention rate stabilised around 0.010 g/day, whereas the calcium production rate stabilised around 0.013-0.016 g/day after 15 days of flooding (molecular weights of Ca^{2+} and Mg^{2+} are 40 g/mol and 24 g/mol, respectively). In all the effluent samples indicated that the dry mass reduced during $MgCl_2$ flow.

When the flow rate increased four times to 0.040 ml/min, the retention rate of magnesium increased to 0.029 – 0.057 g/day and the calcium dissolution rate to 0.047 – 0.060 g/day. Hence, an increase of 3 to 6 times in the magnesium retention rate and 3 to 4 times in the calcium production rate was observed. When the flow rate reduced to 0.010 ml/min, the magnesium retention and calcium production rates dropped to 0.013 g/day and 0.017-0.023 g/day, respectively. When DW was injected, the magnesium retention and calcium production rates fell to zero. The sensitivity to flow rate in the gain of magnesium and loss of calcium (from core perspective) was independent of the wettability and presence of oil implying that sufficient water wet areas existed for the fluid to equilibrate within the core.

The integrated total magnesium retained for the water wet cores was 0.114 moles (2.74 g) for M1 and 0.082 moles (1.96 g) for M2. For the mixed wet cores it was 0.088 moles (2.11 g) for M3 and 0.066 moles (1.58 g) for M4. Similarly, the integrated total calcium dissolved and produced from the cores was 0.078 moles (3.13 g) for M1, 0.086 moles (3.45 g) for M2 for the water wet cores, while for the mixed wet cores 0.085 moles (3.38 g) for M3 and 0.080 moles (3.19 g) for M4 of Ca^{2+} was produced.

Oil production from the mixed wet core (M4) during $MgCl_2$ flow

Oil production as function of time for the core M3 were omitted due to uncertainty in the oil volume readings because of emulsification of the produced fluids. Hence, only measurements for the M4 test are presented here (Table 5). The oil produced, because of $MgCl_2$ flow and compaction, was measured in a gravity separator on the downstream side of the experiment. Readings were recorded from digital photographs taken at frequent time intervals.

Table 5. Initial and final oil and water volumes in mixed wet cores M3 and M4 during $MgCl_2$ brine flow.

Core	M3	M4
Irreducible water volume before test	11.5 ml	12.0 ml
Irreducible water saturation S_{wi}	33.7%	36.4%
Initial oil volume	22.5 ml	21.0 ml
Total oil produced at the end of test	N.A.	11.2 ml
Oil volume after test	N.A.	9.8 ml
Oil Saturation after test S_{or}	N.A.	41.4%
Pore volume before and after test	34.0 ml and 20.4 ml	33.0 ml and 23.7 ml

The irreducible water saturations of M3 and M4 were estimated to be 33.7% and 36.4% with an initial oil in place of 22.5 ml and 21.0 ml before test. For the M4 test, 0.3 ml of oil was produced due to expansion of oil during temperature increase from ambient to 130°C. Figure 9(a) shows the oil with time together with the water volume estimated from equation (13) where the bulk volume, solid volume and pore volume used are displayed in Figure 10, which also displays the porosity evolution with time. In Figure 9(b) the oil saturation inside the core throughout the test from the start of hydrostatic loading using equation (14) is plotted. Before loading, when the sample was mounted, the oil and water volumes were 20.7 ml and 12.3 ml. 1.4 ml of oil was produced during hydrostatic loading to 1.5 times yield, reducing the oil volume to 19.3 ml. During the no-flow period, 3.3 ml of oil was produced due to compaction, which led the oil volume inside the core to further decrease to 16.0 ml by the end of 15th day, in all 4.7 ml oil was produced. During this time, the bulk volume of the sample reduced from 78.4 ml before (Table 1) to 74.2 ml (Figure 10(c)) at 15 days, i.e. a 4.2 ml reduction. Given that the solid volume is constant, the bulk volume reduction equals the reduction in pore volume ($\Delta V_b = \Delta V_p$). This imply that oil is primarily being produced during compaction, while the water is stagnant inside the core during mechanical loading and creep with no flow.

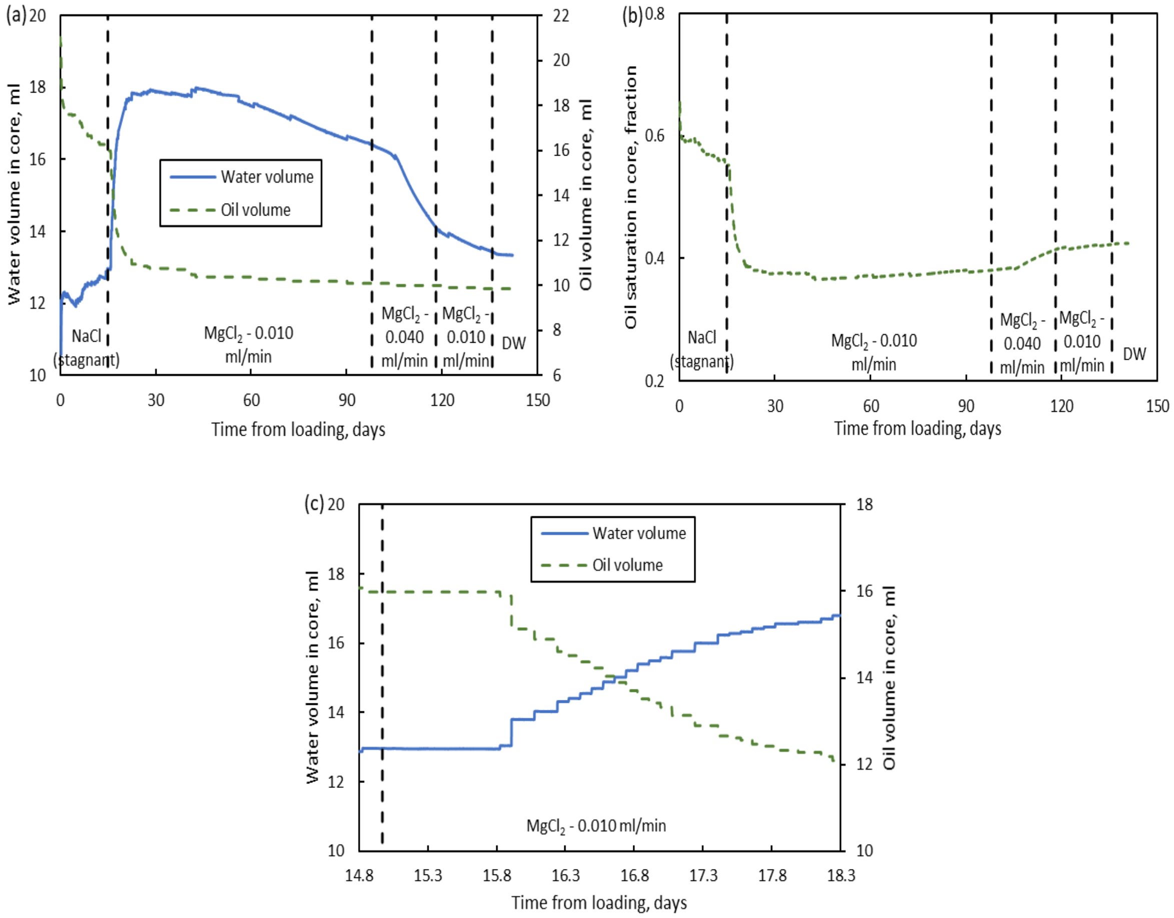

Figure 9. Oil and water volumes with time in the mixed wet sample (M4). (a) Oil and water volumes from measurements of oil volume (separator), bulk volume (compaction) and solid volume (IC effluent analysis), (b) oil saturation in the core with time, and (c) zoomed into oil and water volumes in the core from 14.8 days to 18.3 days. Black dashed vertical lines depict the time when brine composition and/or flow rate changed.

When $MgCl_2$ injection started, a total of 4.8 ml of oil was produced in the first five days (approximately 2.5 PVs), followed by another 1.1 ml in the next 78 days while flooding and compaction co-existed. After increasing the rate to 0.040 ml/min, only 0.2 ml oil produced during the next 20 days, and another 0.1 ml oil produced after reducing it to 0.010 ml/min. At the end of the $MgCl_2$ injection phase the oil volume in the core reduced to 9.8 ml. Figure 9(c) displays a zoomed version of the oil and water volumes in the core at the start of $MgCl_2$ injection phase after the no-flow period. The bulk volume changed during compaction (see equation 9), and the solid volume changed due to non-equilibrium flow (see equation 10).

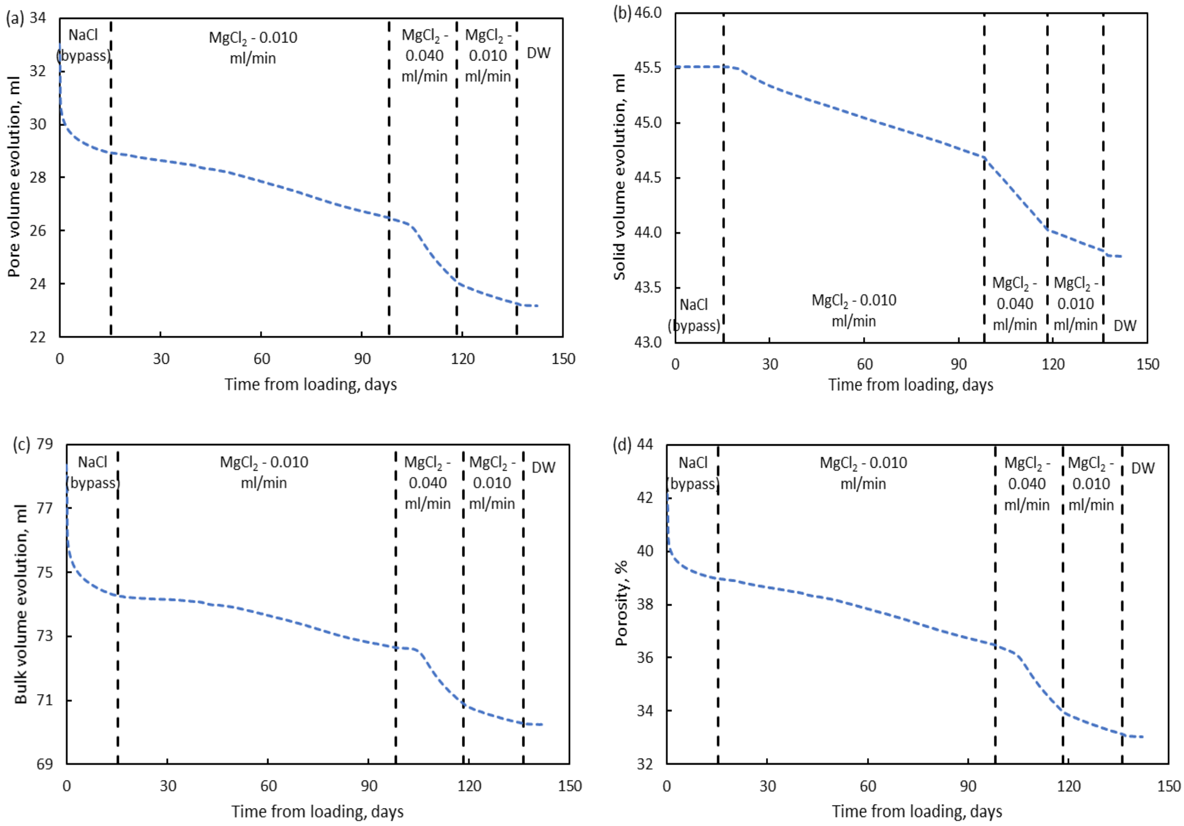

Figure 10. (a) Pore volume, (b) solid volume, (c) bulk volume and (d) porosity evolution with time for mixed wet Mons core M4.

The increase in MgCl$_2$ flow rate to 0.04 ml/min on the 98th day did not lead to any significant additional oil production. At the same time, as presented in (Figure 8), the calcium dissolution and magnesium retention rates (in g/day) increased by a factor of 3 to 6. This did not affect the oil recovery rate. Further on, though pore volume decreased with time because of compaction, only water was expelled from the core. Consequently, the oil saturation increased from 90 days and onwards (Figure 9(b)).

Chromatographic separation test after mechanical test

Chromatographic separation for wettability determination was performed on all four cores after the mechanical tests completed, but before the samples were dismantled from the triaxial cell. The thiocyanate and sulphate concentrations versus PVs of SW1T flooded are shown in Figure 11(a) to (d). The integrated areas between thiocyanate and sulphate curves for all samples are given in Table 6.

Table 6. Integrated areas between thiocyanate and sulphate curves estimated using chromatographic separation tests performed on all samples after mechanical tests. For comparison, water wet cores had an integrated area of 1.41 to 1.59 $\times 10^{-3}$ PV/g and the mixed wet cores had an area of 0.88 to 0.98 $\times 10^{-3}$ PV/g in the wettability determination program (Table 3).

Core	Initial wetting state	Estimated area between sulphate and tracer (PV)	Integrated sulphate – tracer area per gram core ($\times 10^{-3}$ PV/g)	Total MgCl$_2$ flooded (litres)
M1	Water wet	0.238	1.84	2.96
M2		0.294	2.45	3.51
M3	Mixed wet	0.202	1.69	3.26
M4		0.170	1.39	2.61

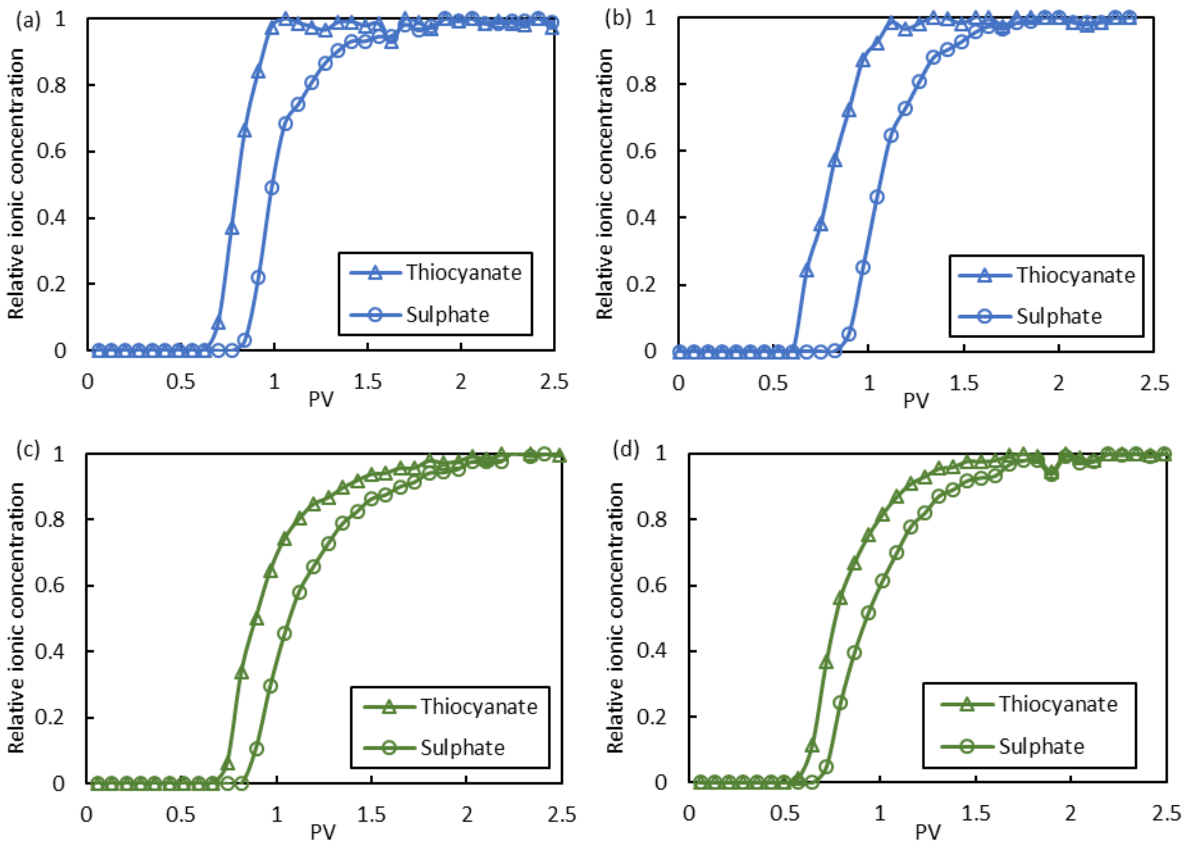

Figure 11. Chromatographic separation tests performed on water wet cores (a) M1 and (b) M2, and mixed wet cores (c) M3 and (d) M4 at ambient temperature after mechanical tests. The plots show reduced ion concentrations of the thiocyanate and sulphate ions for SW1T brine plotted as a function of PVs injected.

All cores showed an increase in the integrated areas compared to the areas obtained in the wettability determination program (Table 3), assumed to be the same for the samples before the mechanical tests. It is observed that the available water wet area increases when more $MgCl_2$ brine is flooded through the cores. From Table 6, the amount of $MgCl_2$ flooded through water wet sample M2 (3.51 litres) is more than that flooded through sample M1 (2.96 litres). The corresponding available water wet area after the mechanical test is also higher for the M2 sample (2.45×10^{-3} PV/g) compared to the M1 sample (1.84×10^{-3}PV/g) (Table 6). The same dependencies are also seen for the mixed wet samples, where more $MgCl_2$ brine through sample M3 (3.26 litres) gave a higher water wet area after the triaxial test (1.69×10^{-3} PV/g) compared to the sample M4 (1.39×10^{-3} PV/g) flooded by 2.61 litres. Dissolution and precipitation processes changes the amount of available mineral surfaces in contact with water and is the only factor at play in the water wet cases, while in the mixed wet cases the increase can also be related to the mobilisation of oil adsorbed on the mineral surfaces.

Analysis of core after test

Basic measurements on all four cores after the mechanical tests are reported in Table 7. The dry mass reduced by 1.3 to 2.1 g for all samples while the solid density increased by 0.02-0.04 g/cm^3, thereby reducing solid volume by 0.8 to 1.4 ml. The samples compacted so bulk volume reduced by 8.2 to 12.7 ml. Thus, the pore volume reduced by 9.3 to 13.6 ml.

Table 7. Basic properties of cores measured after tests. Changes compared to the corresponding initial values are given in parenthesis.

Core	M1	M2	M3	M4
Length (mm)	70.2	66.0	66.1	66.9
Average diameter (mm)	36.2	36.3	35.6	35.8
New dry mass (ΔM_s) (g)	128.1 (-1.3)	118.3 (-1.6)	117.6 (-2.1)	120.3 (-1.7)
Saturated mass (g)	152.8	142.7	138.0	144.0
New bulk volume (ΔV_b) (cm^3)	71.7 (-11.2)	68.2 (-10.4)	65.9 (-12.7)	70.2 (-8.2)
New pore volume (ΔV_p) (cm^3)	24.7 (-10.3)	24.4 (-9.5)	20.4 (-13.6)	23.7 (-9.3)
New porosity (%)	34.4 (-7.8)	35.8 (-7.4)	31.0 (-12.3)	33.8 (-8.3)
New solid density ($\Delta \rho_s$) (g/cm^3) (Pycnometry)	2.72 (0.02)	2.71 (0.04)	2.71 (0.04)	2.71 (0.03)
New solid volume (ΔV_s) (cm^3) (Pycnometry)	47.1 (-0.8)	43.7 (-1.2)	43.4 (-1.4)	44.4 (-1.1)
Ratio of volumetric to axial strain (X)	3.87	3.12	3.99	3.84
Test time (days)	147.9	176.0	158.1	142.2

The tested samples were cut into six sections of almost equal lengths with sections numbered from the inlet (Figure 12). The specific surface area along the sample sections and untested end pieces are reported in Table 8.

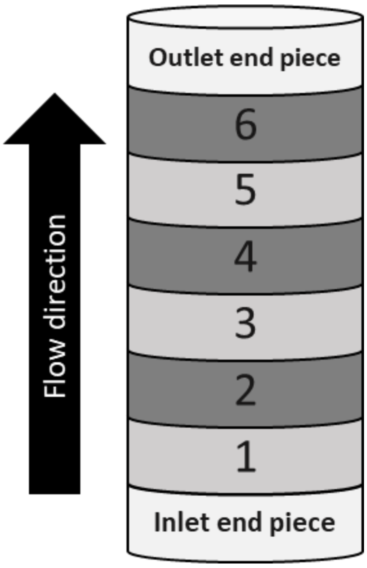

Figure 12. Specific surface area tested along the length of the sample.

Table 8. Specific surface area measurements of unflooded core material from both sides of the core, and for sections along the length of the cores M1 to M4 after tests.

Core	**M1**	**M2**	**M3**	**M4**
Core section	**Water wet**		**Mixed wet**	
	SSA, m^2/g	**SSA, m^2/g**	**SSA, m^2/g**	**SSA, m^2/g**
Outlet end piece (unflooded)	1.82	1.98	2.11	1.96
6	2.33	2.26	2.20	2.02
5	2.47	2.43	2.14	2.08
4	2.45	2.49	2.39	2.44
3	2.45	2.46	2.55	2.45
2	2.47	2.49	3.05	2.82
1	2.18	2.40	3.35	3.02
Inlet end piece (unflooded)	2.13	2.05	2.22	2.17

The SSA of water wet cores M1 and M2 increased from the inlet to the middle and then decreased towards the outlet. Specific surface areas of sections 1 of M1 and M2 were 2.18 m^2/g and 2.40 m^2/g compared to 2.13 m^2/g and 2.05 m^2/g for the unflooded end pieces. They increased to 2.45 m^2/g and 2.49 m^2/g at the middle and then decreased to 2.33 m^2/g and 2.26 m^2/g at the outlet for M1 and M2, respectively. Mixed wet cores M3 and M4 showed a large increase in the SSA of the inlet sections (3.35 m^2/g and 3.02 m^2/g, respectively, compared to 2.22 m^2/g and 2.17 m^2/g for the unflooded end pieces), followed by a gradual decrease from the inlet to the outlet of the flooded samples. The SSA decreased to 2.20 m^2/g and 2.02 m^2/g at the outlet for M3 and M4, respectively.

DISCUSSION

The grain sizes in chalk range from sub-micron to 2-3 microns. This leads to large specific surface areas compared to many other reservoir materials, so that surface interactions with pore fluids become increasingly important to the observed sample dynamics. In effect, water weakening is more likely to occur in chalk than in other reservoir rocks. Wettability of reservoir rock affects the flow and distribution of fluids in the porous media and hence the recovery of oil.

The effect of wettability on stiffness, strength and time-dependent deformation of Mons chalk is documented, and then the results are compared to the Kansas chalk reported in Sachdeva et al. (2019). The key premise is perturbing the experimental conditions (aging time, aging temperature, oil composition, brine composition etc.) to alter the forces at particle level that integrate to the overall core scale geomechanical properties.

Wettability alteration

In the wettability determination program, chromatographic separation was performed on three mixed wet and three reference water wet Mons chalk samples. Based on these measurements, we assume the wettability index of the mixed wet samples in the triaxial test program to be 0.63 ± 0.07 (Table 3). Two aged wettability-altered and two water wet samples were loaded hydrostatically and kept at 1.5 times yield stress over time, and later flooded by $MgCl_2$ brine at varying rate.

Impact of wettability on elastic stiffness and plastic strength

A significant difference in the loading stiffness and yield strength, beyond the experimental uncertainty, was not observed. The initial soft behaviour at low stresses, i.e. the initial large strains of the water wet samples, can be caused by closure of micro-cracks and fractures formed due to the sample handling. Further experiments are required to identify if the mechanical parameters for Mons samples can be altered by aging, e.g. with a more acidic oil, higher aging temperature/time, or by lowering S_{wi} even more before oil is injected.

Oil adsorption impact particle-particle contact forces

The thickness of the charged diffusive layer on calcite surfaces is characterised by the Debye length (Lyklema 2005; Megawati et al. 2013; Voake et al. 2019) that increases with increasing temperature (Andreassen and Fabricius 2010). A thickening of the layer (Debye length) increases the repulsive area between particles causing further weakening of water-saturated samples. Voake et al. (2019) further reported a Debye length of around 200 nm at 130°C using Debye-Huckel theory.

The force between particles in the presence of water is dictated by the sum of attractive van der Waals forces and repulsive electrostatic forces from the overlapping diffusive layer. When oil replace water on surface areas where the double layers would otherwise interact (regions with electrostatic repulsion), the disjoining pressure would reduce and the overall force balance between particles would change. When the normal force between two grains increase (in the case of oil adsorption), it becomes harder for particles to re-organise. This seems to have occurred in Kansas (Sachdeva et al. 2019), which has a Biot coefficient of 0.91 (Voake et al. 2019) and smaller pore size (characterised by the lower relaxation time T_2 estimated from the NMR studies, Voake et al. 2019) than Mons with a Biot coefficient of 0.95 (Figure 13(a) and Table 9 in appendix). If oil adsorbs on mineral surfaces but not on nearby particle contacts, the geomechanical parameters would remain un-affected. This seems to have occurred in Mons (Figure 13(b)).

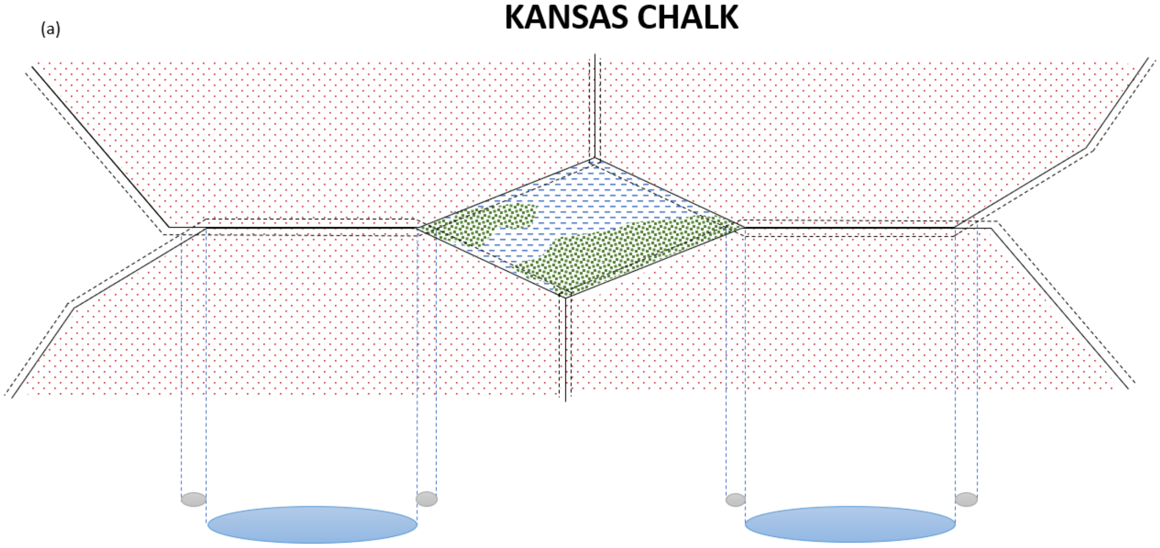

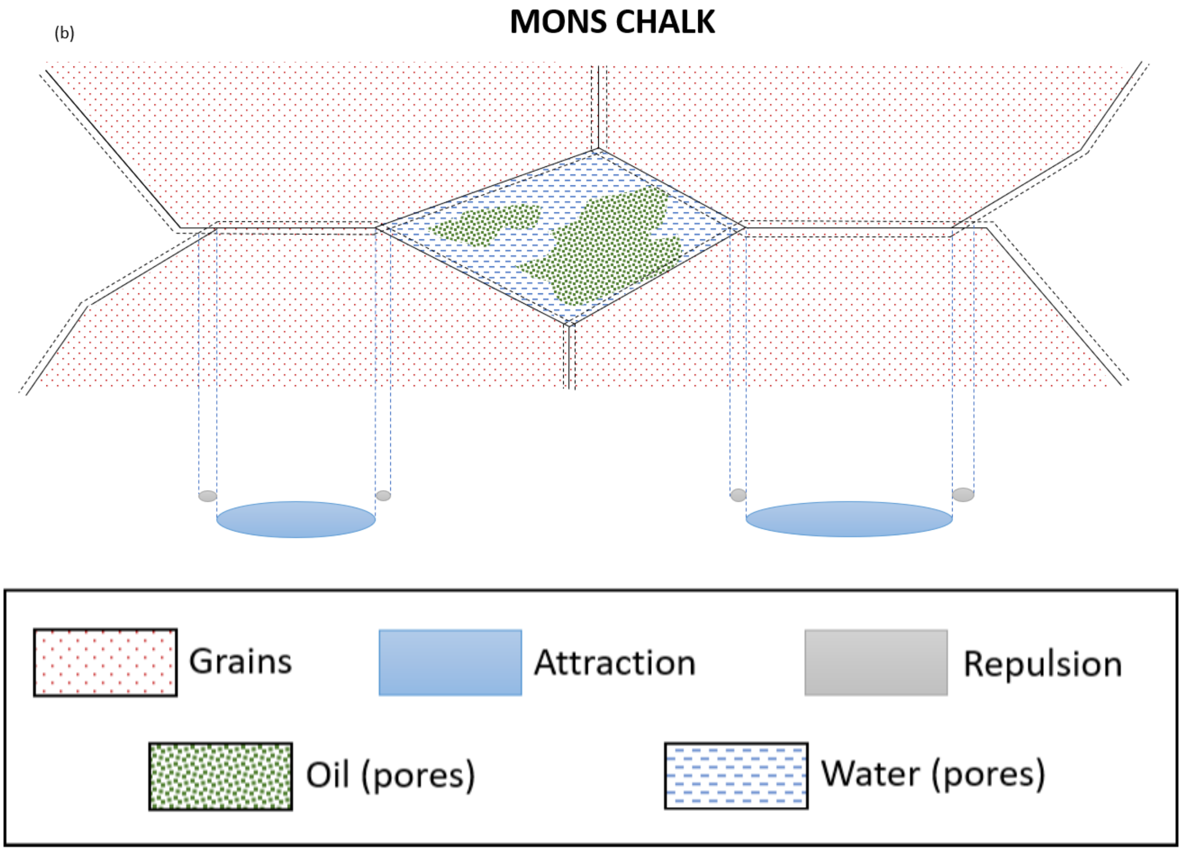

Figure 13. Partitioning of oil and water in pores for (a) Kansas and (b) Mons chalks. Attractive van der Waals and repulsive electrostatic forces present between calcite grains are also shown. Mons chalk has larger pore size and Biot coefficient compared to Kansas chalk (Voake et al. 2019).

With the same oil, brine composition and aging temperature as here, Sachdeva et al. (2018) reported that Kansas chalk remains water wet if the aging time is less than 6 days, and aging for 21 days was enough to obtain a stable mixed wettability. It remains to be tested how mechanical parameters changed for the same oil/water saturation for unaged samples. If the aging conditions were modified, the Mons chalk may become more mixed/oil wet thereby affecting stiffness and strength differently than in this study.

Impact of wettability on creep behaviour during $MgCl_2$ injection

The volumetric creep strain at constant creep stresses (in Table 4) followed a comparable trend for all samples throughout the creep period (Figure 5). The injection of $MgCl_2$ brine induce chemical reactions leading to additional creep rates (Nermoen et al. 2015). When $MgCl_2$ brine was injected at 0.010 ml/min, the strain rate curve continued to follow a decreasing trend for around 15 days, after which it stayed constant (Figure 6). This has also been seen for other clean chalks, e.g. Mons and Stevns Klint (Andersen et al. 2018). All cores showed an accelerated strain when the flow rate was increased to 0.040 ml/min (Figure 5), the strain rate increased by a factor of 3 to 8, and the calcium production and magnesium retention increased by a factor 3 to 6 (Figure 8). This shows how chemical reactions drive solid volume changes (reduce solid mass and increase mineral density), and how this behaviour links to bulk creep strain rate, also seen in Nermoen et al. (2016) and Andersen et al. (2018).

During DW flooding the strain rate dropped down to zero instantly depicting that the electrostatic repulsion between neighbouring particles, when the pores are saturated by salty brines, vanish. It is important to notice that both the chemical reaction dynamics observed by IC analysis and the sensitivity of the creep rate to the chemical reactions are independent of the oil/water saturation and the initial wetness. This is interpreted to be caused by a shift in the overall force balance between particles, occurring in all samples, where the particle-particle dynamics are controlled by the attractive van der Waals forces and a varying electrostatic repulsion. When the electrostatic repulsion is reduced, the particle-particle friction overcome the local shear stresses, thereby halting the re-organisation.

Calcite-NaCl brine interactions during hydrostatic loading and creep

When NaCl brine was injected into Liège chalk, dissolution of calcite was observed (Madland et al. 2011). In our case, the samples were only saturated by NaCl, and not flooded, and as shown in Figure 7 the concentration of calcium produced was in the range 0.001 – 0.003 mol/l. This means that around 0.0001 moles (0.01 g) of calcite dissolved from a 100% NaCl brine saturated core (with a PV of approximately 34 ml), which amounted to approximately 0.01% in mass compared to the initial dry mass of the samples (approximately 125 g). This percentage would be even less for the mixed wet samples due to the initial irreducible water saturation ranging from 31% to 38%. Therefore, the NaCl brine / rock interactions can be neglected.

Adsorption/desorption dynamics on the calcite surfaces

The calcite mineral surface possesses positively charged Ca^{2+} and negatively charged CO_3^{2-} surface sites (Stipp 1999) that leads to the adsorption of positive and negative ions from the pore fluid. When the pore fluid composition is changed, a new surface-equilibrium between the mineral surface and the ion concentration of the pore is established. The desorption and adsorption dynamics occur typically within the first pore volumes injected, dependent upon the ion concentration of the injected brine. When $MgCl_2$ brine was injected through all cores a plateau in the concentration of the produced effluent was established after approximately 15 days (from 16th day till around 30th day i.e. approximately 6.5 PVs injected, Figure 7), after which the magnesium and calcium concentrations are dominated by dissolution and precipitation processes.

Interactions of calcite with DW during sample cleaning

The solubility of calcite in DW at 25°C is 0.013 g/l (Voake et al. 2019) which decreases with increase in temperature (Coto et al. 2012). If the PV is 34 ml, 0.00044 g of calcite could dissolve per PV during DW flow at 25°C. In this study, four PVs of DW were flooded for cleaning at 130°C. Therefore, the dissolved calcite would be less than 0.0018 g, i.e. less than 0.0015% of the initial dry mass (approximately 125 g). Hence, any calcite dissolved during DW flooding can be neglected, as is also shown in the effluent analysis (Figure 7 and Figure 8).

Chemical alterations along the axis of the core

The non-homogeneous chemical replacement dynamics are observed in the specific surface area measurements (Table 8). The SSA of water wet core increases towards the middle of the core and then decreases towards the outlet, whereas the SSA of the mixed wet cores decreases towards the outlet with the highest value observed at the inlet of the samples. Andersen et al. (2018) demonstrated that the SSA of the water wet Mons chalk also decreased from the inlet to the outlet. This difference in our results may be linked to the initial spatial variability in grain size through the cores. The non-homogenous chemical replacement dynamics were also observed in the SSA measurements of Kansas cores as reported in Sachdeva et al. (2019), where the change in SSA was non-uniform through the core. The trends obtained in Kansas cores were not clear, except that the SSA increased from the inlet towards the middle of the samples.

Dynamic bulk, solid and pore volume measurements

Figure 10 shows how $MgCl_2$ flow rate affect the different volumes with time. Solid volume decreases due to the dissolution of larger calcium ions, which forms the solid framework of chalk, and precipitation of smaller magnesium ion forming secondary minerals. Pore volume decreases due to compaction and non-equilibrium flow. The rate of decrease in these volumes is larger when the injection rate of $MgCl_2$ is higher (0.040 ml/min). There is also a transition period of around 5 days observed in the pore volume and bulk volume evolution when the flow rate of $MgCl_2$ is increased from 0.010 ml/min to 0.040 ml/min. During this period the pore and bulk volumes decrease at almost the same rate as before, followed by a decrease at an accelerated rate. This transient period in Figure 10 (also observed in Figure 5 at the start of $MgCl_2$ flooding at a higher rate of 0.040 ml/min) shows the delayed weakening during reactive flow of $MgCl_2$, i.e. a delay in the accelerated strain by increased pore collapse rate at constant stress and temperature conditions. The rock framework (acting as force chains) can withstand the chemical reactions for some time, which are dependent upon stresses focussing the dissolution to the load bearing parts (which in our case is the solid framework or the grain-grain contacts following the force chains) of the material, and thus a delayed failure occurs. During the flooding of DW before demounting, no change in the pore volume, solid volume and bulk volume is observed.

Comparing the observed mechanical response with Kansas chalk

Kansas chalk is coccolithic mudstone or wackestone characterised by moderately preserved coccolithopores, whereas Mons chalk is pure coccolithic mudstone (Andersen et al. 2018). Both Kansas and Mons chalks are from Cretaceous age. Mons chalk has > 99 wt% calcite content, whereas Kansas chalk has around 95-97 wt% calcite content. Kansas chalk has gone through a higher degree of diagenesis (Finn and Johnson 2005) than the Mons chalk (Pirson et al. 2008). Previous XRD analyses of the clay fraction (< 2 μm) from these two chalk types have shown differences in their mineralogical assemblage, indicative of different diagenetic conditions (Bertolino et al. 2013; Andersen et al. 2018).

The mechanical parameters of Mons chalk obtained in this study are compared to those obtained from Kansas chalk reported by Sachdeva et al. (2019). We observe that these chalk types differ in their wettability values with the same aging procedure and their mechanical response to chalk at imposed stresses at 130°C. The wettability for the mixed wet Kansas chalk was reported to be 0.55 ± 0.05, whereas mixed wet Mons chalk gave the wetting indices of 0.63 ± 0.07 (Table 3). During loading with stagnant and inert fluids inside the pores, the behaviour observed for Mons differs from Kansas chalk, where a clear difference in both stiffness and strength in response to wettability alteration between the mixed wet samples and water wet samples were seen (Sachdeva et al. 2019).

During time-dependent creep period, water wet and mixed wet Kansas chalk gave a similar creep trend irrespective of the presence of oil (Sachdeva et al. 2019). Similar comparable trends were observed for Mons chalk as well. Strain rates reduced for all Mons cores at the start of $MgCl_2$ flood (Figure 6). It was followed by an increase in strain rates for all cores after approximately 15 days of $MgCl_2$ injection. All strain rates increased even more when flow rate was increased four-fold, followed by a reduction in strain rates when flow rate was reduced again. These rates dropped down to zero for all cores during DW injection. The creep slope was observed to be not the same for all cores, but the response to change in brine and flow rates was the same. Similar observations were also documented for Kansas cores (Sachdeva et al. 2019).

Oil production during compaction and flow

During hydrostatic loading and no-flow creep period (up to 15th day), 4.7 ml oil was produced from mixed wet Mons M4 core. Hence, deformation contributed to 43% of the total oil recovered after the initial thermal expansion. This value is comparable to the bulk volume loss of the sample (i.e. $\Delta V_s = \Delta V_p = \Delta V_{oil}$). Given that the water was not mobilised implies that oil was the mobile phase during compaction. After the first 15 days of creep, $MgCl_2$ was injected. In this phase, all the oil was oil was produced during the initial 2-3 PVs, and after which despite the ongoing chemical reaction and compaction negligible oil volume was produced from the core. This shows that the non-equilibrium rock-fluid interactions between the calcite surface and $MgCl_2$ brine did not contribute to any tail-end recovery after the initial viscous displacement. When the observed oil production is compared to the chromatographic separation tests after mechanical tests, it can be deduced that the observed increase in the integrated area of the mixed wet samples is related to the creation of new mineral phases due to precipitation rather than the mobilisation of oil volumes wetting the mineral phases.

On the other hand, no oil was produced during the loading and the creep phase due to compaction and further, no oil was recovered during $MgCl_2$ injection through mixed wet Kansas chalk after the initial displacement (Sachdeva et al. 2019). The recovery of oil from Mons chalk due to compaction is likely due to the fact that it is more water wet (W_i of 0.63 ± 0.07, Table 3) to start with compared to the mixed wet Kansas chalk (W_i of 0.55 ± 0.05). Mixed wet Mons M4 core also have a larger volumetric strain during loading and creep in the stagnant phase compared to the Kansas mixed wet cores, which could also have resulted in production of oil. Kansas chalk also has a smaller pore size than Mons (Voake et al. 2019) and due to the capillary forces, they need the extra flow energy from the injection brine to produce oil. However, it remains to be tested how compaction-driven multiphase flow and geomechanical properties are changed for unaged oil/water saturated Kansas and Mons chalk samples.

Summary of the discussion

The results on Mons and Kansas chalks have shown that the initial wettability and oil/water saturation does not play a role in determining the effect of pore fluids on chalk mechanics. Even though $MgCl_2$ brine leads to weakening of chalk, it does not lead to any additional recovery of oil at the defined flow rates, which is likely due to one of these two reasons as reported by Sachdeva et al. (2019): (a) even though a change in the wetting state is observed for mixed wet Mons cores M3 and M4, $MgCl_2$ brine was not able to mobilise the oil stuck on the walls, meaning the new surfaces formed due to precipitation of magnesium-bearing minerals were all in contact with the water phase, and/or (b) pressure difference across the oil ganglia is insufficient to overcome capillary forces. Hence the combined observations from Kansas chalk showed that both compaction and non-equilibrium flow do not contribute to oil production after the initial displacement (Sachdeva et al. 2019), whereas these observations from Mons showed that compaction contributes to oil production up to a certain extent, but non-equilibrium flow does not. It will be important to study, in the future, the effect of increasing the flow rate even more to study the potentiality of $MgCl_2$ brine to improve oil recovery at higher rates.

CONCLUSIONS

We have investigated how injection of $MgCl_2$ brine through hydrostatically compacted Mons chalk impact a) stiffness and strength, b) time-dependent deformation at constant stresses, and c) oil production rates. All samples were loaded to a stress level of 150% of the compaction yield stress. The experiments were performed on both water wet and mixed wet samples. We have compared the observed mechanical response to a similar test series conducted on a different chalk type (Kansas) to display how petrophysical differences impact the overall dynamics.

The water wet and wettability-altered Mons samples were found to have a similar strength, but further investigations are required to define the stiffness relationship. On the other hand, the wettability altered Kansas samples were stiffer and stronger than their water wet counterparts. Hence, the initial wettability was shown to control the elastic stiffness and plastic strength measurements in both chalk types.

The volumetric creep strain and creep strain rate for different wettability cores followed a comparable trend during the stagnant fluid period. The creep response to the injection of $MgCl_2$ brine was also the same, irrespective of the wettability and oil/water saturation. These observations were found for both the Kansas and Mons chalks. The results seem to indicate that the presence of oil in pores does not prevent brines to access intergranular contacts, i.e. the water weakening by $MgCl_2$ injection prevails.

Further, IC analysis displayed that the chemical reactions were also insensitive to oil in the samples implying that the injected brine can interact with the mineral surfaces. The chemical replacement observed by ion chromatography was insensitive to the presence of oil in the pores, so the outcome from experiments performed on water wet samples can be applied to actual oil reservoir scenarios.

The oil production with time measurements due to compaction in Mons chalk showed a 43% additional oil recovery before the start of reactive brine flooding, whereas no additional oil recovery was seen during this stage in Kansas chalk. After the initial oil was produced during the first 2-3 PVs of $MgCl_2$ injection, neither compaction nor chemical interactions through both the Kansas and Mons chalks led to additional oil recovery.

ACKNOWLEDGEMENT

The authors acknowledge the Research Council of Norway and the industry partners, ConocoPhillips Skandinavia AS, Aker BP ASA, Eni Norge AS, Equinor ASA, Neptune Energy Norge AS, Lundin Norway AS, Halliburton AS, Schlumberger Norge AS, Wintershall Norge AS, and DEA Norge AS, of The National IOR Centre of Norway for support.

AVAILABILITY OF DATA

The data that support the findings of this study are available on request from the corresponding author.

APPENDIX

The main differences between Kansas and Mons chalk types used to discuss the results are reported in Table 9.

Table 9. Differences between Kansas and Mons chalk types.

	Kansas	**Mons**
Carbonate content, %	95-97	> 99
Initial wettability index (Sachdeva et al. 2019)	0.55 ± 0.05	0.63 ± 0.07
Biot coefficient (Voake et al. 2019)	0.91	0.95
Initial porosity, % (Sachdeva et al. 2019)	35-38	42-44
Initial water saturation, % (Sachdeva et al. 2019)	26-29	31-38
Relaxation time T_2 from NMR studies, ms (Voake et al. 2019)	15-80	35-200

REFERENCES

Ahsan, R. and Fabricius, I.L., 2010. Sorption of magnesium and sulfate ions on calcite. In 72nd EAGE Conference and Exhibition incorporating SPE EUROPEC 2010, Extended Abstracts, SP13.

Alam, M.M., Ahsan, R., Shaik, A.K., and Fabricius, I.L., 2010. Surface charge of calcite and its influence on the electrical conductivity in chalk. In 80th Annual International Meeting, Society of Exploration Geophysicists, Expanded Abstracts, 2686-2691.

Andersen, P.Ø., Wang, W., Madland, M.V., Zimmermann, U., Korsnes, R.I., Bertolino, S.R.A., Minde, M., Schulz, B., and Gilbricht, S., 2018. Comparative Study of Five Outcrop Chalks Flooded at Reservoir Conditions: Chemo-mechanical Behaviour and Profiles of Compositional Alteration. *Transport in Porous Media*, **121**(1), 135-181.

Andreassen, K.A. and Fabricius, I.L., 2010. Biot critical frequency applied to description of failure and yield of highly porous chalk with different pore fluids. *Geophysics*, **75**(6), E205-E213.

Bertolino, S.A.R., Zimmermann, U., Madland, M.V., Hildebrand-Habel, T., Hiorth, A., and Korsnes, R.I., 2013. Mineralogy, geochemistry and isotope geochemistry to reveal fluid flow process in flooded chalk under long term test conditions for EOR purposes. In XV International Clay Conference, Brasil, **676**.

Borromeo, L., Egeland, N., Minde, M.W., Zimmermann, U., Andò, S., Madland, M.V. and Korsnes, R.I., 2018. Quick, Easy, and Economic Mineralogical Studies of Flooded Chalk for EOR Experiments Using Raman Spectroscopy. *Minerals*, **8**(6), 221. ISSN 2075-163X. DOI: https://doi.org/10.3390/min8060221.

Brunauer, S., Emmett, P.H., and Teller, E., 1938. Adsorption of gases in multimolecular layers. *Journal of the American Chemical Society*, **60**(2), 309-319.

Coto, B., Martos, C., Peña, J. L., Rodríguez, R., and Pastor, G., 2012. Effects in the solubility of $CaCO_3$: Experimental study and model description. *Fluid Phase Equilibria*, **324**, 1-7.

Fabricius, I.L. and Borre, M.K., 2007. Stylolites, porosity, depositional texture, and silicates in chalk facies sediments. Ontong Java Plateau–Gorm and Tyra fields, North Sea. *Sedimentology*, **54**(1), 183-205.

Fan, T. and Buckley, J.S., 2007. Acid number measurements revisited. *SPE Journal*, **12**(04), 496-500.

Finn, T.M. and Johnson, R.C., 2005. Niobrara Total Petroleum System in the Southwestern Wyoming Province. Chapter 6 of *Petroleum Systems and Geologic Assessment of Oil and Gas in the Southwestern Wyoming Province, Wyoming, Colorado, and Utah*, U.S. Geological Survey Digital Data Series DDS-69-D, U.S. Geological Survey, Denver, Colorado.

Gauer, P.R., Sylte, J.E., and Nagel, N.B., 2002. Ekofisk Field Well Log Decompaction. Paper SPE/ISRM 78177 presented at the Rock Mechanics Conference, Irving, Texas, October 20-23.

Heggheim, T., Madland, M.V., Risnes, R., and Austad, T., 2005. A Chemical Induced Enhanced Weakening of Chalk by Seawater. *Journal of Petroleum Science and Engineering* **46**, 171-184.

Hellmann, R., Renders, P.J.N., Gratier, J.P., and Guiguet, R., 2002a. Experimental pressure solution compaction of chalk in aqueous solutions. Part 1. Deformation behavior and chemistry. *Water-Rock Interactions, Ore Deposits, and Environmental Geochemistry: A Tribute to David A. Crerar*, **7**(7), 129–152.

Hellmann, R., Gaviglio, P., Renders, P.J.N., Gratier, J.P., Bekri, S., and Adler, P., 2002b. Experimental pressure solution compaction of chalk in aqueous solutions. Part 2. Deformation examined by SEM, porosimetry, synthetic permeability, and X-ray computerized tomography. *Water-Rock Interactions, Ore Deposits, and Environmental Geochemistry: A Tribute to David A. Crerar*, **7**(7), 153–178.

Hermansen, H., Landa, G.H., Sylte, J.E., and Thomas, L.K., 2000. Experiences after 10 years of waterflooding the Ekofisk field, Norway. *Journal of Petroleum Science and Engineering*, **26**, 11–18.

Hiorth, A., Cathles, L.M., and Madland, M.V., 2010. The impact of pore water chemistry on carbonate surface charge and oil wettability. *Transport in porous media*, **85**(1), 1-21.

Hofmann, S., Voïtchovsky, K., Spijker, P., Schmidt, M., and Stumpf, T., 2016. Visualising the molecular alteration of the calcite (104) – water interface by sodium nitrate. *Scientific reports*, **6**, 21576.

Korsnes, R.I., Madland, M.V., and Austad, T., 2006a. Impact of Brine Composition on the Mechanical Strength of Chalk at High Temperature. *Eurock 2006: Multiphysics Coupling and Long Term Behaviour in Rock Mechanics*, Taylor and Francis, London, 133-140.

Korsnes, R.I., Strand, S., Hoff, O., Pedersen, T., Madland, M.V., and Austad, T., 2006b. Does the Chemical Interaction between Seawater and Chalk affect the Mechanical Properties of Chalk? *Eurock 2006: Multiphysics Coupling and Long Term Behaviour in Rock Mechanics*, Taylor and Francis, London: p. 427-434.

Korsnes, R.I., Madland, M.V., Austad, T., Haver, S., and Røsland, G., 2008. The Effects of Temperature on the Water Weakening of Chalk by Seawater. *Journal of Petroleum Science and Engineering*, **60**, 183-193.

Liu, J., Wani, O.B., Alhassan, S.M., and Pantelides, S.T., 2018. Wettability Alteration and Enhanced Oil Recovery Induced by Proximal Adsorption of Na^+, Cl^-, Ca^{2+}, Mg^{2+}, and SO_4^{2-} Ions on Calcite. *Physical Review Applied*, **10**(3), 034064.

Lyklema, J., 2005. *Fundamentals of interface and colloid science: soft colloids*, **5**. San Diego, USA: Elsevier, Academic Press.

Madland, M.V., Hiorth, A., Korsnes, R.I., Evje, S., and Cathles, L., 2009. Rock Fluid Interactions in Chalk Exposed to Injection of Seawater, $MgCl_2$, and NaCl Brines with Equal Ionic Strength. Paper A22 presented at the 15th European Symposium on Improved Oil Recovery, Paris, France, April 27-29.

Madland, M.V., Hiorth, A., Omdal, E., Megawati, M., Hildebrand-Habel, T., Korsnes, R.I., Evje, S., and Cathles, L.M., 2011. Chemical Alterations Induced by Rock-Fluid Interactions when Injecting Brines in High Porosity Chalks. *Transport in Porous Media*, **87**, 679-702.

Madland, M.V., Midtgarden, K., Manafov, R., Korsnes, R.I., Kristiansen, T.G., and Hiorth, A., 2008. The Effect of Temperature and Brine Composition on the Mechanical Strength of Kansas Chalk. Paper SCA2008-55 presented at the International Symposium of the Society of Core Analysts, Abu Dhabi, UAE, October 29-November 2.

Maury, V., Piau, J.M., and Halle, G., 1996. Subsidence induced by water injection in water sensitive reservoir rocks: The example of Ekofisk. Paper SPE 36890 presented at the SPE European Petroleum Conference, Milan, Italy, October 22-24.

Megawati, M., Andersen, P.Ø., Korsnes, R.I., Evje, S., Hiorth, A., and Madland, M.V., 2011. The effect of aqueous chemistry pH on the time-dependent deformation behavior of chalk experimental and modelling study. In: Pore2Fluid International Conference. 16–18 Nov, Paris, France.

Megawati, M., Hiorth, A., and Madland, M.V., 2013. The impact of surface charge on the mechanical behavior of high-porosity chalk. *Rock Mechanics and Rock Engineering*, **46**(5), 1073-1090.

Megawati, M., Madland, M.V., and Hiorth, A., 2015. Mechanical and physical behavior of high-porosity chalks exposed to chemical perturbation. *Journal of Petroleum Science and Engineering*, **133**, 313–327. http://dx.doi.org/10.1016/j.petrol.2015.06.026.

Minde, M.W., Haser, S., Korsnes, R.I., Zimmermann, U., and Madland, M.V., 2017. Comparative Studies of Mineralogical Alterations of Three Ultra-long-term Tests of Onshore Chalk at Reservoir Conditions. In: 19th European Symposium on Improved Oil Recovery/IOR Norway 2017. European Association of Geoscientists and Engineers. ISBN 978-94-6282-209-2.

Minde, M.W., Zimmermann, U., Madland, M.V., Korsnes, R.I., Schulz, B. and Gilbricht, S., 2018a. Mineral Replacement in Long-Term Flooded Porous Carbonate Rocks. Submitted to *Geochimica et Cosmochimica Acta*, publication under review.

Minde, M.W., Wang, W., Madland, M.V., Zimmermann, U., Korsnes, R.I., Bertolino, S.R., and Andersen, P.Ø., 2018b. Temperature effects on rock engineering properties and rock-fluid chemistry in opal-CT-bearing chalk. *Journal of Petroleum Science and Engineering*, **169**, 454-470.

Nagel, N.B., 1998. Ekofisk Field Overburden Modelling. Paper SPE 47345 presented at the SPE/ISRM Rock Mechanics in Petroleum Engineering, Trondheim, Norway, July 8-10.

Nagel, N.B., 2001. Compaction and subsidence issues within the petroleum industry: From Wilmington to Ekofisk and beyond. *Physics and Chemistry of the Earth, Part A: Solid Earth and Geodesy*, **26**(1-2), 3-14.

Nermoen, A., Korsnes, R.I., Hiorth, A. and Madland, M.V., 2015. Porosity and Permeability Development in Compacting Chalks during Flooding of Non-Equilibrium Brines: Insights from Long-Term Experiment. *Journal of Geophysical Research: Solid Earth*, **120**, doi: 10.1002/ 2014JB011631.

Nermoen, A., Korsnes, R.I., Aursjø, O., Madland, M.V., Kjørslevik, T.A., and Østensen, G., 2016. How stress and temperature conditions affect rock-fluid chemistry and mechanical deformation. *Frontiers in Physics*, **4**, 2.

Nermoen, A., Korsnes, R.I., Storm, E.V., Stødle, T., Madland, M.V., and Fabricius, I.L., 2018. Incorporating electrostatic effects into the effective stress relation - Insights from chalk experiments. *Geophysics*, **83**(3), MR123-MR135.

Neveux, L., Grgic, D., Carpentier, C., Pirnon, J., Truche, L., and Girard, J.P., 2014a. Influence of hydrocarbon injection on the compaction by pressure solution of a carbonate rock: An experimental study under triaxial stresses. *Marine and Petroleum Geology*, **55**, 282–294.

Neveux, L., Grgic, D., Carpentier, C., Pironon, J., Truche, L., and Girard, J.P., 2014b. Experimental simulation of chemomechanical processes during deep burial diagenesis of carbonate rocks. *Journal of Geophysical Research: Solid Earth*, **119**(2), 984–1007. https://doi.org/10.1002/2013JB010516

Pirson, S., Spagna, P., Baele, J.M., Damblon, F., Gerrienne, P., Vanbrabant, Y., and Yans, J., 2008. An Overview of the Geology of Belgium. *Memoirs of the Geological Survey of Belgium*, **55**(5), 26.

Ricci, M., Spijker, P., Stellacci, F., Molinari, J.F., and Voïtchovsky, K., 2013. Direct visualization of single ions in the Stern layer of calcite. *Langmuir*, **29**(7), 2207-2216.

Risnes, R., 2001. Deformation and Yield in High Porosity Outcrop Chalk. *Phys. Chem. Earth* (A), **26**, 53-57.

Risnes, R., Haghighi, H., Korsnes, R.I., and Natvik, O., 2003. Chalk-Fluid Interactions with Glycol and Brines. *Tectonophysics*, **370**, 213-226.

Sachdeva, J.S., Nermoen, A., Korsnes, R.I., and Madland, M.V., 2019. Impact of Initial Wettability and Injection Brine Chemistry on Mechanical Behaviour of Kansas Chalk. *Transport in Porous Media*. https://doi.org/10.1007/s11242-019-01269-z

Sachdeva, J.S., Sripal, E.A., Nermoen, A., Korsnes, R.I., Madland, M.V., and James, L.A., 2018. A Laboratory Scale Approach to Wettability Restoration in Chalk Core Samples. SCA2018-020 paper presented at the International Symposium of the Society of Core Analysts, Trondheim, Norway, August 27-30.

Standnes, D.C. and Austad, T., 2000a. Wettability alteration in chalk: 1. Preparation of core material and oil properties. *Journal of Petroleum Science and Engineering*, **28**(3), 111-121.

Standnes, D.C. and Austad, T., 2000b. Wettability alteration in chalk: 2. Mechanism for wettability alteration from oil-wet to water-wet using surfactants. *Journal of Petroleum Science and Engineering*, **28**(3), 123-143.

Stipp, S.L.S., 1999. Toward a conceptual model of the calcite surface: Hydration, hydrolysis and surface potential. *Geochimica et Cosmochimica Acta*, **63**(19/20), 3121 – 3131.

Strand, S., Standnes, D.C., and Austad, T., 2006a. New Wettability Test for Chalk Based on Chromatographic Separation of SCN^- and SO_4^{2-}. *Journal of Petroleum Science and Engineering*, **52**, 187-197.

Strand, S., Høgnesen, E.J., and Austad, T., 2006b. Wettability alteration of carbonates - Effects of potential determining ions (Ca^{2+} and SO_4^{2-}) and temperature. *Colloids and Surfaces A: Physicochemical and Engineering Aspects*, **275**(1-3), 1-10.

Strand, S., Hjuler, H.L., Torsvik, R., Pedersen, J.I., Madland, M.V., and Austad, T., 2007. Wettability of chalk: Impact of silica, clay content and mechanical properties. *Petroleum Geoscience*, **13**(1), 69-80.

Sulak, R.M., 1991. Ekofisk Field: The First 20 Years. *Journal of Petroleum Technology*, **43**(10), 1-265.

Sulak, R.M. and Danielsen, J., 1989. Reservoir Aspects of Ekofisk Subsidence. *Journal of Petroleum Technology*, **41**(7), 709-716, SPE 17852-PA.

Sylte, J.E., Thomas, L.K., Rhett, D.W., Bruning, D.D., and Nagel, N.B., 1999. Water Induced Compaction in the Ekofisk Field. Paper SPE 56426 presented at the SPE Annual Technical Conference and Exhibition, Houston, Texas, October 3-6.

Voake, T., Nermoen, A., Ravnås, C., Korsnes, R.I., and Fabricius, I.L., 2019. Influence of temperature cycling and pore fluid on tensile strength of chalk, *Journal of Rock Mechanics and Geotechnical Engineering*, https://doi.org/10.1016/j.jrmge.2018.12.004.

Zhang, P. and Austad, T., 2005. The Relative Effects of Acid Number and Temperature on Chalk Wettability. Paper SPE 92999 presented at SPE International Symposium on Oilfield Chemistry, Houstan, Texas, USA, February 2-4.

Zhang, P. and Austad, T., 2006. Wettability and oil recovery from carbonates: Effects of temperature and potential determining ions. *Colloids and Surfaces A: Physicochemical and Engineering Aspects*, **279**(1-3), 179-187.

Zhang, P., Tweheyo, M. T., and Austad, T., 2007. Wettability alteration and improved oil recovery by spontaneous imbibition of seawater into chalk: Impact of the potential determining ions Ca^{2+}, Mg^{2+}, and SO_4^{2-}. *Colloids and Surfaces A: Physicochemical and Engineering Aspects*, **301**(1-3), 199-208.

Zimmermann, U., Madland, M.V., Nermoen, A., Hildebrand-Habel, T., Bertolino, S.A.R., Hiorth, A., Korsnes, R.I., Audinot, J.N., and Grysan, P., 2015. Evaluation of the compositional changes during flooding of reactive fluids using scanning electron microscopy, nano-secondary ion mass spectrometry, x-ray diffraction and whole rock geochemistry. *AAPG (Am. Assoc. Pet. Geol.) Bulletin*, **99**(5), 791–805. http://dx.doi.org/10.1306/12221412196.

Paper IV

Sachdeva, J.S., Sripal, E.A., Nermoen, A., Korsnes, R.I., Madland, M.V., and James, L.A. (2018). A Laboratory Scale Approach to Wettability Restoration in Chalk Core Samples. Paper SCA2018-117 presented at the International Symposium of the Society of Core Analysts, Trondheim, Norway, 27-30 August.

A LABORATORY SCALE APPROACH TO WETTABILITY RESTORATION IN CHALK CORE SAMPLES

Jaspreet S. Sachdeva[1,2], Edison A. Sripal[3], Anders Nermoen[1,2,4], Reidar I. Korsnes[1,2],
Merete V. Madland[1,2], Lesley A. James[3]
[1]The National IOR Centre of Norway
[2]University of Stavanger
[3]Department of Process Engineering, Memorial University of Newfoundland
[4]International Research Institute of Stavanger
Corresponding Author: Dr. Lesley A. James (ljames@mun.ca)

This paper was prepared for presentation at the International Symposium of the Society of Core Analysts held in Trondheim, Norway, 27-30 August 2018

ABSTRACT

Wettability in chalk has been studied comprehensively to understand fluid flow mechanisms impacting coreflooding experiments. Wettability becomes paramount in understanding the parameters influencing chalk-fluid interactions. The main objective of this work is to evaluate as to which degree the wettability in chalk core samples can be controlled in the laboratory. Kansas chalk samples saturated with brine (1.1 M/64284 ppm NaCl) and an oil mixture (60% - 40% by volume of Heidrun oil and heptane) were aged at a constant temperature of 90°C with aging time as the laboratory control variable. A multimodal method incorporating contact angle measurements, wettability index via USBM test, and SEM-MLA analysis was applied in evaluating wettability. A systematic approach was applied with the three different methods to quantify the degree of uncertainty linked to a) wettability estimation and b) the aging procedure to control wettability alteration of Kansas chalk. With a comprehensive suite of samples, we were successfully able to alter the wettability of chalk cores.

INTRODUCTION

Wettability is the tendency of one fluid to spread on, or adhere to, a solid surface in the presence of another immiscible fluid. Wettability is of paramount importance in oil recovery from low permeability chalk as it controls the flow and distribution of fluids [1]. In the past, numerous studies have indicated a number of factors influencing wettability including the composition of oil, rock mineralogy, fluid saturation, brine composition, temperature, and time of aging [2]. Although carbonate reservoirs tend to be intermediate to strongly oil wet, in the laboratory restoration to oil wet characteristics is fraught with uncertainties [3].

One of the simplest experimental control variables is the aging time. Anderson [2] indicated that 1000 hours (40 days) of aging at reservoir temperature is sufficient for wettability equilibrium for sandstones. In order to ensure that brine chemistry are not ignored during the aging process it is important to saturate the core with brine prior to any flooding of oil.

Wettability can be quantified using contact angle measurements of a drop placed on top of the surface and/or the USBM method (United States Bureau of Mines). For a reservoir rock to be termed oil wet, the contact angle in an oil-brine-rock system should be greater than 105° [2,4,5], or the wettability index for the USBM method to be close to -1, calculated from drainage and imbibition capillary pressure vs saturation curves. Robin et al. [6] developed a qualitative description of how to differentiate between oil wet and water wet capillary pressure curves. In addition to the contact angle and USBM methods, Scanning Electron Microscopy (SEM) analyses using Cryo Scanning Electron Microscope (Cryo-SEM) and Environmental Scanning Electron Microscope (ESEM) methods [6,7] have been used to determine wettability in rocks and packed glass beads saturated with reservoir fluids. These analyses had uncertainties as it often compromised the sample integrity due to extreme changes in the physical state because of cooling and polishing. In a newly developed method [8], SEM-MLA (Mineral Liberation Analysis) has been applied by testing the samples without any changes to their physical state.

In this paper we try to determine the threshold duration beyond which the aging does not change the wetting state of outcrop chalk. After aging the chalk cores at high temperature for varying periods of time, wettability determination was performed using contact angle measurements, USBM method and SEM-MLA analysis. Specifically, the study was carried out on outcrop chalk samples as laboratory core flooding and SCAL experiments are routinely performed on core samples from restored state [9]. Similar work had been carried out previously on Rørdal chalk samples [1] wherein the chalk samples were submerged into crude oil for wettability alteration, and then after aging the crude oil was flushed out by decahydronapthalene, which subsequently was flushed out by decane for imbibition tests. Graue et al. [1] reported that a stable wettability was obtained for cores aged more than 14 days using a different set of fluids.

EXPERIMENTAL METHODODLOGY

Porous Medium

The porous media used for this work was outcrop chalk from Kansas, from the Niobrara formation, Fort Hays Member, USA (Late Cretaceous). The Kansas chalk used here displayed a permeability ranging from 1.90 to 2.10 mD, and a porosity ranging from 36.93 to 38.57 %. Its carbonate content is approx. 95-97%, the Biot coefficient is 0.91 and the induration is H3 [10,11], which imply that Kansas chalk is partially cemented compared to other high porous chalks.

Fluids

The physical properties of the 1.1 M NaCl-brine used to determine the saturation porosity, brine-permeability, and for initial saturation are presented in Table 1. Heidrun (offshore Norway) dead crude oil with 6 cP viscosity and 858 kg/m^3 density was mixed with n-heptane (60% - 40% by volume) and used as the non-wetting phase. The total acid number (TAN) of the Heidrun crude oil was analyzed and found to be 2.82 mg KOH/g (reported to be 3 mg KOH/g in [12]), while the mixture obtained an acid number of 2.12 mg KOH/g using potentiometric titration method. The oil mixture was filtered (5 μm filter paper) and degassed by vacuuming for 48 hours to prevent gas production during the drainage. The physical properties of Heidrun crude oil are tabulated in Table 2. The composition of the oil mixture was analyzed using *Agilent 7890A Gas Chromatograph with Simulated Distillation* (SIMDIS) system (see Table 3).

Experimental Method

Sample Preparation and Basic Sample Characterization

7 full sized cylindrical core samples ('cores') of 1.5" (38.1 mm) diameter and 2" (50 mm) lengths, and 5 mm length end pieces from both ends (top and bottom, 14 in total) were drilled out from a single block. The cores and end pieces were sonicated to remove fines and then dried at 90^{o}C for two days. Then the dry weight of the cores was measured before being vacuumed and saturated by NaCl brine for wet weight measurements. The saturation porosity could then be estimated (the porosity of the end pieces was assumed to be the same). The 7 cores were mounted in flow-cells and the brine-permeability was estimated from differential pressure measurements and Darcy's law. The saturation porosity and brine permeability estimates are given in Table 4.

Centrifuge for Primary Drainage

The 7 brine saturated cores including the 14 top and bottom end pieces with filter paper in between, were mounted into the core holders of the centrifuge (*Rotosilenta 630RS* centrifuge from Vinci Technologies). An overburden/confining pressure of 200 psi (1.38 MPa) was used, and the centrifuge was operated in drainage mode to displace the brine with oil to irreducible water saturation. Drainage was performed in 7 steps from 500 rpm to 3500 rpm in increments of 500 rpm with 3 hours of equilibration time for each step. The capillary pressure was calculated at any position, r, along the core length using the Hassler-Brunner equation [13]:

$$P_c(r) = \frac{1}{2}\Delta\rho\omega^2(r_1^2 - r^2) \tag{1}$$

where $\Delta\rho = \rho_{out} - \rho_{in}$ is the density difference between the fluid expelled from the core (ρ_{out}) and the fluid entering the core (ρ_{in}), ω is the angular rotation speed of the centrifuge, and $r_1 \simeq 22.1$ cm (for drainage mode of centrifuge) and 16.5 cm (for imbibition mode of centrifuge) and r (varying from 0 to 5 cm) are the distances from the rotational axis to the outlet face and any point along the core length, respectively. In addition to Hassler Brunner method, Forbes and Forbes-splines method were also applied, but there was no significant improvement in the model fit. According to Forbes [16], it is assumed that the pressure field in the core is linear, (neither radial nor centrifugal), and gravity is neglected. These assumptions can be satisfied for very short and narrow samples spun far from the rotation axis. In the case of Vinci centrifuge, the geometry is such that (sample being far from the rotation axis), the pressure field in the core is almost linear which is not the case with other centrifuge's (Beckmans). Hence this was determined to be reason for very little difference between the results of Hassler Brunner and Forbes equations in our case.

After reaching an equilibrium between the oil/water saturation and capillary pressure, hence when no more brine is being produced, the brine expelled from the core was measured and the average water saturation for each rotation speed was obtained. This water saturation (%) was plotted against the capillary pressure estimated from equation (1) to produce the capillary pressure curve.

Aging

After the centrifuge the confining pressure was reduced to 100 psi and then the core holders with cores and end pieces inside were placed in the oven to age at 90°C for aging time ranging from 6 to 30 days (Table 4).

After aging, the 7 full sized cores were used for USBM wettability measurement, and the 7 top and 7 bottom end pieces were used for the contact angle measurements and SEM-MLA analyses, respectively.

Wettability determination by USBM of cores

After the primary drainage (oil displaced brine) and aging, the NaCl brine was forcibly imbibed (primary imbibition) into the cores using the centrifuge in imbibition mode to obtain residual oil saturation S_{or} – before a secondary drainage (oil displaced brine) was performed to reach the irreducible water saturation, as described by McPhee et al. [14]. The receiving tubes coupling cups to core holders, were saturated by the same fluid as the cups holding the fluid that enters the cores. A confining pressure of 200 psi and 7 centrifugal steps from 500 to 3500 rpm at 500 rpm increments for 3 hours equilibration time was used. Areas under the secondary drainage curve (A_1) and primary imbibition curve (A_2), when plotting the capillary pressure against water saturation enabled us to estimate the wettability index I_w via:

$$I_w = log\ (A_1/A_2) \tag{2}$$

The trapezoidal method was used to estimate the area under the curves. In conjunction to the formula above, the wettability index I_w is greater than 0 for water wet, smaller than 0 for oil wet and around 0 for neutral wet systems.

Wettability determination by Contact Angle Measurements of the top end pieces

The top end piece of the aged core sample was mounted in a *Vinci IFT 700* instrument to measure the contact angle by sessile drop method. The same NaCl brine (Table 1) was used as the droplet fluid and each droplet was of size $\sim 5 \cdot 10^{-4}$ ml (radius of 0.5 mm). The sessile drop method uses a contact angle goniometer, which allows the user to measure the contact using digital photography for immobile and permanently attached droplets placed by a syringe onto the chalk end piece surface. 8-10 photographs were acquired over 2 minutes each enabling us to observe how the droplet obtained a stable geometry over time. The contact angle measurement was done on trimmings that were on top of the consolidated sample. These trimmings were at the oil front during the primary imbibition process. Hence it was assured that the saturation was uniform. Contact angle was measured at multiple spots (about 10 to 12) on the surface of the trimming and an average value was taken as the contact angle for that particular samples resulting in 150 to 300 data points for each sample. Initially, brine drops were left for a longer duration to observe the change in contact angle, but this largely due to evaporation of the brine droplet. Also, leaving the brine droplet for a longer duration resulted in formation of salt crystals on the surface causing discrepancies in the contact angle measurements. Hence, contact angle measurement at multiple spots on the rock surface was performed an average value of the contact angle measurement is reported. On the other hand it was understood that roughness will impact contact angle measurements. It is understood that the contact angles measured are effective and will vary depending on surface treatment. But in this case all samples were treatment the same way and that the contact angles can be compared. All the sample trimmings were cut with the same saw using SS blade (1/16”). The chalk samples that were used for contact angle and SEM-MLA were also cut in the same way. We don’t believe the surface roughness influenced the contact angle measurement within our measurements as the shape of the droplet did not change from sample to sample or within a sample.

Wettability determination by SEM-MLA analysis of the bottom end pieces

In the last stage, the bottom end piece of the aged core sample was used for SEM-MLA analysis [8]. A *FEI Quanta 650 FEG* SEM, equipped with Bruker high throughput Energy Dispersive X-ray (EDX) system and backscattered electron detectors was used for this purpose. Imaging of the flat sample surfaces was carried out at very low vacuum conditions (0.6 Torr) [15]. Additionally, the end pieces were not subjected to any metallic or carbon coating on the surface, which is a standard procedure for SEM-MLA analysis, except for liquid graphite coating on the sample holder. The instrument conditions and parameters were: high voltage of 25 kV, spot size of 5.75, working distance of 13.5 mm, 10 nA beam current, 16 µs BSE dwell time, 10-pixel minimum size (400-pixel frame resolution for 1 mm High Full Well (HFW) capacity), and 12 ms spectrum dwell for EDX. The MLA acquisitions were performed using the 3.1.4.683 MLA™ software and each acquisition took between 3 and 4 hours per sample. Minerals and fluids in the core sample were calculated through a custom classification script that accounted for porosity and mineralogy. The results for individual samples were acquired as a digital map of the minerals and a data table listing their mineral composition. Prior to testing the individual aged end pieces, two pure chalk pieces; one with a drop of the oil mixture and another with a drop of 1.1M NaCl-brine on it, were analyzed to determine the oil and NaCl-brine (termed ‘halite’) signature and added to the SEM mineral database. The aged end pieces were then analyzed to determine the relative quantity of oil, halite and carbonate in percent. The premise is to link the oil/halite concentrations to the overall wetness of the mineral surface, which in this study is controlled by the aging time.

RESULTS AND DISCUSSION

The premise of this work was to measure wettability of aged Kansas chalk using three techniques at varying aging time while keeping brine and oil composition, and aging temperature fixed.

Before aging, the samples were brought to irreducible water saturation (S_{wi}) using the primary drainage method. From trial and error, it was found that a confining pressure of 200 psi (1.38 MPa) was optimal to avoid disintegration of the cores during centrifuge tests. The irreducible water saturation was found to be 54.15 to 64.71% for all cores (Table 4).

After the samples were aged they were imbibed by NaCl brine (primary imbibition) from S_{wi} to the residual oil saturation (S_{or}, see Figure 1 and Table 4). The area under the P_c vs S_w curve during primary imbibition is termed A_2. Then, the cores were taken out of the holders which were switched to drainage mode before secondary drainage was performed (in which oil expelled brine). The area spanned by the P_c vs S_w curve is termed A_1.

The wettability index I_w from USBM method was estimated using the log10 of the ratio A_1 by A_2 in equation (2). From the WI reported in Table 4, it can be seen that, except from chalk number 5 (18 days), an increasing aging time leads to a lowered wettability index, ranging from 0.36 and 0.51 for 6 and 9 days aging to around zero for 12, 15 and 21 days, and -0.15 for 30 days aging. Figure 2 (left) gives a plot of wettability index estimated by USBM method as a function of aging time. The abnormality with result from sample aged 18 days is quite uncertain. But during the USBM tests it was observed that number of tests have to be repeated as the samples disintegrated due to excess overburden pressure. This resulted in additional tests to optimize the confining pressure required for successful drainage and imbibition tests on the samples. Even though the confining pressure was optimized by trial and error, and the confining pressure used for the sample with 18 days aging time is the same as the other samples, we suspect that this outlier may have been caused by natural fractures present in chalk which led to further disintegration during the primary imbibition and secondary drainage that was not visible during the initial tests.

In summary each method provided a conclusion that could not be perceived as unanimous. This discrepancy in the experimental data may have originated mainly from the USBM method. Although the data shows only 7 samples with 7 aging times, more than 30 samples were tested with almost half of them breaking apart. Initially the samples were not able to withstand the confining pressure and with that reduced and optimized, we had samples coming out intact in the primary drainage stage. The core samples (used for USBM) went through further damage during the primary imbibition and secondary drainage. Hence it was with great difficulty we were able to get reliable data for the USBM method. This was not the case for the trimmings used for the contact angle measurement and the SEM-MLA analysis. In these cases, the trimmings being just a few millimeters, we were able to get a saturated and a more reliable sample after few attempts. The trimmings for the SEM-MLA were selected once the primary drainage test was found to be reliable as the data was similar for all the samples. For SEM-MLA analysis, the trimmings being barely few millimeters were put though the primary drainage process and selected for aging. This again took number of attempts to eventually select the 7 samples and age them.

The top end pieces were analyzed with contact angle measurement in which a brine droplet was placed on the sample. It was found impossible to place a stable droplet onto the samples aged for 6 and 9 days, as the droplet initially had a maximal contact angle of around 65°, but within only a few seconds, it started to spread out and got sucked into the chalk developing into a contact angle of 0° in time. Hence, obtaining a stable, time independent, contact angle measurement was not possible for samples with 6 and 9 aging days. For samples aged for 12 days and 30 days the sessile droplets formed enabling stable contact angle measurements. For the 12 and 15 days samples contact angles of 78° and 85° were found respectively. Increasing the aging time to 18, 21 and 30 days the contact angle increased to 102, 110, and 108°, respectively (Figure 2 (right) and Figure 3, Table 4). Hence, as the aging time is increased to 18 days and beyond, the contact angle reached a plateau of more than 100° which is in-line with oil wet characteristics, said to be greater than 105° [2,4,5]. Figure 2 (right) gives a plot of contact angle as a function of aging time.

The lower end pieces were analyzed using SEM–MLA in which the oil/brine content of the surface of the samples was determined (Table 5). The use of a pre-defined signature of the oil, calcite mineralogy and brine in the MLA-database simplified the analysis compared to a similar study using Berea sandstone [8]. Based on the individual surface measurements (reported in Table 5) for the amount of oil/brine/calcite of the aged chalk samples, we report the SEM-MLA wettability estimate in Table 4. Figure 4 provides two examples of mineral/fluid MLA maps and SEM images of samples aged for 6 days and 30 days showing how an increasing aging time results in an increased oil signature on the chalk samples.

The wettability measurements reported here, from all three methods, imply that an aging time exceeding 21 days was sufficient to ensure that the Kansas chalks are oil wet when the samples were saturated by 1.1 M NaCl-brine and 2.12 mg KOH/g oils and aged at 90°C.

CONCLUSIONS

1. 7 outcrop Kansas chalk cores together with 5 mm thick top and bottom end pieces were acquired from the same block and their wettability were altered by aging for varying durations. The aging temperature, brine and oil compositions were kept fixed for all 7 aged samples.
2. Wettability was measured using three different methods viz. contact angle, wettability index via USBM method and oil saturation using SEM-MLA analysis.
3. USBM method: Increasing oil wet characteristics, i.e. close to zero meaning that the ratio of A_1 by A_2 equals 1, was observed with increasing aging time from 12 days onward. The 18 days' experiment seemed to be an outlier result as it did not match the 12 and 15 days' (close to zero, positive value), and 21 and 30 days tests (close to zero,

negative value). To ensure that the sample remained intact a confining pressure of 200 psi had to be used to prevent disintegration of the sample.

4. Contact angle measurement: With increasing aging time, the chalk samples indicated increasing oil wet characteristics, especially after 12 days aging and onwards. Contact angle values varied from 65° (unstable readings from 6 and 9 days tests – water wet) to 110° (very stable readings for 18, 21 and 30 days test – oil wet).
5. The newly developed SEM-MLA method for oil/brine chalk surface determination provided a direct observation of the chemical composition of the end-pieces. An increasing amount of oil present on the samples was measured using MLA analysis. It was found that the oil fraction increased steadily from 10% to 46% when aging time was increased from 6 to 30 days. Interestingly MLA analysis on chalk samples was straight forward compared to Berea as the mineral list was limited.
6. Based upon the three presented measures, an aging time exceeding 21 days, at 90°C saturated by 1.1 M NaCl-brine and 2.12 mg KOH/g oils, was sufficient to ensure that the Kansas chalks are oil wet. This conclusion was largely driven by the contact angle results indicating a wettability condition above 21 days. The USBM method indicated oil wet characteristics starting from 21 days added to the discrepancy on 18 days was forcing us to lean towards 18 days timeline to ensure oil wet characteristics. Hence a timeline of 21 days have been conclude to restore oil wet characteristics in chalk.
7. The tests can further be strengthened by varying brine salinity, aging temperature and the wettability tests broadened to include Amott tests in addition.

ACKNOWLEDGEMENTS

The authors acknowledge the Research Council of Norway and the industry partners, ConocoPhillips Skandinavia AS, Aker BP ASA, Eni Norge AS, Total E&P Norge AS, Equinor ASA, Neptune Energy Norge AS, Lundin Norway AS, Halliburton AS, Schlumberger Norge AS, Wintershall Norge AS, and DEA Norge AS, of The National IOR Centre of Norway for support. The authors would also like to thank Chevron Canada, Hibernia Management and Development Company (HMDC), Research and Development Corporation of Newfoundland and Labrador (RDC), Natural Sciences and Engineering Research Council of Canada (NSERC), and the Canadian Foundation for Innovation (CFI) for financial support. We thank our colleagues in the Hibernia EOR Research Group for technical support.

REFERENCES

1. Graue, A., Viksund, B.G., & Baldwin, B.A., “Reproducible Wettability Alteration of Low-Permeable Outcrop Chalk,” (1999), Society of Petroleum Engineers. doi:10.2118/55904-PA
2. Anderson, W.G., “Wettability Literature Survey - Part 1: Rock/Oil/Brine Interactions and the Effects of Core Handling on Wettability”. *Journal of Petroleum Technology*, (1986) **38,** 10, 1125-1144.

3. Zangiabadi, B., Korsnes, R.I., Madland, M.V., Hildebrand-Habel, T., Hiorth, A., & Kristiansen, T.G., “Mechanical Properties of High And Lower Porosity Outcrop Chalk At Various Wetting States,” (2009), Presented at Asheville 2009, the 43rd US Rock Mechanics Symposium and 4th US-Canada Rock Mechanics Symposium, Asheville, NC, 28 June-1 July.
4. Andersen, P.O., Ahsan, R., Evje, S., Bratteli, F., Madland, M.V., & Hiorth, A., “A Model for Brine-Dependent Spontaneous Imbibition Experiments with Porous Plate,” (2013), Society of Petroleum Engineers. doi:10.2118/164901-MS
5. Cuiec, L.E., Bourbiaux, B., & Kalaydjian, F., “Oil Recovery by Imbibition in Low-Permeability Chalk,” (1994), Society of Petroleum Engineers. doi:10.2118/20259-PA
6. Robin, M., Combes, R., Degreve, F., & Cuiec, L., “Wettability of Porous Media from Environmental Scanning Electron Microscopy: From Model to Reservoir Rocks”, (1997), Paper SPE-37235, Presented at the International Symposium on oilfield Chemistry, Houston, Texas, USA, 18-21 February.
7. Schmatz, J., Klaver, J., Jiang, M., & Urai, J.L., “Nanoscale Morphology of Brine/Oil/Mineral Contacts in Connected Pores of Carbonate Reservoirs: Insights on Wettability From Cryo-BIB-SEM,” (2017), Society of Petroleum Engineers. doi:10.2118/180049-PA
8. Sripal, E., & James, L.A., “Application of an Optimization Method for the Restoration of Core Samples for SCAL Experiments,” *Petrophysics*, (2018) **59,** 1, 72-81.
9. Hirasaki, G.J., Rohan, J.A., Dubey, S.T., & Niko, H., “Wettability Evaluation During Restored-State Core Analysis,” (1990), Paper SPE-20506, Presented at the SPE Annual Technical Conferences and Exhibition, New Orleans, Louisisana, USA, 23-26 September.
10. Henriksen, A.D., Fabricius, I.L., Borre, M.K., Korsbech, U., Theilgaard, A.T., & Zandbergen, J.B., “Core density scanning, degree of induration and dynamic elastic moduli of Palaeogene limestone in the Copenhagen area,” *Quarterly Journal of Engineering Geology and Hydrogeology*, (1999) **32**, 107-117.
11. Voake, T., Nermoen, A., Ravnås, C., Korsnes, R.I., & Fabricius, I.L., “The influence of temperature cycling and pore fluid on the tensile strength of chalk,” Submitted for publication, (2018).
12. Warner, R., “Western European refineries and acidity in crude oil,” S&P Global Platts, (2017), Available at https://www.platts.com/IM.Platts.Content/InsightAnalysis/IndustrySolutionPapers/SR-western-european-refineries-and-acidity-in-crude-oil.pdf [Accessed 26 April 2018].
13. Hassler, G.L., & Brunner, E. “Measurement of capillary pressures in small core samples,” Trans. AIME, (1945) **160**, 114-123.
14. McPhee C., Reed, J., & Zubizarreta, I., *Core Analysis: A Best Practice Guide*, Elsevier, Amsterdam, Netherlands, (2015), **64**, 313-345.
15. Kumar, M., Fogden, A., Senden, T., & Knackstedt, M.A., “Investigation of Pore-Scale Mixed Wettability,” Paper SPE-129974, *SPE Journal*, (2012), **17,** 1, 20–30. doi: 10.2118/129974-PA.
16. Frobes,P.L., 1997, Centrifuge Data Analysis Techniques: An SCA Survey on the Calculation of Drainage Capillary Pressure Curves from Centrifuge Measurements,

paper SCA 1997 – 14, Presented at The International Symposium of the Society of Core Analysts, Calgary, Canada.

Table 1. Composition and properties of brine at 25°C

Brine Salinity (ppm)	Density (kg/m^3)	Viscosity (cP)	IFT with oil (Nm/m)
64,284	1060	1.05	70.8

Table 2. Properties of Heidrun Crude oil at 25°C

Color	Density (kg/m^3)	Viscosity (cP)	TAN (mg KOH/g)	Asphaltene content (%)
Light brown	858	6	2.82	< 1

Table 3. Composition of the 60-40 Heidrun/Heptane oil mixture from GC-analyses

Component	Mass fraction	Mole fraction	Volume fraction
CO_2	0.0000	0.0000	0.0000
N_2	0.0000	0.0000	0.0000
C1	0.0000	0.0000	0.0000
C2	0.0000	0.0000	0.0000
C3	0.0002	0.0009	0.0003
i-C4	0.0003	0.0012	0.0005
n-C4	0.0018	0.0070	0.0026
i-C5	0.0028	0.0086	0.0040
n-C5	0.0054	0.0165	0.0075
C6	0.0163	0.0427	0.0206
C7+	0.9732	0.9231	0.9646

Table 4. Experimental measurements for Kansas chalk

Core No.	Sat. porosity (%)	Brine Permeability (mD)	Aging Time (days)	S_{wi} (%)	S_{or} (%)	Contact Angle (°)*	SEM-MLA oil %	I_w (USBM)
1	38.57	2.10	6	64.71	19.23	65 (29.4)	10	0.368
2	38.49	1.90	9	54.32	13.82	66 (26.8)	19	0.510
3	37.76	2.01	12	58.10	6.10	78 (9.1)	27	0.005
4	36.93	1.92	15	62.61	8.81	85 (7.5)	37	0.053
5	38.04	1.96	18	54.15	4.13	102 (6.2)	37	0.864
6	38.06	2.00	21	54.33	4.28	110 (4.2)	39	-0.018
7	37.63	1.95	30	58.64	2.15	108 (4.5)	46	-0.165

** 150 to 300 data points were collected with average value presented and the standard deviation presented in brackets*

Table 5. Mineral list from the SEM-MLA analysis for Kansas chalk samples 1 to 7, number of aging days in parenthesis: 1(6), 2(9), 3(12), 4(15), 5(18), 6(21) and 7(30).

Colour	Mineral	% Area Coverage by Sample						
		#1 6 days	#2 9 days	#3 12 days	#4 15 days	#5 18 days	#6 21 days	#7 30 days
🟪	Carbonate	8	21	61	3	57	50	31
🟨	Halite	82	60	12	60	6	11	23
🟧	Oil	10	19	27	37	37	39	46
◼	Others	0	3	3	4	3	1	2

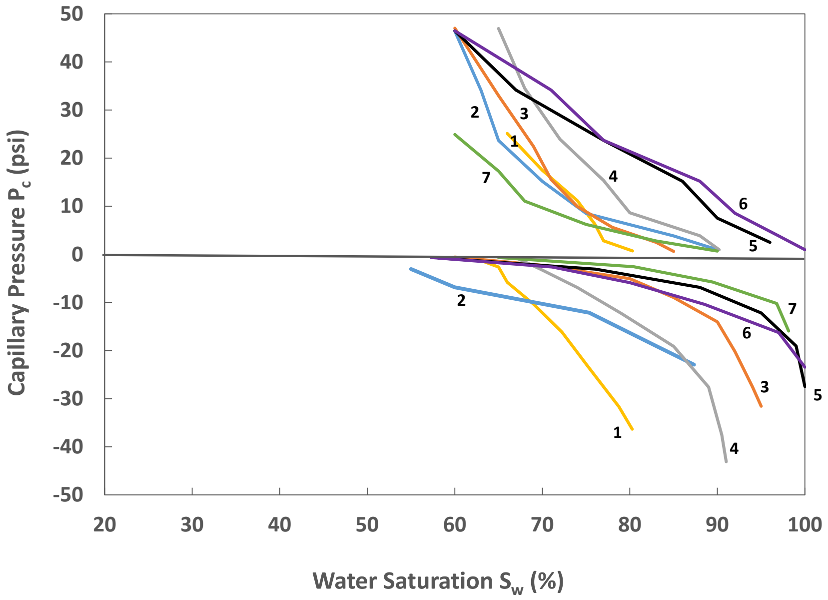

Figure 1. Primary imbibition (brine displacing oil, $P_c < 0$) and secondary drainage (oil displacing brine, $P_c > 0$) for Kansas chalk samples 1 to 7, number of aging days in parenthesis: 1 (6-yellow), 2 (9-blue), 3 (12-orange), 4 (15-grey), 5 (18-black), 6 (21-purple) and 7(30-green).
Note: For samples 5 and 6, the primary imbibition data was adjusted to 100% maximum saturation as the experiments overestimated the saturations to beyond 100%. The S_{or} reported for samples 5 and 6 in Table 4 are assumed to be the penultimate points after the saturations were adjusted to 100%.

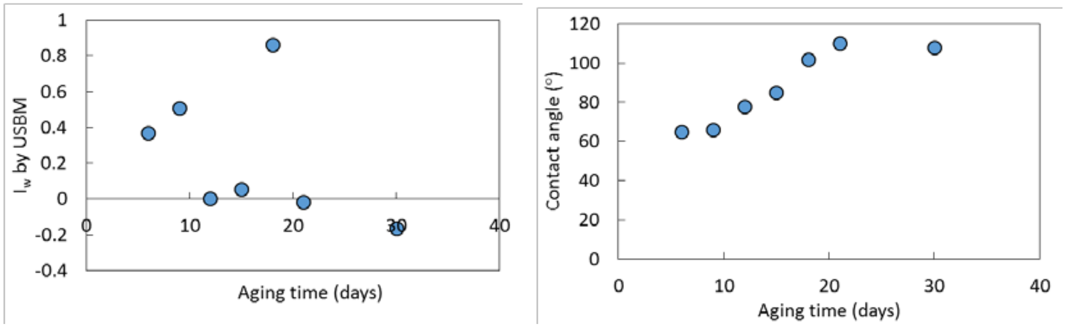

Figure 2. Left: Wettability index measurement using USBM method as a function of aging time. Right: Contact angle on the top end piece of aged chalk cores as a function of aging time.

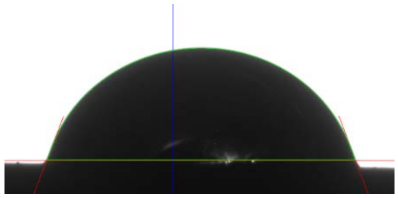

Sample 1 (θ = 65°) Age time: 6 days

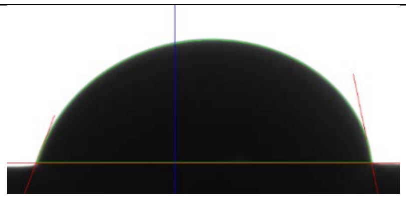

Sample 2 (θ = 66°) Age time: 9 days

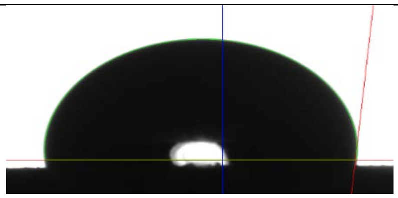

Sample 3 (θ = 78°) Age time: 12 days

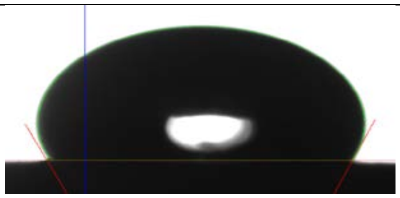

Sample 4 (θ = 85°) Age time: 15 days

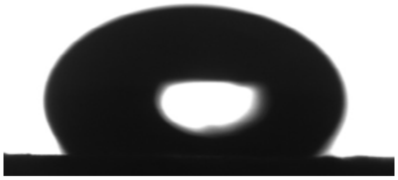

Sample 5 (θ = 102°) Age time: 18 days

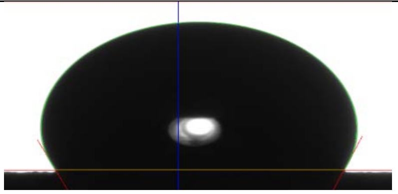

Sample 7 (θ = 108°). Age time: 30 days

Figure 3. Brine droplet of size $\sim 5 \cdot 10^{-4}$ *ml placed onto the aged top end piece.*
The contact angle is shown for differently aged chalk samples.

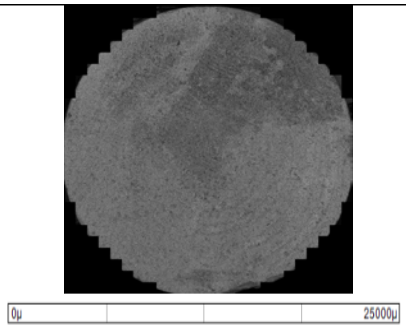

Chalk sample 1 (aged 6 days) SEM

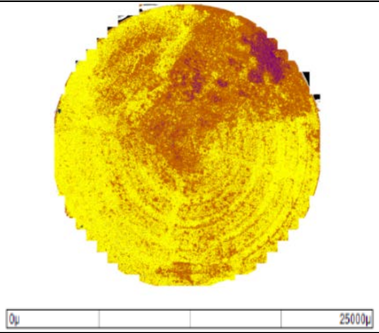

Chalk sample 1 (aged 6 days) MLA

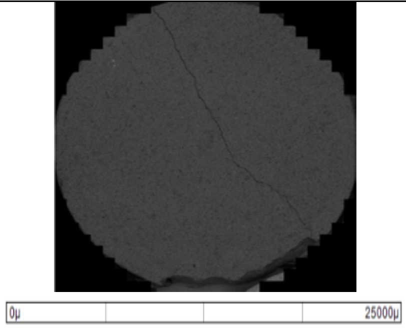

Chalk sample 7 (aged 30 days) SEM

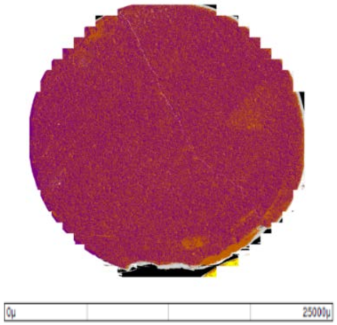

Chalk sample 7 (aged 30 days) MLA

Figure 4. SEM Images and MLA image of different aged chalk samples

Paper V

Sachdeva, J.S., Nermoen, A., Korsnes, R.I., and Madland, M.V. (2017). Elastic and Plastic Behavior of Chalks at Deviatoric Stress Condition: Experiments Performed with Four Different Brines. Paper Tu P030 presented at the IOR Norway 2017 – 19th European Symposium on Improved Oil Recovery, Stavanger, Norway, 24-27 April.

Paper VI

Sachdeva, J.S., Nermoen, A., Madland, M.V., and Korsnes, R.I. (2016). How Wetting Conditions Dictate Chalk Mechanics at Uni-axial Strain Conditions – Insights from Experiments Performed at In-situ Stress, Temperature and Pore Pressure. Paper SCA2016-068. *International Symposium of the Society of Core Analysts 2016*, Snowmass, Colorado, USA.

HOW WETTING CONDITIONS DICTATE CHALK MECHANICS AT UNI-AXIAL STRAIN CONDITIONS – INSIGHTS FROM EXPERIMENTS PERFORMED AT IN-SITU STRESS, TEMPERATURE AND PORE PRESSURE

Jaspreet S. Sachdeva[1,2], Anders Nermoen[1,2,3], Merete V. Madland[1,2], Reidar I. Korsnes[1,2]
[1]University of Stavanger, Norway
[2]The National IOR Centre of Norway
[3]International Research Institute of Stavanger, Norway

This paper was prepared for presentation at the International Symposium of the Society of Core Analysts held in Snowmass, Colorado, USA, 21-26 August 2016.

ABSTRACT

This paper document how the mechanical strength of chalk depends on the chemistry of pore fluids. Three experiments with different pore fluid compositions were performed at uni-axial strain conditions maintaining constant overburden stress during pore pressure depletion and subsequent compaction phase. The pore fluids were: i) 100% NaCl-brine, ii) 10%-90% NaCl-brine and oil mixture and iii) 100% oil. Significant differences were observed during the depletion and time-dependent compaction phase. The oil-saturated core was stronger than core saturated by brine-oil mixture, while the brine-saturated core accumulated most strain. During compaction, seawater was injected that led to additional strain; most so in the oil-saturated core, intermediate additional strain in the brine-oil mixed core, and least additional strain was observed in the brine-saturated core. This is in line with earlier results on how the ion composition of seawater significantly impacted chalk mechanics. Other significant observations include the additional side stress required to maintain the zero radial strain requirement, and irrespective of the original fluid composition, it is found that after only 2.5 PVs of seawater injection the creep rate for all three cases attained the same value. This indicates that the seawater induced weakening is abrupt, and it is more prominent when there is less water in the core originally.

INTRODUCTION

During primary phase oil production from a reservoir, the extraction of pressurized fluids reduce the pore fluid pressure leading to an increase in the effective stress, which in turn drives compaction. Reservoirs can be re-pressurized by injecting seawater to reduce the effective stress and mobilize oil. Even though the pressure is maintained, there is still considerable amount of compaction observed in the reservoirs. This compaction has been linked to the interaction of ions in the brines with the rock itself. Considerable research has been carried out concerning this water induced compaction in chalk reservoirs in the past few decades [1-4]. These studies have been carried out on water-wet chalk. This research has primarily shown that the pore fluid composition alters the mechanical integrity of chalk, as seawater and other simplified brines affect the mechanical strength. Different ions in the water, e.g. sulphates and magnesium ions, change the macroscopic mechanical behaviour of chalk, thus altering the way in which the brines and oils move through the porous rock and hence affecting oil recovery [2-4]. In recent studies of isotropic (hydrostatic) loading tests [5,6], it was shown that values characterizing the mechanical properties of chalk decreased when the wetting state was changed towards more water-wet. However, how do the results in [5,6] apply to high fluid pressures at uni-axial strain condition? In addition, how does the initial water condition dictate the mechanical response after the core has been flooded by seawater? This paper deals with the cases where the cores are initially saturated by different fluids and then the wettability is altered by aging to more mixed-wet state.

MATERIAL, EQUIPMENT, AND EXPERIMENTAL PROGRAM

Test Material and Saturation Fluids

The experiments in this study are performed on an outcrop chalk from a quarry in west-central Kansas in the USA (~39% porosity). The Kansas chalk type is considered to be a pure chalk with a non-carbonate content in the range 1-3% [2,7] and a permeability in the range 1-2 mD. This chalk is from Late Cretaceous geological age. Tang and Firoozabadi [7] argue that it is a good analogue to some clean North Sea reservoir chalks in regards to porosity, capillary pressure, and absolute and relative permeability.

Three different initial fluid saturations were used: Core K01 was saturated and flooded by 1.1M NaCl-brine. NaCl-brine was used as a simplified formation brine to minimize rock-fluid interactions prior to seawater flooding. Core K02 was saturated by approx. 10% NaCl-brine and 90% of Heidrun and Heptane oil that were mixed in 60%-40% (by volume). This oil was filtered through a 6.5μm filter. Core K03 did not contain any brine and was saturated only by the same oil. Both cores K02 and K03 were flooded with two pore volumes of this oil in each direction at 50°C. After the cores, K02 and K03, were saturated, they were submerged into the same oil and aged for 3 weeks at 8 bar and 90°C. The aging was performed to alter the wettability properties of the chalk cores. Wettability was not measured after aging. The aging procedure followed here would yield a wettability along the same lines as the results of Zangiabadi et al. [6] where they aged the cores with the same oil together with 20% brine, which gave a wettability index of 0.65. The wettability index (WI) is a measure of the available sulphate adsorption sites, where a WI equal to 0 means completely oil-wet and 1 means completely water-wet [6]. Strand et al. [8] reported wettability indexes below 0.5 on Stevns Klint chalk that were aged after being completely saturated by 60%-40% Heidrun/heptane mixture without initial water. Zangiabadi et al. [6] also reported acid number 1.92 mg KOH/g oil for the same oil mixture that is used in this study as well. Zangiabadi et al. [6] and Strand et al. [8] conclusively report that by increasing the acid number in the oil, the cores become more oil-wet after aging.

The Triaxial Cell Setup

The chalk cores were mounted into the triaxial cell that allows for continuous measurements of the axial and radial strains during flooding fluids at elevated stresses, pressures, and temperatures. The cell was equipped with a heating element and a regulating system with precise temperature control. Four pumps were connected to the triaxial cell to control the axial stress (σ_{ax}), confining pressure (σ_{rad}), flooding rate (Gilson pump) and pore pressure on the downstream side (P_p). An external linear voltage differential transducer (LVDT) monitored the length of the plug (L). The circumferential diameter on the middle of the core was measured with an extensometer. All the tests were performed at uni-axial strain conditions, with varying radial stress to ensure zero lateral (radial) strain and constant overburden stress such that the stress-path is similar to those that are occurring in the real field scenarios. In these tests, the deformation only took place in the axial direction and a constant axial stress was maintained. The extensometer attached around the core plug measured the radial deformation in the core as a function of time. The signal from extensometer was sent to the computer (LabView software) and was used to change confining pressure for the purpose of avoiding any radial deformation and maintaining zero radial strain. Changes in the confining pressure also affected the axial stress, so the piston pressure was automatically regulated to ensure constant axial stress.

Test Procedure

The experiments were performed at uni-axial strain conditions according to the following procedure: i) Mount the core in the triaxial cell; ii) Increase confining pressure (σ_{rad}) to 1.2 MPa and pore pressure (P_p) to 0.7 MPa simultaneously; iii) Increase temperature to 130°C; iv) Increase σ_{rad} to 40 MPa and P_p to 38 MPa simultaneously; v) Increase axial stress (σ_{ax}) to 42.5 MPa; vi) Start uni-axial strain test. Pore pressure depletion from 38 MPa to 15 MPa; vii) Observe creep at constant overburden; viii) Inject seawater according to the recipe shown in Zangiabadi et al. [6] and observe the creep strain.

During pore pressure depletion in uni-axial strain experiments, Hooke's law is modified such that Young's Modulus is calculated using,

$$E\delta\varepsilon_{ax} = \frac{3\alpha\delta P_p \delta\sigma_{rad} - 2(\delta\sigma_{rad})^2}{\delta\sigma_{rad} - 2\alpha\delta P_p} \qquad (1)$$

where E defines the Young's or elastic modulus, δP_p defines the change in the pore pressure from 38 MPa to the point where the core starts to yield, $\delta\sigma_{rad}$ defines the change in the radial stress and $\delta\varepsilon_{ax}$ defines the change in the axial strain corresponding to the same pore pressure values, and α is the Biot coefficient taken equal to 1 for calculations.

RESULTS

Pore Pressure Depletion Phase

Pore pressure depletion is carried out from 38 MPa to 15 MPa at uni-axial strain conditions. The yield, total axial strain and Young's Modulus values for the three cores during the pore pressure depletion phase are given in

Table 1. For the K03 core (100% oil), the yield strength and elastic modulus is found to be 2 and 1.4 times larger, respectively, than the results for the K01 core (100% brine). The total axial strain after loading is 4 times larger for the K01 core compared to the K03 core. The axial stress vs axial strain curves for all cores are given in Figure 1(a).

Uni-Axial Strain Compaction and Seawater Injection

The uni-axial compaction at constant overburden and pore pressures observed for the three cores is shown in Figure 1(b). The uni-axial compaction observed for K01 and K02 is 5.6% and 2.3%, before seawater injection, which goes up to 8.6% and 5.3%, respectively, after injecting seawater for 40 days. No compaction is observed for K03 prior to seawater injection, but shoots up to 7.5% after injecting the seawater for only 15 days. The strain rates before and after seawater injection for all tests are given in Figure 1(c). The strain rates for K01 and K02 prior to seawater injection are 0.05%/day and 0.07%/day, which increase to 0.17%/day and 0.19%/day, respectively, immediately after the start of injection. The strain rate shoots up to 0.77%/day from zero for K03 immediately after the start of seawater injection. After 2.5 PVs (5 days) of injection, all three cores attain the same value of around 0.17%/day strain rate. Please note that the starting time of seawater injection is taken as zero time (reference time) to make it easy to analyse the results.

DISCUSSIONS

The uni-axial compaction experiments, similar to Omdal et al. [9], have been performed, where the radial stress is automatically adjusted to ensure zero radial strain. The experiments have been carried out by depleting pore pressure whilst keeping the overburden stress constant, before the pore pressure was kept constant at 15 MPa over time. This experimental setup opens up for a range of studies in addition to the mechanical consequences reported here. For example, we can simulate the actual reservoir history with respect to stress, temperature and pore fluid composition, how the pore pressure affects the mobility of oil and water at actual PVT-values, and, to which extent adsorption, dissolution and precipitation depend on pore pressure and stress.

As expected from simpler hydrostatic tests reported by e.g. Zangiabadi et al. [6], we observe that K03 (100% oil) obtains the highest elastic modulus and highest yield during pressure depletion and that these values decrease with increasing brine content.

Prior to seawater injection, the side stresses are automatically reduced as the core compacts (Figure 1(d)). This is interpreted as a signature of work hardening during time, since less stress is required to keep the core at zero radial strain. However, when seawater is injected, the core weakens. Because of that, both the axial strain is increased, and similarly, the side stress required to maintain zero radial strain is increased. The side stress for the oil-saturated core increased by 6.3 MPa whilst the 10% and 100 % brine-saturated cores obtained approx. 3% additional axial strain, and correspondingly, the extra side stress required to sustain zero radial strain was 2.3 MPa and 1.7 MPa, respectively. We expect that a similar phenomenon could occur in reservoir systems when seawater is injected. In these cases, it is expected that the horizontal stresses would increase, since the uni-axial strain condition applies to reservoirs with large width to height ratios.

In Figure 1(c) before seawater injection, the compaction (strain) rate is different for all tests. However, irrespective of the original fluid composition, it is found that after only 2.5 PVs of seawater injection the creep rate for all three cases attained the same value. This shows that the wetting conditions have minor impact on the compaction rate after flooding 2.5 PVs of seawater through the core. In addition, it shows that the seawater induced weakening is abrupt and more prominent when there is almost zero initial water in the core. Thus in mixed wet cores, oil is not blocking seawater access to the intergranular contacts.

CONCLUSIONS

1. Completely oil-saturated core is found to be stronger compared to partially or completely brine-saturated cores.
2. Uni-axial compaction rate accelerates when seawater is injected.
3. The initial accelerated compaction by seawater injection is affected by the initial fluid chemistry.
4. After injecting 2.5 PVs of seawater, initial saturation and wetting state have minor effects on compaction rate.

ACKNOWLEDGEMENTS

The authors would like to thank the Research council of Norway and the industry partners; ConocoPhillips Skandinavia AS, BP Norge AS, Det Norske Oljeselskap AS, Eni Norge AS, Maersk Oil Norway AS, DONG Energy A/S, Denmark, Statoil Petroleum AS, ENGIE E&P NORGE AS, Lundin Norway AS, Halliburton AS, Schlumberger Norge AS, Wintershall Norge AS of the National IOR Centre of Norway for support.

REFERENCES

1. Sylte, J.E., L.K. Thomas, D.W. Rhett, D.D. Bruning and N.B. Nagel, “Water Induced Compaction in the Ekofisk Field”, Presented at the SPE Annual Technical Conference and Exhibition, Houston, Texas, SPE 56426 (1999).
2. Megawati, M., A. Hiorth, and M.V. Madland, “The impact of surface charge on the mechanical behaviour of high-porosity chalk”, *Rock Mechanics and Rock Engineering*, (2012) **46**(5), 1073-1090.

3. Madland, M.V., A. Hiorth, E. Omdal, M. Megawati, T. Hildebrand-Habel, R.I. Korsnes, S. Evje, and L.M. Cathles, “Chemical Alterations Induced by Rock-Fluid Interactions when Injecting Brines in High Porosity Chalks”, *Transport in Porous Media*, (2011) **87**, 679-702.
4. Korsnes, R.I., M.V. Madland, T. Austad, S. Haver, and G. Røsland, “The Effects of Temperature on the Water Weakening of Chalk by Seawater”, *Journal of Petroleum Science and Engineering*, (2008) **60**, 183-193.
5. Zangiabadi, B., T.A. Davidian, R.I. Korsnes, K.A.N. Vorland, T.G. Kristiansen and M.V. Madland, “The effect of wetting conditions on the mechanical strength of chalk”, *Proceedings of the 3rd International Conference on Coupled T-H-M-C Processes in Geo-systems, Lille, France*, (2008), 179-186.
6. Zangiabadi, B., R.I. Korsnes, M.V. Madland, T. Hildebrand-Habel, A. Hiorth and T.G. Kristiansen, “Mechanical Properties of High and Lower Porosity Outcrop Chalk at Various Wetting States”, Presented at the 43rd US Rock Mechanics Symposium and 4th U.S.-Canada Rock Mechanics Symposium, Asheville, NC, ARMA 09-139 (2009).
7. Tang, G. and A. Firoozabadi, “Effect of pressure gradient and initial water saturation on water injection in water-wet and mixed-wet fractured porous media”, *SPE Reservoir Evaluation & Engineering*, (2001) **4**(6), 516-524.
8. Strand, S., M.L. Hjuler, R. Torsvik, J.I. Pedersen, M.V. Madland and T. Austad, “Wettability of Chalk: Impact of Silica, Clay Content and Mechanical Properties”, *Petroleum Geoscience,* (2007) **13**, 69-80.
9. Omdal, E., M.V. Madland, T.G. Kristiansen, N.B. Nagel, R.I. Korsnes and A. Hiorth, “Deformation Behavior of Chalk Studied Close to In-Situ Reservoir Conditions”, *Rock Mechanics and Rock Engineering,* (2010) **43**, 557-580.

FIGURES AND TABLES

Table 1: Mechanical properties of the chalk cores

Core		K01	K02	K03
Yield Stress	MPa	8.85	14.92	18.45
Total depletion strain	%	2.72	1.16	0.64
Young's Modulus	GPa	2.81	3.47	4.05

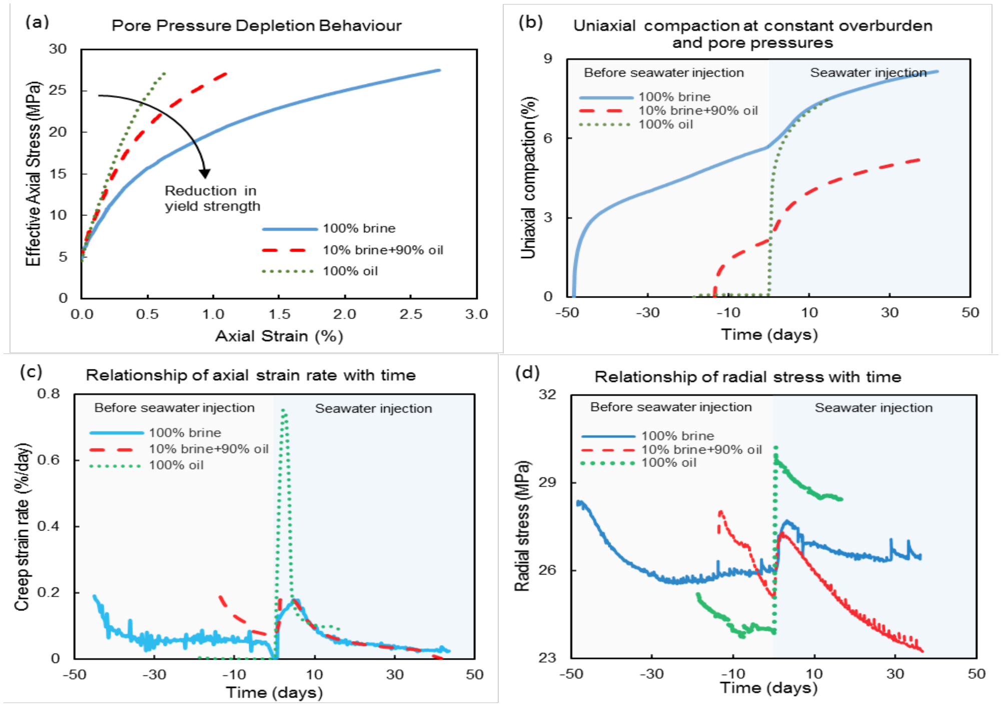

Figure 1: (a) Axial stress vs axial strain for all cores. (b) Compaction curves for all tests. (c) Compaction strain rate for all tests. (d) Radial stress curves for all tests. Please note that the starting time of seawater injection is taken as t=0 days in (b), (c) and (d).